Distribution Agreement

In presenting this thesis or dissertation as a partial fulfillment of the requirements for an advanced degree from Emory University, I hereby grant to Emory University and its agents the non-exclusive license to archive, make accessible, and display my thesis or dissertation in whole or in part in all forms of media, now or hereafter known, including display on the world wide web. I understand that I may select some access restrictions as part of the online submission of this thesis or dissertation. I retain all ownership rights to the copyright of the thesis or dissertation. I also retain the right to use in future works (such as articles or books) all or part of this thesis or dissertation.

Signature:

_____ _____

Xinru Huang Date

Comparing Measures of Global and Local Material Properties of Polystyrene under Different Boundary Conditions: Smooth, Chain-Tethered, and Rough Walls

By

Xinru Huang
Doctor of Philosophy

Physics

_____

Connie B. Roth
Advisor

_____

Eric R. Weeks
Committee Member

_____

Justin C. Burton
Committee Member

_____

Kurt Warncke
Committee Member

_____

James T. Kindt
Committee Member

Accepted:

_____

Lisa A. Tedesco, Ph.D.
Dean of the James T. Laney School of Graduate Studies

_____

Date

Comparing Measures of Global and Local Material Properties of Polystyrene under Different Boundary Conditions: Smooth, Chain-Tethered, and Rough Walls

Xinru Huang
B.Sc., Shihezi University, 2012

Advisor: Connie B. Roth, PhD

An abstract of
A dissertation submitted to the Faculty of the
James T. Laney School of Graduate Studies of Emory University
in partial fulfillment of the requirements for the degree of
Doctor of Philosophy
in Physics
2018

Abstract

Comparing Measures of Global and Local Material Properties of Polystyrene under Different Boundary Conditions: Smooth, Chain-Tethered, and Rough Walls
By Xinru Huang

In this dissertation, I measure both global and local material properties of polystyrene (PS) under different substrate conditions using ellipsometry and fluorescence. The first part of my dissertation focuses on investigating the correlation between the temperature-dependent specific volume v_{sp} and the variations in the glass transition temperature T_g for supported PS films. I find that both liquid and glassy v_{sp} behave nonmonotonically as a function of film thickness h. They start to deviate from bulk at ~120 nm, and at 65 nm have a maximum increase of (0.4 ± 0.2) % before dropping back to the bulk value at ~40 nm. This small amount of increase in v_{sp} is the same order of magnitude as Lipson's theoretical prediction and all within the experimental error of previous studies ± 1 %. The dramatic density increase for films thinner than 30 nm is consistent with some previous studies, but I believe this is not real due to the breakdown of Lorentz-Lorenz formula.

For rest parts of this dissertation, I use fluorescence spectroscopy to locally measure the glass transition temperature Tg near end-tethered and rough substrates without the free surface effect, which is ill-defined and uncontrollable. To achieve such local measurements, a 12 ± 1 nm chemically labeled PS layer with trace amounts of a fluorescent Tg sensitive pyrene dye is inserted at a position z away from different interfaces, thereby mapping out local Tg(z) profiles. I observe an optimum grafting density of σ = 0.011 chains/nm2 that results in a maximum Tg increase of 49 ± 2 K, which corresponds to the "mushroom-to-brush" crossover regime. The length scale over which this Tg(z) perturbation persists from the interface is ~100-125 nm. Then, I make rough interfaces by exposing flat silica substrates to hydrogen fluoride vapor for different lengths of time to achieve various roughnesses. The local Tg(z = 0) right at the rough substrates increases monotonically up to 111 ± 2 ^{0} C with increasing root-mean-square roughness Rrms from 0.5 nm to 10.9 nm. Comparing these two studies suggests chain tethering plays a dominant role in deciding the long length scale of Tg(z) near dissimilar polymer-polymer interfaces.

Comparing Measures of Global and Local Material Properties of Polystyrene under Different Boundary Conditions: Smooth, Chain-Tethered, and Rough Walls

Xinru Huang
B.Sc., Shihezi University, 2012

Advisor: Connie B. Roth, PhD

A dissertation submitted to the Faculty of the
James T. Laney School of Graduate Studies of Emory University
in partial fulfillment of the requirements for the degree of
Doctor of Philosophy
in Physics
2018

Acknowledgements

First and foremost, I would like to thank my advisor Connie B. Roth for her great guidance and support throughout all my years at Emory University. Connie is such a thoughtful person who patiently listens to all my words and generously shares all her past experience to inspire me. Her selfless help improves every aspect of me from research, writing, communicating to career planning, all of which well prepared me to move onto the next stage of my life. A big thank you goes out to my former lab member Roman Baglay for his expert advice and encouragements. I also need to thank all current and past group members, especially my former lab mentor Justin Pye, and all the current members Michael Thees, Yannic Gagnon and Yixuan Han for bringing inspiring talks and laughs into and outside the lab.

I would like to thank my committee members, Eric R. Weeks, Justin C. Burton, Kurt Warncke and James T. Kindt for working with me throughout this busy thesis writing season and taking your time to bring this dissertation to your highest standards. I also need to thank you for being so flexible that I successfully set up my defense time on the first try.

A big thank you also goes to Horace Dell and Cody Anderson for doing fantastic job on our home-designed equipment. I also need to thank Lowell Ramsey for helping me "dissect" our heaters. I would like to thank Jason Boss and Art Kleyman to keep our computers operating smoothly. Last but not the least, I must thank all the physics department staff, with a special thank you to Calvin Jackson, Barbara Conner and Susan Cook.

I would like to say thank you to my fiancé, Ryan Freeman, who endures all the frustration from me throughout all this process. Looking forward to marrying you in May! Finally, I need to thank my parents, Yineng Huang and Wenping Yan for unconditionally support and trust. To everybody I met along the way, thank you.

Table of Contents

List of Figures

List of Tables

Chapter 1

Introduction

This dissertation is about measuring global and local material properties of polystyrene (PS) under different boundary conditions, as measured by ellipsometry and fluorescence. In this introductory chapter, I will briefly discuss some basics of polymers, the glass transition and how it is known to change in thin films due to different polymer interfacial interactions. This will provide some necessary background to understand this dissertation and provide a sense of the state of the field prior to my contributions. I will end with an overview of the following chapters.

1.1 Polymer basics

Polymers are long molecules consisting of many repeat units. One of the first things we must consider is what the "size" of a polymer molecule is. There are two possibilities: one has to do with the contour length of a polymer chain and the other to the spatial extent. In the former case, the standard term is molecular weight (MW) with the unit of g/mol. A closely related concept, the degree of polymerization N is also commonly used, which is given by the ratio of M, the molecular weight of a given chain, to the molecular weight of the repeat unit M_0 ($N = \frac{\mathrm{M}}{M_0}$). A real polymer system contains many molecules with a variety of degrees of polymerization, so we use the number-average molecular weight M_n and weight-average molecular weight M_w in this dissertation to denote the molecular weight of polymers. The ratio of M_w to M_n is defined as the polydispersity index PDI, providing the information about the breath of the chain length distribution. In the latter case, because of the easy access through experiments, we commonly

use radius of gyration R_g, which is the average distance of all monomers from the center of mass, representing how much space a polymer coil occupies. For polymer chains resembling a random walk, $R_g \sim N^{1/2}$, with usually, R_g on the scale of tens nanometers. These long flexible chains cause entanglements in polymer systems and give polymers mechanical strength, flexibility, elasticity, etc.. More physical properties of polymers can also be obtained or tuned by the structure of polymers (branches, stars, brushes …), physical stereoregularity of polymer chains (isotactic, syndiotactic and atactic), polymer compositions (polymer mixtures, polymer nanocomposites …) and so on. Nevertheless, for this dissertation I will stick to simple and linear polystyrene chains.

The long chain aspect of polymers results in one of their most distinctive features, viscoelasticity. A material is viscoelastic when it behaves like a solid on short time scales and like a liquid on long time scales.[1] As virtually all polymers are processed in the liquid state, the viscosity part of polymer materials plays a central role in the optimization and control of processing. On the other hand, solid polymers have broad applications due to their various mechanical properties. The scientific reason behind this viscoelastic behavior is the multiple relaxation time scales in polymer systems.

To better understand the multiple time scales in polymer systems, we can take a look at the modulus master curve shown in Figure 1.1. At short timescales or above the glass transition temperature (see section 1.2), the modulus is that of a rigid solid of order GPa, and then it drops by 3~4 orders of magnitude to MPa for long entangled polymers. For those long entangled polymers, the existence of entanglements makes the moduli stay constant to a longer time scale and postpones the terminal liquid flow. This is the so-called rubbery plateau. The difference

between long entangled polymers and small molecules is that, for small molecules and low molecular weight unentangled polymers, their moduli drop to zero and immediately flow like a liquid. The transition of the modulus change from GPa to MPa is associated with the glass transition (see section 1.2). The glass transition is formally only defined on cooling, typically corresponding to when the cooperative segmental relaxation (α-relaxation) time reaches ~100 s, which is roughly the middle of the transition zone in Figure 1.1. The glass transition for polymers is associated with packing frustration at a segmental level and not that of the entire chain. Thus, theories universally applied to structural glasses can be equally applied to polymers.

The effect of chain connectivity for polymers comes in when they enter the liquid state above T_g. The Rouse model is the first successful molecular model of polymer dynamics to describe the different relaxation modes of the chain, a bead-spring model where the chain is represented as $N + 1$ beads connected by N springs. The shortest relaxation time within the Rouse model is that of a single bead-spring segment τ_{seg}, while the longest Rouse mode relaxation time accounts for the whole polymer chain, with a total of N relaxation times. The relaxation time τ_e corresponds to the Rouse mode for the average length of chain found between entanglements. To describe how entanglements with other chains in the melt restrict flow to even longer time scales, de Gennes used the concept of the tube, originally proposed by Edwards,[2] to introduce the reptation model to describe chain motion under such effects of entanglements.

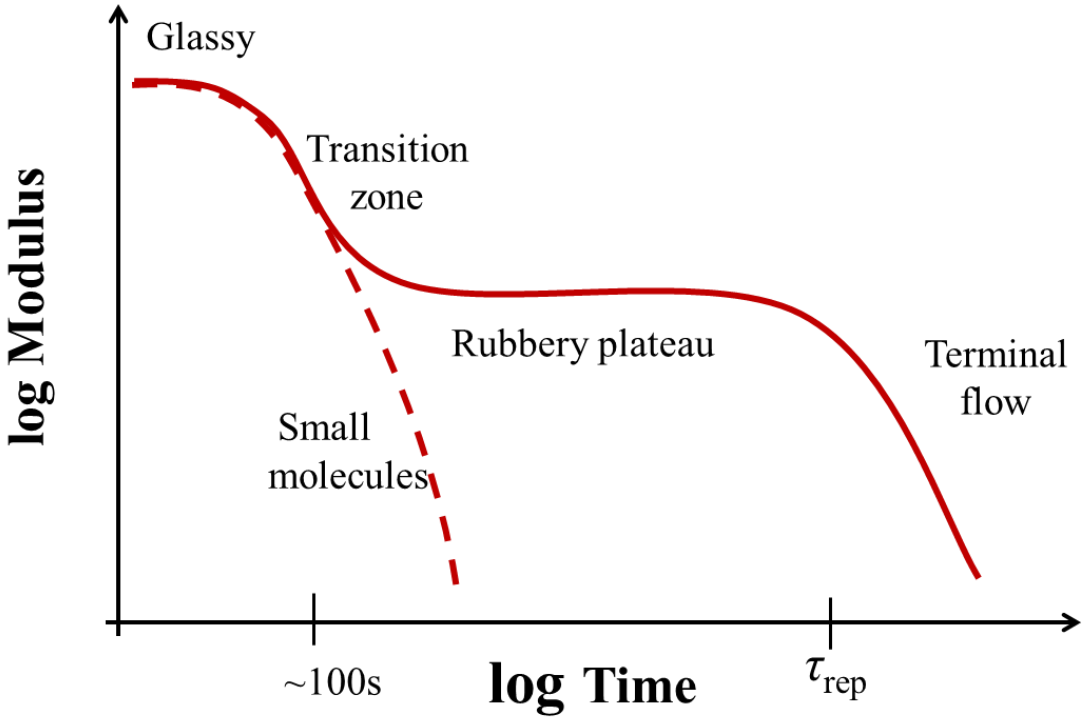

Fig. 1.1: Modulus master curve as a function of logarithmic time for polymers of molecular weight below and above the entanglement density. The dashed red curve shows low MW flow right after the glass transition zone with modulus dropping to zero. Solid red line is an illustration of the viscoelastic response of highly entangled polymer melts going through multiple relaxation regimes. Due to the existence of entanglements, a rubbery plateau postpones terminal flow until the reptation time τ_{rep} is reached.

The reptation model was originally developed to study a flexible chain trapped in a permanent polymer network,[3] after which Doi and Edwards extended this theory to describe the linear and nonlinear rheological response of polymer melts.[4] Imagine a chain trapped in a field of obstacles with spacing *d* and we can define a confining "tube" of diameter *d* with a set of fixed obstacles, shown in Figure 1.2. To realize large scale motions, the polymer chain needs to

escape from the confining tube and erase its original memory, but unfortunately, the polymer chain is unable to move tangentially to the direction of the tube and moves in a one dimensional diffusion process along the length of the tube, which is called reptation. The relaxation time corresponding to the moment when the middle segments of the chain finally escape from the tube is defined as the reptation time τ_{rep}, the time needed to completely erase the confining tube's memory. For times between the end of glass transition and τ_{rep}, the modulus is almost constant in time and most of the deformation energy is stored rather than dissipated, the material behaves as a rubbery solid with 3-4 orders of magnitude smaller in modulus compared to the glassy state. This so-called rubbery plateau can persist for some decades in time depending on the molecular weight of the polymer. The release of the initial constrains after a time of τ_{rep} finally gives way to flow in the terminal regime, allowing for viscous flow like a liquid.

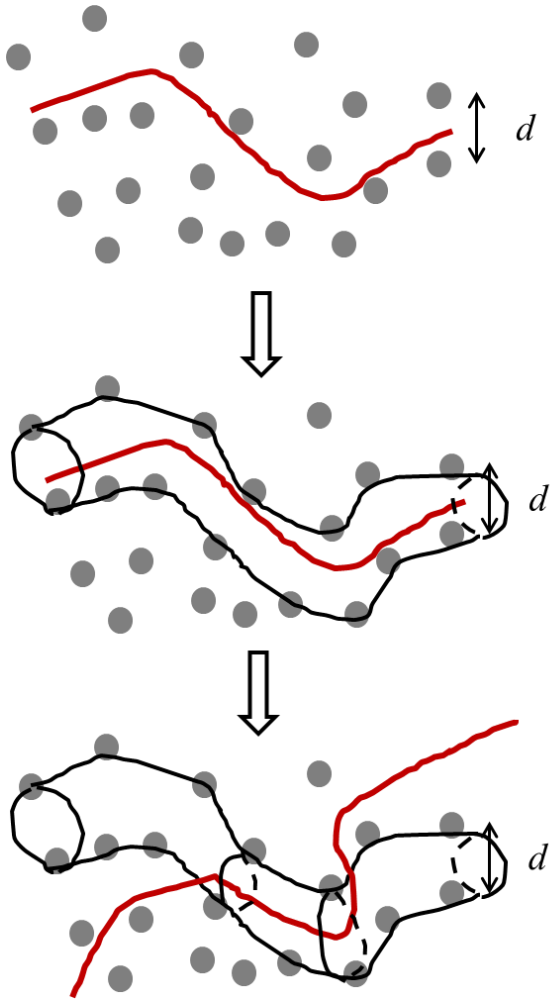

Fig. 1.2: A single chain (red solid curve) trapped in an array of obstacles (gray disks), spaced at an average distance *d*. The obstacles can be replaced by a tube with diameter *d* and the chain eventually loses its memory of the original tube through reptation, when the middle part of the chain moves out of the tube.

Among these relaxation regimes, the rubbery plateau is unique to polymers because of long chain entanglements. The length of this rubbery plateau associated with the reptation time τ_{rep} is mainly affected by the molecular weight of polymers. Within the "tube" model, reptation time τ_{rep} can be approximated by the following equation:[5]

$$\tau_{rep} \approx \frac{M^3}{M_0^2 M_e}\tau_{seg} \qquad (1)$$

where M is the molecular weight, M_0 is the monomer molecular weight, and M_e is the molecular weight in between entanglements. The reptation model predicts that the viscosity η of an entangled polymer melt is linearly proportional to the reptation time τ_{rep}.[4] As a result, the reptation model gives us that the viscosity of polymers is proportional to M^3. However, the experimental scaling observed $\eta \sim M^{3.4}$ has a stronger molecular weight dependence than that predicted simply by reptation. These deviations at high MW ($M > M_e$) are partially because the displacement of monomers at the two ends of the tube fluctuate, leading to an additional stress relaxation process, so in reality polymer chains relax faster than simple reptation predictions. Besides free chain-end fluctuations, we can bring reptation predictions into closer agreement with experiments by adding other additional relaxation processes such as constraint release and contour length fluctuations.[6] Deviations from the 3.4 power law at low MW ($M < M_e$) are because those chains are too short to be entangled.

The complete span of time scales from the segmental relaxation time to the reptation time can reach 12 or more orders of magnitude for high MW polymers,[7] so it is impossible to collect the modulus master curve of Figure 1.1 by one single experiment. The Rouse model as well as other molecular models describing the motion of polymer chains, assumes that the relaxation time associated with each mode has the same temperature dependence. The consequence of this is the expectation that it should be possible to superimpose linear viscoelastic data taken at different temperatures, commonly known as time-temperature superposition (TTS). TTS tells us a measurement at a certain temperature and time is equivalent to a measurement at a higher temperature and shorter times. Experimentally, this is

extraordinarily useful such that a plot like Figure 1.1, that covers more than 10 orders of magnitude in time, far larger than the range of any technique, can be gathered simply by collecting data at different temperatures and then building a master curve by shifting the timescales until all of the data overlap. For TTS to apply, the materials need to be homogeneous and isotropic, which are both true for the PS systems I am studying in this disertation.

1.2 Glass Transition

At high temperatures, materials are equilibrium liquids, as we cool them down, some of them will go through crystallization and solidify into crystals with well-defined unit cells, while others will vitrify into amorphous glasses with no long-range order or symmetry in the packing of the molecules. Glasses are non-equilibrium materials that have many relaxation procedures going on. When a material vitrifies into an amorphous glass, we say that this material is going through the glass transition and we associate with each material a glass transition temperature, T_g.

The value of T_g is the most important material property I am studying in this dissertation. Figure 1.3 shows two common ways of measuring T_g, one is to measure the change in the slope of volume *V* or enthalpy *H* as a function of temperature *T*, and the other is to measure the step change in temperature of the thermal expansion coefficient α ($\alpha = \frac{1}{h_0}\frac{dh}{dT}$) or heat capacity c_p ($c_p = \frac{\partial H}{\partial T}$). The glass transition is typically broad such that the exact position of the measured T_g can vary from experimental method to method, which will be discussed later in Chapter 2. The glass transition occurs when the molecular rearrangements required to reach equilibrium become slower than the rate at which the temperature is being changed. This demonstrates the value of T_g

is cooling rate dependent. Also for polymers, the value of the glass transition temperature T_g does not depend on MW after an initial saturation value of a couple of hundred monomers.[8] In the sense that the glass transition turns materials into non-equilibrium glasses and T_g is cooling rate dependent, generally we treat the glass transition as a kinetic phenomenon where the amorphous material is dynamically arrested. However, it is still debatable whether or not there is a thermodynamically "ideal" glass that can be formed under infinitely slow cooling rates.[9]

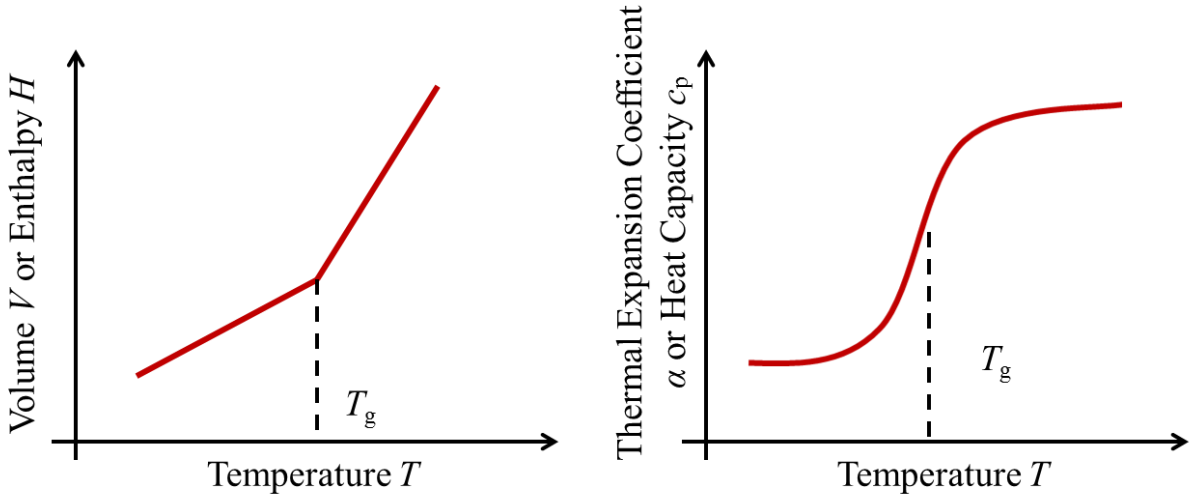

Fig. 1.3: Sketch of two ways to determine T_g. Left panel: volume V or enthalpy H as a function of temperature T. T_g is defines as the temperature when the slope changes from the liquid to glassy regimes on cooling. Right panel: thermal expansion coefficient α or heat capacity c_p as a function of temperature T. T_g is often associated with the midpoint of the step change.

To date, there is not yet a single theory that can completely explain the glass transition behavior mainly because of the remarkable changes in dynamics that occur in the supercooled region, defined as the temperature range in between T_g and the theoretical crystallization temperate T_m.[10] For example, viscosity is extraordinarily sensitive near T_g such that it can

reasonably change by ~14 orders of magnitude in 50 K approaching T_g.[11,12,13] The relaxation time of a glassy system approaching T_g fits well to the Kohlrausch-Williams-Watts (KWW) function,[13] whose stretching exponent informs us the glass transition is heterogeneous in time. Experimental and simulation evidence suggests that spatial heterogeneity happens near the glass transition with fast and slow regions.[12,14,15]

The running joke is that there are more theories than theorists in our field trying to understand these dramatic changes in glassy systems. Thus, I will simply mention some of the most popular theories and the ones that are meaningful to my dissertation. In 1965, Adam and Gibbs proposed the concept of a cooperatively rearranging region (CRR) with the idea that subunits of the material need to move in a cooperative fashion to make any significant change occur.[16] In 1984, Lentheuss et. al.[17] and Bengtzelius et. al.[18] used Mode Coupling Theory (MCT) to explain glassy dynamics dealing with a cage effect formed by a given particle's surrounding neighbors. In order to move at least the diameter of a particle, the cage has to be opened and this requires the cooperative rearrangement of many other neighbors. However, MCT does not work at lower temperatures when approaching T_g, as a result, MCT does not anticipate any properties of glassy dynamics, singularities, power laws and the like.[19] Long and Lequeux[20] introduced a percolation type model to explain the local dynamics in glassy materials. Percolation theory is the simplest fundamental model in statistical mechanics that exhibits critical phenomena signaled by the emergence of giant connected subunits of the material.[21] Sadly, the specific percolation thresholds are dependent on the lattice structure used in the model, which is not quantitatively meaningful for glassy systems with no long-range order. The Adam and Gibbs hypothesis, MCT, and Long and Lequeux's percolation model all assume the subunits of the materials are

independent, but Random First Order Transition (RFOT)[22] theory and a recent theory proposed by Schwiezer[23,24,25] introduce different interactions among the subunits of the materials. Despite the difficulties in studying glassy systems theoretically, the non-equilibrium glassy state has many interesting practical properties including memory effects,[26] structural recovery,[27,28] and physical aging.[29,30]

1.2.1 Glass transition in thin polymer films

Polymer thin films have many applications ranging from protective coatings, separation membranes, adhesives, lubrication layers to sensors and devices. However, shrinking the size of polymer films may make them more vulnerable to the surrounding environment and eventually change their material properties. The glass transition temperature T_g, which is one of the most important parameters for a certain application, also changes as a function of film thickness. This variation in T_g for polymer thin films was first observed by Keddie, Jones and Cory in 1994, who measured T_g as a function of film thickness h for supported PS films on hydrogen passivated silicon wafers with single wavelength ellipsometry.[31] They found a monotonic decrease in T_g starting from ~60 nm down to 12 nm with a maximum T_g change of 30 K. This behavior was not found to be molecular weight dependent, implying this thin film effect is not simply due to chain confinement and distortion of chain conformations.[32,33] Keddie, Jones and Cory fit their data to a semi-empirical equation with three fitting parameters:

$$T_g(h) = T_g^{bulk}\left[1 - \left(\frac{A}{h}\right)^{\delta}\right] \qquad (2)$$

Their best fit resulted in a T_g^{bulk} = (373.8 ± 0.7) K, a characteristic length A = (3.2 ± 0.6) nm, and exponent δ = 1.8 ± 0.2. Interestingly, T_g starts to deviate from the bulk behavior at a thickness around 60 nm which is much bigger than the characteristic length A and the ~1-3 nm cooperative length scale found in polymers near T_g.[12,34,35] This suggests there may exist a longer length scale also associated with the glass transition.

Keddie, Jones and Cory proposed competing effects from both the substrate interface and the free surface lead to an overall T_g change in thin supported films.[31,36] This has since been tested experimentally using local T_g measurements next to different interfaces by Torkelson's group.[37,38] The presence of the free surface leads to fewer constraints on relaxations and alters cooperative motion to occur more easily near the free surface.[10,39,40] The increasing mobility at the free surface eventually makes it harder to "freeze" the system such that the glass transition happens at a lower temperature. Similarly, different interactions between polymers and the substrate will change the local mobility near the substrate which results in changes in T_g, see Section 1.2.1.2. Keddie, Jones and Cory's work set off the field of polymer thin films and the same T_g reduction behavior has since been observed using X-ray reflectivity, dielectric spectroscopy, positron annihilation lifetime spectroscopy (PALS), local thermal analysis and fluorescence.[41]

The next interesting question was to understand how the altered dynamics from near a free surface (or substrate) propagates into the film, eventually recovering bulk dynamics far from the interface. The first direct measurement was done experimentally by Ellison and Torkelson in 2003 with a fluorescence technique designed to locally measure T_g.[37] They created a multilayer sample to isolate either the effect from the free surface or substrate. The key to this method,

which differed from their previous work,[42] is to covalently bond pyrene dye to the PS backbone. The advantage of doing this is that covalent bonding stops the pyrene dye from diffusing throughout the whole polymer film and makes the entire fluorescence signal come from a specific location. By inserting the pyrene labeled PS layer in between different PS layers, they achieved measuring local material properties of PS. When isolating the substrate interface, they observed no T_g change for PS next to a silica substrate, while, T_g was reduced by 32 K at the free surface and found to propagate ~30-40 nm into the polymer film before bulk dynamics were recovered.[37] Many simulation works also have studied the local dynamics inside polymer films and similar gradient in dynamics near an interface are observed.[40,43,44]

1.2.1.1 Polymer-air interface (free surface)

Besides adding an underlayer to isolate the free surface effect, a more efficient way to have a double influence from the polymer-air interface is to perform measurements on freestanding polymer films. Forrest et al.[45–47] and Mattsson et al.[48] found that for PS freestanding films with M_w < 368 kg/mol, $T_g(h)$ follows the same functional form as Eq. (2) but with T_g roughly equivalent to that measured for supported films of half the film thickness, consistent with double the amount of free surface being present. For freestanding films that have M_w > 575 kg/mol, $T_g(h)$ was found to decrease linearly and have a very strong dependence on the molecular weight. This strong molecular weight dependent behavior was later confirmed with dielectric spectroscopy,[49,50] Raman spectroscopy,[51] X-ray reflectivity[52] and fluorescence,[53] but there does not exist a well-accepted explanation.

In 2011, using transmission ellipsometry, Pye and Roth measured the thermal expansion and glass transition behavior of high molecular weight PS (M_n > 820 kg/mol) freestanding films over an extended temperature range.[54] They observed two distinct reduced T_gs, separated by up to 60 K for films thinner than 70 nm. The upper glass transition is stronger with no MW dependence, while the lower transition follows the previously seen MW dependent, linear $T_g(h)$ behavior seen in high MW freestanding PS films. This result suggests two mechanisms can propagate enhanced mobility from the free surface into the polymer films simultaneously, and helped explain why low and high MW PS freestanding films have different MW behaviors.

1.2.1.2 Polymer-substrate interface (wall)

For supported polymer thin films, polymer-substrate interactions affected by different polymer species can significantly alter T_g behavior. For example, previous studies on supported poly(2-vinyl pyridine) (P2VP) films on silicon wafers showed a monotonic T_g increase up to ~ 40 K as a function of decreasing film thickness using both ellipsometry and fluorescence.[38,55,56] It is worth noting that a more recent study from Glor et al. observed two T_gs in the same system and the higher T_g also increases as a function of decreasing film thickness h.[57] The side group of P2VP can form a hydrogen bond with the SiO_x substrate presumably leading to a mobility decrease, as a result, the T_g increase at the polymer-substrate interface wins over the faster dynamics at the free surface, showing an overall T_g increase in supported P2VP films.[38] Similarly, the average T_g of supported poly(methyl methacrylate) (PMMA) films shows only a small increase in T_g with decreasing film thickness due to the competing effects from the perturbative interfaces effectively canceling each other out. For PMMA, it seems the perturbations from

hydrogen bonding with SiO_x are comparable to those from the polymer-air interface.[58] On the other hand, PS does not interact with the silicon substrate and provides the best example of a solely free surface perturbation.[37]

The strength of different interactions near substrates not only depends on the chemistry of particular polymers, but also can be affected by grafting polymer chains and changing the surface roughness at substrates. Grafting polymer chains onto interfaces has many applications since it can provide an efficient way to tune the interfacial energy between the polymer matrix and the substrate. These substrates can be either flat like silicon wafers[59-60] or curved like rods[61] or particles.[62] It is popular for people in the polymer nanocomposites field to tether polymer chains to nanoparticles in order to enhance their material properties such as optical clarity, self-passivation, and reduced permeability.[63] Besides their use in polymer nanocomposites, grafted polymer chains are well-suited to offer performance gains in biotechnology, including prevention of bacterial adherence, cell attachment and formation of colloidal crystals.[64]

There are two methods to tether polymer chains to different substrates,[65] called "grafting to" and "grafting from", shown in Figure 1.4. The "grafting to" technique uses a chemical reaction between functionalized polymers with a surface containing a complementary functional group. Very narrow polydispersity brushes can be obtained by this method depending on the original functionalized polymer used.[66] We can regulate the grafting density by simply changing the allowed reaction time and any residual ungrafted polymers can be removed by solvent extraction. However, this "grafting to" method does not produce very high grafting densities because the attachment of chains can be impeded by the presence of previously attached chains. Zhou et al. pushed the upper limits of grafting density for the "grafting to" method by

crystallizing polymer chains in advance to increase the density of adsorbing sites.[67] On the other hand, the "grafting from" technique involves in situ polymerization of an initiator functionalized surface with monomers. Many living and conventional vinyl polymerizations have been applied using this method.[65,68] The biggest advantage of the "grafting from" method is that it can produce polymer brushes of high grafting density because there is little steric impediment to monomers approaching the surface to polymerize to grafted sites. Nevertheless, this chemically more complex method also is limited by initiator surface coverage and efficiency. The effect of side reactions may also be more prevalent than in bulk polymerizations, leading to a broader molecular mass distribution. In order to know exactly what the molecular weight is for the resulting brushes, chains need to be removed from the substrate to be measured by some size exclusion measuring instrument like gel permeation chromatography (GPC).

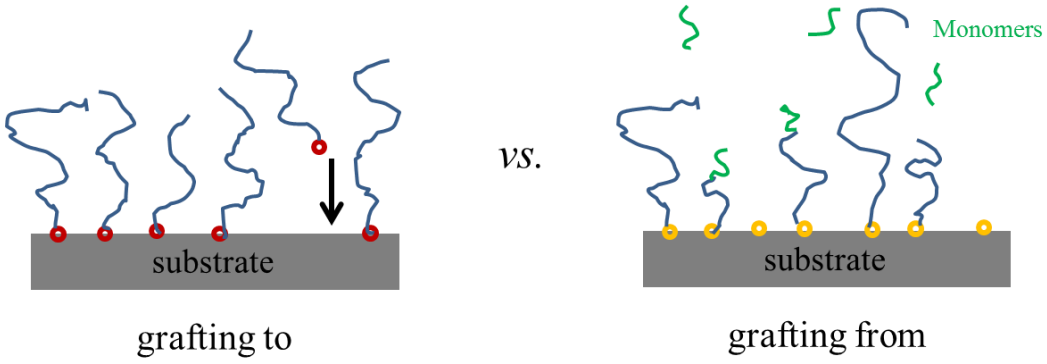

Fig. 1.4: Comparison of two different grafting methods. Left panel: "grafting to" technique requires end-functional groups (red circles), as a part of polymer chains to chemically react with complementary groups on the substrates. Right panel: "grafting from" method involves an in situ polymerization procedure. Yellow circles correspond to the original initiator spread on the substrate, which regulates the bonding position of grown polymer brushes.

Roughening of the substrate theoretically provides another efficient way to tailor the interfacial interactions between the polymer matrix and the substrate.[69] Experimentally, no published study has yet measured glass transition polymer dynamics next to a rough wall. An attempt by Panagopoulou et al. looked into how surface roughness influenced the segmental mobility of thin polymer films using dielectric spectroscopy.[70] However, their results contradict with the slowing down motion observed in many simulation works.[71–75] There are many experimental difficulties associated with such studies next to a rough substrate. First is the important question of what is an appropriate roughness scale to perturb local glass transition dynamics, and how to meaningfully quantify surface roughness since there are numerous roughness parameters to choose from? Then the next challenge is how to make a roughened surface without changing the surface chemistry and substrate compliance.

There are many existing methods that can be used to make rough surfaces, but in general, they are either mechanical operations or chemical erosions. Popular machining methods are lapping, sand blasting, evaporation, sputtering and so on. For the former two techniques, typical roughnesses are on the micrometer scale.[76] Even though physical vapor deposition methods can easily reach nanometer scale roughness, their upper limit in roughness is constrained by the highest deposition rate which is usually only a couple of nanometers per second. Alternatively, chemical etching methods provide a continuous range of roughness from nanometers to micrometers. For a silica substrate, use of hydrofluoric acid creates a violent chemical reaction.[77] To have more control of these extremely fast chemical reactions, people usually use buffered

oxide etching (BOE), a solution which is a mixture of ammonium fluoride (NH_4F) and hydrogen fluoride (HF) to create a constant slow etching rate.[78]

Fully characterizing a rough surface is an impossible mission because the real surface geometry is so complicated that a limited number of roughness parameters cannot provide a full description. If the number of parameters used is increased, a more accurate description can be obtained. Then the tricky question is how to choose from a big pool of surface roughness parameters[79] to get a sufficient description of a rough surface. The following introduction of some amplitude (vertical direction) and spacing (horizontal direction) roughness parameters can help you better understand my choices in Chapter 5. All the roughness quantifications are based on a mean surface level line defined mathematically as,[80]

$$\sum_{i=1}^{N} z_i = 0 \qquad (3)$$

with *N* height measurements of *z*, shown as the dashed black line in Figure 1.5.

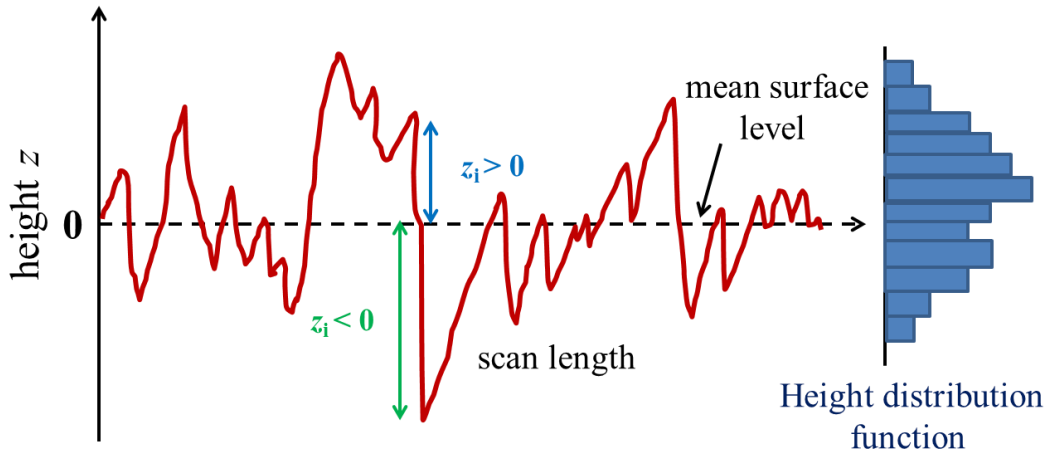

Fig. 1.5: Cartoon sketch of the surface profile on a random rough interface. The dashed line is the mean surface level, above which measured heights are positive and negative below the line.

The bar chart on the far right is the height distribution function projected from the measured heights z_i. The shape of this height distribution function defines skewness (symmetry) and kurtosis (sharpness), which tells us about the deviations of heights from the normal distribution.

Root-mean-square roughness R_q (frequently denoted as R_{rms}) is the most commonly used amplitude roughness parameter. It is defined as,[80]

$$R_q = \sum_{i=1}^{N} \sqrt{\frac{(z_i - z_o)^2}{N}} \quad (4)$$

where $(z_i - z_o)$ is the distance between the i[th] vertical coordinate and the mean plane. Another very close roughness parameter to R_q is the mean roughness R_a, which can be calculated as,[80]

$$R_a = \frac{1}{N} \sum_{i=1}^{N} |z_i| \quad (5)$$

If a surface has a profile that contains no large deviations from the mean surface level, the values of R_q and R_a will be similar. However, neither R_q nor R_a informs us about the preferences of bumps or holes on the surface. To extract more information about up and downs on the surface, we need to first introduce the idea of a height distribution function. A height distribution function is the projection of measured height values onto a probability graph. Depending on the shape of the height distribution function, we can define skewness and kurtosis to separately describe its symmetry and sharpness:[80]

$$skewness = \frac{1}{R_q^3} \frac{1}{N} \sum_{i=1}^{N} z_i^3 \quad (6)$$

$$kurtosis = \frac{1}{R_q^4} \frac{1}{N} \sum_{i=1}^{N} z_i^4 \quad (7)$$

Skewness is a nondimensional quantity which is typically evaluated in terms of positive or negative. A skewness of zero suggests an even distribution of data around the mean plane. When skewness is strongly non zero, an asymmetric, one-tailed distribution is indicated, such as a flat plane having a small, sharp spike (>0), or a small, deep pit (<0). Graphically, kurtosis indicates whether data are arranged flatly or sharply about the mean plane. The kurtosis of any normal distribution is 3, so it is common to compare the kurtosis of a distribution to 3. When kurtosis is < 3, it means the *z* value distribution has fewer and less extreme outliers; while when kurtosis is > 3, it means more extreme *z* values exist.

The power-spectral-density (PSD) function is the most common spatial roughness parameter people use. As the Fourier transformation of the real rough surface, it informs us of the characteristic length scales constructing the specific roughness profile.[80] Figure 1.6 shows two extreme examples of periodic and totally irregular rough surfaces. A totally irregular rough surface has continuous spatial frequencies, where the lowest frequency will be restricted by the scanning window size.

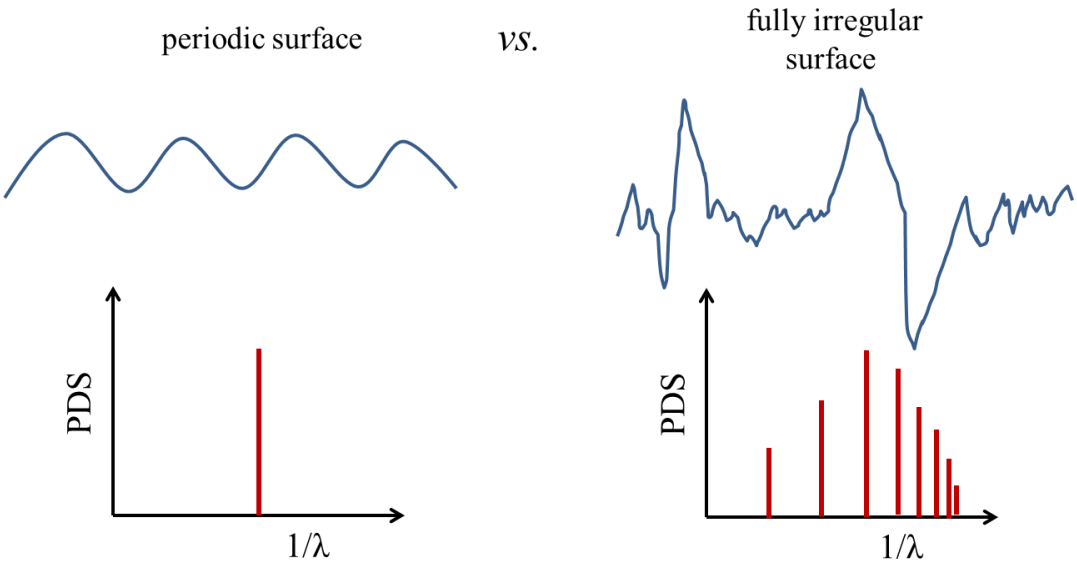

Fig. 1.6: The power-spectral-density (PSD) functions for two rough surfaces. Left panel: PSD for a periodic surface only has one characteristic length scale, resulting in a delta function. Right panel: PSD for a fully irregular surface which ideally has an infinite number of characteristic length scales.

Besides using rough walls to perturb polymer systems and make changes in dynamics, rough walls have great applications across different scientific and engineering fields. For example, rough metal surfaces enhance heat transfer of electronics cooling leading to better thermal management in microprocessors.[81] Understanding how rough interfaces alter microscopic properties at the nanoscale is a fundamental goal for both material engineering and polymer science.

1.2.1.3 Polymer-polymer interface

With the invention of new synthesis and processing technologies, polymer blends and new block copolymers with domain sizes reaching ~100 nm scale are possible for macroscopic material fabrication.[82-83] Understanding how dynamics couple across polymer-polymer interfaces at the nanoscale becomes essential in designing functionalities of polymer blends. Besides the engineering benefits of studying polymer-polymer interfaces, scientifically, it provides another type of perturbation that can effectively alter the cooperative dynamics of polymer materials.

Previously, Baglay and Roth[84-85] studied the local $T_g(z)$ profiles across and near dissimilar polymer-polymer interfaces and found the perturbations in local T_g can be quite long-ranged (spanning 350-400 nm) and asymmetric (biased to the glassy side). This is in contrast to expectations based on miscible blends, which would predict a sharp transition in dynamics across a dissimilar polymer-polymer interface essentially following the composition profile. However, the measured dynamics do not correlate with the ~5 nm wide symmetric composition profile of the interface.[84] The local $T_g(z)$ length scales appear to be universally grouped according to the measured T_g.[85] If the polymer side has a higher or lower T_g compared to the other side, then this is referred to as hard or soft confinements.[85] Most recently, they sandwiched a 300 nm thick PS film in between two bulk poly(n-butyl methacrylate) (PnBMA) films to mimic periodic boundary conditions used in simulations.[87]

Comparing polymer-polymer interfaces to the other two perturbations mentioned earlier in Section 1.2.1(polymer-air interfaces and polymer-substrate interfaces), Baglay and Roth[85] proposed three possible factors that may help explain these hundred nanometer long length scales in the $T_g(z)$ profiles. First, there is a broadening of the interfacial region during annealing of the polymer-polymer interfaces. The interfacial width at a polymer-air interface is only about

0.5 nm, which is ten times smaller than the equilibrium interfacial width at polymer-polymer interfaces. Depending on the interaction parameters between PS and the other polymers, the interfacial width can be varied. For instance, the interfacial width for a PS/PMMA interface is 5 nm[86] compared to 7 nm for PS/PnBMA.[84,88] In general, the polymer-polymer interfacial width for the polymer pairs studied by Baglay and Roth is around 5 nm.[85] Second, chain connectivity across the interface could also play an important role in modifying polymer-polymer interfacial dynamics. Third, an increased interfacial roughness at polymer-polymer interfaces due to the reduced interfacial energy compared to polymer-air and polymer-substrate interfaces is also expected.

Chapter 4 in this dissertation aims to study how chain connectivity alters the local dynamics by measuring T_g right next to tethered substrates. The "grafting to" method mentioned in Section 1.2.1.2 provides an efficient way to tailor the interfacial energy between polymer and a "hard" confinement interface by varying the grafting density of tethered chains on silica substrates. Unfortunately, there only exists theory and simulation works that study how the interfacial roughness affects the local dynamics next to rough substrates.[69,71,73–75] Chapter 5 of this dissertation is the first experimental study of measuring the local glass transition temperature T_g next to rough interfaces with tunable surface roughness. One of the biggest contributions of my dissertation is to disentangle the impact of these factors proposed by Baglay and Roth,[85] studying individually how surface tethering and roughness affect the local cooperative dynamics of polymer films.

1.3 Outline of dissertation

This dissertation is comprised of six chapters detailing the research I accomplished towards the goal of understanding how different boundary conditions affect both global and local glass transition and related properties of polymers. Chapter 2 describes the two main experimental apparatuses I use to measure the glass transition behavior of polymer films. The details of ellipsometry and fluorescence techniques are presented, including a brief history of these techniques, components parts of the instruments and their working principles. Towards the end of Chapter 2, I also compare the reported T_g difference between ellipsometry and fluorescence.

The fundamentals of the $T_g(h)$ decrease behavior of supported PS thin films have puzzled the field for more than two decades.[31] An open question at present is what other material properties change in PS thin films corresponding to the large shifts in $T_g(h)$. In 2011, White and Lipson proposed a thermodynamic model with no adjustable parameters and predicted that a small ~0.5 % increase in the specific volume may explain the decrease in $T_g(h)$ for freestanding PS thin films.[89] To test White and Lipson's theory,[89] in Chapter 3, I use ellipsometry to investigate the temperature-dependent specific volume for supported polystyrene (PS) films of different thicknesses. Using the Lorentz-Lorenz parameter as a measure of the relative change in film density, I calculate the specific volume from temperature-dependent measurements of the index of refraction. I find that both the liquid and glass specific volume start to deviate from bulk at ~120 nm, and at 65 nm has a maximum increase of (0.4 ± 0.2) % before dropping back to the bulk value at ~40 nm. This percent increase in specific volume is the same order of magnitude as Lipson's theoretical prediction[89] and all within the experimental error of previous studies ± 1 %.[90,91] For films thinner than 30 nm, we see a dramatic density increase which is consistent

with some previous studies but I believe this is not real due to the breakdown of Lorentz-Lorenz formula. A version of this chapter was published as:

> Xinru Huang and Connie B. Roth, Changes in the Temperature-Dependent Specific Volume of Supported Polystyrene Films with Film Thickness. *Journal of Chemical Physics* **144**, 234903 (2016).

The specific volume study in Chapter 3 is under the influence of the free surface, whose perturbation to the dynamics is not well understood. For the rest of this dissertation, I am going to avoid the free surface effect and only focus on perturbations from the polymer substrate interfaces. In Chapter 4, I end-graft polystyrene (PS) chains to silica substrates and measure the local glass transition temperature T_g as a function of distance z from the substrate interface. I observe an optimum grafting density of $\sigma = 0.011$ chains/nm^2 that results in a maximum T_g increase of 49 ± 2 K, which corresponds to the "mushroom-to-brush" crossover regime. Within this near substrate region, only ~10 % is the end-tethered PS chains, which tells us it does not take many grafted chains to have a big impact on T_g. The length scale over which this $T_g(z)$ perturbation persists from the interface is ~100-125 nm, and it is comparable to our group's recent work of PS next to a higher-T_g polymer such as polysulfone. This suggests to us that chain tethering may play a dominant role in deciding the long ranged $T_g(z)$ profiles across polymer-polymer interfaces. A version of this chapter was published as:

> Xinru Huang and Connie B. Roth, Optimizing the Grafting Density of Tethered Chains to Alter the Local Glass Transition Temperature of Polystyrene near Silica Substrates: the Advantage of Mushrooms over Brushes. *ACS Macro Letters* **7**, 269-274 (2018).

Another way to alter interfacial interactions is roughening the substrate. To date, only theory and simulation work exists on studying polymer behavior next to rough walls.[69,71,73-75] Hanakata et al. found that roughness, stiffness and polymer-substrate interactions can all change

the local glass transition temperature T_g and fragility m of polymers as a function of film thickness h.[73,74] In Chapter 5, I create rough substrates with root-mean-square roughness R_q ranging from 0.5 nm to 10.9 nm without changing the surface chemistry through exposing silica substrates to HF vapor for different lengths of time. Analysis using the power-spectral-density (PSD) function indicates that the rough interfaces do not have a characteristic length scale. The local $T_g(z = 0)$ right at the rough substrates increases monotonically with increasing R_q up to 111 $\pm$ 2 ^{0}C. These results suggest that interfacial roughness may not play as important a role as chain tethering in deciding the $T_g(z)$ profiles next to dissimilar polymer-polymer interfaces. A version of this chapter is prepared as:

> Xinru Huang, Michael F. Thees and Connie B. Roth, Experimental Study of Substrate Roughness on the Local Glass Transition of Polystyrene. *Journal of Chemical Physics*, to be submitted.

1.4 References

[1] E. Riande, *Polymer Viscoelasticity Stress and Strain in Practice*, Marcel Dekker, New York (2000).

[2] S.F. Edwards, Proc. Phys. Soc. London, **92**, 9, (1967).

[3] P.G. de Gennes, J. Chem. Phys. **55**, 572 (1971).

[4] M. Doi and S.F. Edwards, J. Chem. Soc. Faraday Trans. 2 **74**, 1789 (1978).

[5] P.C. Hiemenz and T.P. Lodge, *Polymer Chemistry*, CRC Press (2007).

[6] M. Rubinstein and R.H. Colby, *Polymer Physics*, Oxford University Press (2003).

[7] J.D. Ferry, *Viscoelastic Properties of Polymers*, 3rd Ed.; Wiley: New York (1980).

[8] C.B. Roth and R.R. Baglay, *Fundamentals of Polymers and Glasses*, *Polymer Glasses*, editor C.B. Roth, CRC Press (2016).

[9] G. Biroli and J.P. Garrahan, J. Chem. Phys. **138**, 12A301 (2013).

[10] G. Tarjus, An Overview of the Theories of the Glass Transition. In *Dynamical Heterogeneities in Glasses, Colloids and Granular Media*; L. Berthier, G. Biroli, J.P. Bouchaud, L. Cipelletti, and W. van Saarloos, International Series of Monographs on Physics; Oxford University Press (2011).

[11] C.A. Angell, K.L. Ngai, G.B. McKenna, P.F. McMillan, and S.W. Martin, J. Appl. Phys. **88**, 3113 (2000).

[12] M.D. Ediger, Annu. Rev. Phys. Chem. **51**, 99 (2000).

[13] R. Richert, J. Phys: Condens. Matter **14**, 703 (2002).

[14] C. Donati, J.F. Douglas, W. Kob, S.J. Plimpton, P.H. Poole, and S.C. Glotzer, Phys. Rev. Lett. **80**, 2338 (1998).

[15] E.R. Weeks, J. C. Croker, A.C. Levitt, A. Schofield, and D.A. Weitz, Science **287**, 627 (2000).

[16] G. Adam and J.H. Gibbs, J. Chem. Phys. **43**, 139 (1965).

[17] E. Leutheusser, Phys. Rev. A **29**, 2765 (1984).

[18] U. Bengtzelius, W. Götze, and A. Sjolander, J. Phys. C: Solid State Physics **17**, 5915 (1984).

[19] W. Götze, J. Phys. Condens. Matter **11**, A1 (1999).

[20] D. Long and F. Lequeux, Eur. Phys. J. E **4**, 371 (2001).

[21] M. Sahimi, *Application of Percolation Theory*, CRC Press (1994).

[22] A. Cavagna, Phys. Rep. **476**, 51 (2009).

[23] S. Mirigian and K.S. Schweizer, J. Phys. Chem. Lett. **4**, 3648 (2013).

[24] S. Mirigian and K.S. Schweizer, J. Chem. Phys. **141**, 161103 (2014).

[25] S. Mirigian and K.S. Schweizer, J. Chem. Phys. **143**, 244705 (2015).

[26] T. Xie, Nature **464**, 267 (2010).

[27] G.B. McKenna, J. Phys. Condens. Matter **15**, S737 (2003).

[28] G.B. McKenna and S.L. Simon, Macromolecules **50**, 6333 (2017).

[29] L.C.E. Struik, *Aging in Amorphous Polymers and Other Materials*, Elsevier, Amsterdam **17**, 78 (1978).

[30] J.E. Pye, K.A. Rohald, E.A. Baker, and C.B. Roth, Macromolecules **43**, 8296 (2010).

[31] J.L. Keddie, R.A.L. Jones, and R.A. Cory, Europhys. Lett. **27**, 59 (1994).

[32] O.K.C. Tsui and H.F. Zhang, Macromolecules **34**, 9139 (2001).

[33] C.J. Ellison, M.K. Mundra, and J.M. Torkelson, Macromolecules **38**, 1767 (2005).

[34] E. Hempel, G. Hempel, A Hensel, C. Schick, and E. Donth, J. Phys. Chem. B **104**, 2460 (2000).

[35] U. Tracht, M. Wilhelm, A. Heuer, H. Feng, K. Schmidt-Rohr, and H. Spiess, Phys. Rev. Lett. **81**, 2727 (1998).

[36] J.L. Keddie, R.A.L. Jones, and R.A. Cory, Faraday Discuss. **98**, 219 (1994).

[37] C.J. Ellison and J.M. Torkelson, Nat. Mater. **2**, 695 (2003).

[38] C.B. Roth, K.L. McNerny, W.F. Jager, and J.M. Torkelson, Macromolecules **40**, 2568 (2007).

[39] K.F. Mansfield and D.N. Theodorou, Macromolecules **24**, 6283 (1991).

[40] R.J. Lang and D.S. Simmons, Macromolecules **46**, 9818 (2013).

[41] C.B. Roth and J.R. Dutcher, J. Electroanal. Chem. **584**, 13 (2005).

[42] C.J. Ellison, S.D. Kim, D.B. Hall, and J.M. Torkelson, Eur. Phys. J. E **8**, 155 (2002).

[43] S. Peter, H. Meyer, J. Baschnagel, and R. Seemann, J. Phys. Condens. Matter **19**, 205119 (2007).

[44] R.A. Riggleman, K. Yoshimoto, J.F. Douglas, and J.J. De Pablo, Phys. Rev. Lett. **97**, 045502 (2006).

[45] J.A. Forrest, K. Dalnoki-Veress, J.R. Stevens, and J.R. Dutcher, Phys. Rev. Lett. **77**, 2002 (1996).

[46] J.A. Forrest, K. Dalnoki-Veress, and J.R. Dutcher, Phys. Rev. E **56**, 5705 (1997).

[47] J.A. Forrest and J. Mattsson, Phys. Rev. E **61**, R53 (2000).

[48] J.Mattsson, J.A. Forrest, and L. Börjesson, Phys. Rev. E **62**, 5187 (2000).

[49] C. Rotella, S. Napolitano, and M. Wübbenhorst, Macromolecules **42**, 1415 (2009).

[50] S. Napolitano and M. Wübbenhorst, Polymer **51**, 5309 (2010).

[51] H. Liem, J. Cabanillas-Gonzalez, P. Etchegoin, and D.D.C. Bradley, J. Phys. Condens. Matter **16**, 721 (2004).

[52] T. Miyazaki, R. Inoue, K. Nishida, and T. Kanaya, Eur. Phys. J. Spec. Top. **141**, 203 (2007).

[53] S. Kim, S.A. Hewlett, C.B. Roth, and J.M. Torkelson, Eur. Phys. J. E **30**, 83 (2009).

[54] J.E. Pye and C.B. Roth, Phys. Rev. Lett. **107**, 235701 (2011).

[55] J.H. van Zanten, W.E. Wallace, and W.L. Wu, Phys. Rev. E **53**, R2053 (1996).

[56] C.H. Park, J.H. Kim, M. Ree, B.H. Sohn, J.C. Jung, and W.C. Zin, Polymer **45**, 4507 (2004).

[57] E.C. Glor, G.V. Angrand, and Z. Fakhraai, J. Chem. Phys. **146**, 203330 (2017).

[58] R.D. Priestley, M.K. Mundra, N.J. Barnett, L.J. Broadbelt and J.M. Torkelson, Aust. J. Chem. **60**, 765 (2007).

[59] A. Clough, D. Peng, Z. Yang, and O.K.C. Tsui, Macromolecules **44**, 1649 (2011).

[60] R.S. Tate, D.S. Fryer, S. Paqualini, M.F. Montague, J.J. De Pablo, and P.F. Nealey, J. Chem. Phys. **115**, 9982 (2001).

[61] N. Tsubokawa, Polym. J. **37**, 637 (2005).

[62] J.F. Moll, P. Akcora, A. Rungta, S. Gong, R.H. Colby, B.C. Benicewicz and S.K. Kumar, Macromolecules **44**, 7473 (2011).

[63] K.I. Winey and R.A. Vaia, MRS Bulletin, **32**, 314 (2007).

[64] N. Ayres, Polym. Chem. **1**, 769 (2010).

[65] W.J. Brittain and S. Minko, J. Polym. Sci. Part A Polym. Chem. **45**, 3505 (2007).

[66] B. Zdyrko and I. Luzinov, Macromol. Rapid Commun. **32**, 859 (2011).

[67] T. Zhou, H. Qi, L. Han, D. Barbash, and C.Y. Li, Nat. Commun. **7**, 11119 (2016).

[68] B. Zhao and W.J. Brittain, Prog. Polym. Sci. **25**, 677 (2000).

[69] J.F. Douglas, Macromolecules **22**, 3707 (1989).

[70]A. Panagopoulou and S. Napolitano, *Impact of Substrate Roughness on the Segmental Mobility of Thin Polymer Films*, presented at APS March Meeting, New Orleans, LA, USA (2017)

[71] P. Scheidler, W. Kob, and K. Binder, J. Phys. Chem. B **108**, 6673 (2004).

[72] P.Z. Hanakata, J.F. Douglas, and F.W. Starr, J. Chem. Phys. **137**, 244901 (2012).

[73] P.Z. Hanakata, J.F. Douglas, and F.W. Starr, Nat. Commun. **5**, 4163 (2014).

[74] P.Z. Hanakata, B.A. Pazmiño Betancourt, J.F. Douglas, and F.W. Starr, J. Chem. Phys. **142**, 234907 (2015).

[75] T. Davris and A.V. Lyulin, J. Chem. Phys. **143**, 074906 (2015).

[76] E. Gnecco, *Fundamentals of Friction and Wear,* Springer (2007).

[77] G.A.C.M. Spierings, J. Mater. Sci. **28**, 6261 (1993).

[78] S. Wolf and R.N. Tanber, *Silicon Processig for theVLSI Era: Volume 1- Process Technology*, Lattice Press (1986).

[79] E.S. Gadelmawla, M.M. Koura, T.M. Maksoud, I.M. Elewa, and H.H. Soliman, J. Mater. Process. Technol. **123**, 133 (2002).

[80] J.M. Bennett and L. Mattsson, *Introduction to Surface Roughness and Scattering* (Optical Society of America, Washington, DC (1989), pp. 38–56.

[81] L. Ventola, F. Robotti, M. Dialameh, F. Calignano, D. Manfredi, E. Chiavazzo, and P. Asinari, Int. J. Heat Mass Transf. **75**, 58 (2014).

[82] D.A. Bernards and T.A. Desai, Soft Matter **6**, 1621 (2010).

[83] R.A. Segalman, B. McCulloch, S. Kirmayer, and J.J. Urban, Macromolecules **42**, 9205 (2009).

[84] R.R. Baglay and C.B. Roth, J. Chem. Phys. **143**, 111101 (2015).

[85] R.R. Baglay and C.B. Roth, J. Chem. Phys. **146**, 203307 (2017).

[86] J. Brandup, E.H. Immergut and E.A. Grulke, Polymer Handbook, 4th Edition, John Wiley & Sons, Inc. (1999)

[87] R.R. Baglay and C.B. Roth, ACS Macro Lett. **6**, 887 (2017).

[88] D.F. Siqueira, D.W. Schubert, V. Erb, M. Stamm, and J.P. Amato, Colloid. Polym. Sci. **273**, 1041 (1995).

[89] R.P. White and J.E.G. Lipson, Phys. Rev. E **84**, 041801 (2011).

[90] W.E. Wallace, N.C.B. Tan, W.L. Wu, and S. Satija, J. Chem. Phys. **108**, 3798 (1998).

[91] J.A. Forrest, K. Dalnoki-Veress, and J.R. Dutcher, Phys. Rev. E **58**, 6109 (1998).

Chapter 2

Experimental Methods

In this chapter, I am going to describe two approaches to characterize the glass transition temperature T_g in polymers: ellipsometry and fluorescence spectroscopy. In fact, there are many other possible experimental probes, but these two are the ones used in this dissertation. Ellipsometry is a very old technique, the fundamental principles of which are well known for studying surfaces and thin films. The fluorescence technique to measure T_g was originally developed by Ellison and Torkelson.[1] We can utilize it to characterize the local dynamics inside polymer films, understanding how strong the perturbations at different interfaces are and how they propagate across polymer systems.

2.1 Measurements with ellipsometry

In general, ellipsometry measures the change in the polarization state of elliptically polarized light reflected off or transmitted through films. According to this description, the instrument of ellipsometry (an ellipsometer) requires: a light source, an optical element to convert unpolarized light to linearly polarized light, an optical element to convert linearly polarized light to elliptically polarized light, a sample of interest, an optical element to determine the state of polarization of the resulting light beam and a detector for measuring light intensity.[2] Thanks to the appearance of many optical elements in the late 1800s, especially "quarter undulation plate" by Spottiswoode,[3] ellipsometry was in practice already in 1890s but without an official name. In 1901, Drude described an early optical instrument used for studying changes in polarization upon reflection with a polarizer, an analyzer and a compensator.[4] The name of

"ellipsometry" was introduced in 1945 by Alexandre Rothen when measuring the thickness of barium films on stainless steel slides.[5] For many years, the detector used to determine the null position of the analyzer was a human eye because the charge couple device (CCD) was not invented until 1969.[6]

In our lab, a J. A. Woollam M-2000 ellipsometer is used and its schematic is shown in Figure 2.1. Our light source is a quartz tungsten halogen (QTH) bulb with wavelengths from 350 nm to 1200 nm, which covers the entire visible light regime. The fixed polarizer (+ 45°) converts the unpolarized light from the QTH bulb to linearly polarized light, and then sends it into a continuously rotating compensator − a quarter-wave plate. The compensator introduces a phase difference in the light polarized perpendicular (*s*) and parallel (*p*) to the plane of incidence, resulting in elliptically polarized light (circular if the polarized light is parallel to the fast axis of the quarter-wave plate) traveling through the sample. It is worth noting that the sample is also an optical element and it reflects the polarized light into another fixed analyzer (- 45°) with a different polarization state. Eventually, a detector measures hundreds of wavelengths simultaneously when the light beam disperses across a CCD array. Data is fit to all wavelengths, but we choose to report the index of reflection *n* at 632.8 nm for historical reasons.

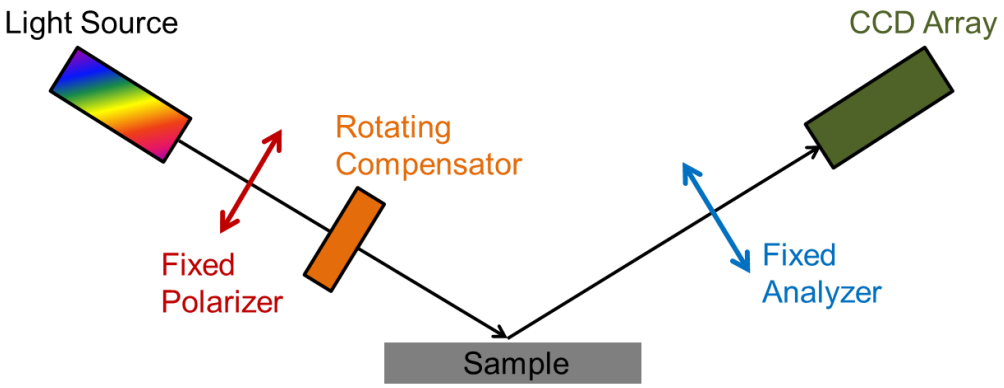

Fig. 2.1: A schematic of J. A. Woollam M-2000 ellipsometer. The light source is a QTH bulb, which emits light with wavelengths from 350 nm to 1200 nm. The fixed polarizer and analyzer are orthogonal. The rotating compensator introduces elliptically polarized light and by measuring the phase and magnitude difference after reflecting off the sample, we can extract sample information including thickness, refractive index, and adsorption coefficient. The reflected light is dispersed onto a CCD detector array to allow spectroscopic measurements.

The reason why we need to introduce an elliptically polarizing element in the light path is that elliptically polarized light has a phase and magnitude difference between the orthogonal and parallel polarization components. Both of these parameters can be found through measuring the complex reflectivity ratio ρ:[2]

$$\rho = \frac{r_p}{r_s} = \tan(\Psi)e^{i\Delta}$$

where r_p and r_s are the Fresnel reflection coefficients of *p* and *s* polarized light, tan(ψ) is the amplitude ratio of the *p* and *s* polarizations, *i* is the imaginary unit, and Δ is the phase shift between the polarizations. Ellipsometry is measuring ψ and Δ as a function of wavelength λ. However, in reality, samples are usually multilayers and this causes the problem of translating ψ(λ) and Δ(λ) into useful sample properties. As a result, we need to establish a sample model with distinctive layers depending on what specific system we are interested in.

In this dissertation, I have a three layer model including a silicon substrate, with a 1.25 nm thick native silicon oxide layer, and a PS film, which is modeled as a Cauchy layer:[7]

$$n(\lambda) = A + \frac{B}{\lambda^2} + \frac{C}{\lambda^4}$$

where *A*, *B* and *C* are the fitting parameters in this dispersion function for transparent materials. To accommodate the requirement of the modeled layer being transparent, we only fit the data from 400 nm to 1000 nm for PS samples. The way the computer finds the desired values for the film thickness *h* and refractive index $n(\lambda)$ of the film is to generate model $\psi(\lambda)$ and $\Delta(\lambda)$ values for the specific layer model of the sample. By minimizing the difference between the measured and the modeled $\psi(\lambda)$ and $\Delta(\lambda)$, the best fit results determine the film's properties.

To determine the glass transition temperature T_g of polymer films, we need to plot the film's properties as a function of temperature (as was illustrated in Fig. 1.3). Most commonly, T_g can be defined as the intersection of the extrapolated liquid and glassy fit lines of a film thickness *h* vs. temperature *T* plot. Also, we can use the derivative of $h(T)$ data to calculate the thermal expansion coefficient $\alpha = \frac{1}{h}\frac{dh}{dT}$ as a function of temperature, where T_g is determined from the midpoint in the step change. All of this works perfectly for relative thick films, however, for very thin films, the glass transition broadens and this leads to difficulties in selecting temperature regimes for the fits in the liquid and glassy regimes, and significant noise in the data for thin films becomes amplified during differentiation.[8] To obtain reliable measures of the thermal expansion coefficient in such a case, we usually average the data or the thermal expansion coefficient is calculated by the slope of a linear fit to the film thickness vs. temperature plot.

Ellipsometry, just like every other technique, has its own limitations. First of all, it has difficulty measuring extremely thin films. Figure 2.2 shows ψ vs. Δ trajectories for various refractive indices. Each curve is constructed for a different value of *n* with a given curve traced out counterclockwise for increasing film thickness starting with zero thickness at the film-free

point. The curves shown in Figure 2.2 are all for an angle of incidence $\varphi = 65^0$ at a wavelength of $\lambda = 632.8$ nm, where the periodicity *d* of these curves can be calculated by:[2]

$$d = \frac{\lambda}{2\sqrt{n^2 - (\sin\varphi)^2}}$$

Near the film-free point, the different index of refraction curves are very close to each other causing difficulty during ellipsometry fitting to distinguish them. Especially for films thinner than 10 nm, the fits become poorly defined.[9] Measurements of such thin films are routinely done, but part of the fitting parameters (*A*, *B* and *C*) of index of refraction are held fixed because of this issue.

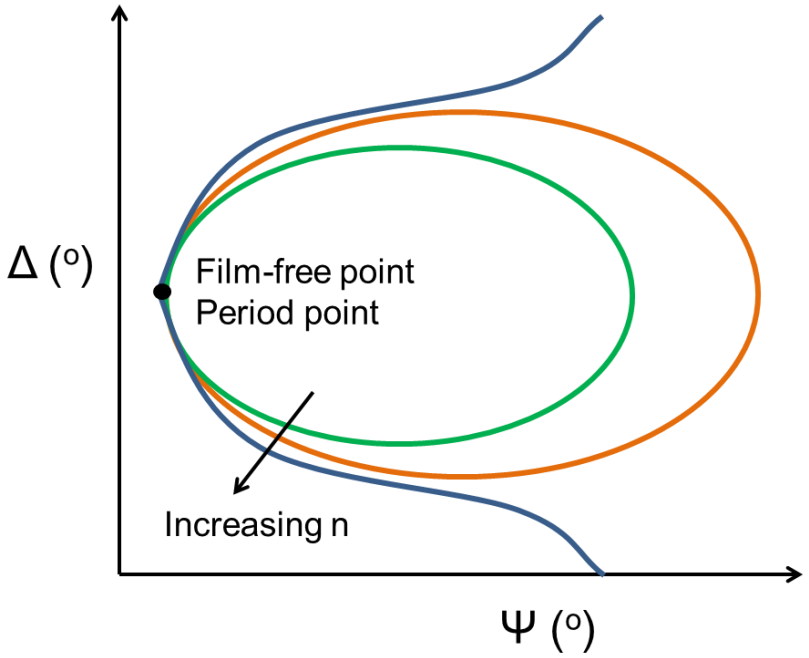

Fig. 2.2: ψ vs. Δ trajectories for different refractive indices *n* with an angle of incidence $\varphi = 65^0$ at a wavelength of $\lambda = 632.8$ nm. All the curves trace out counterclockwise with increasing film thickness starting with zero thickness at the film-free point. Near the film-free point or period point, fitting ellipsometry results becomes difficult because the different index of refraction

curves are very close to each other. To reliably determine the fits for films thinner than ~10 nm, we hold the fitting parameters C fixed or A, B and C fixed at their bulk values to reduce the number of fitting parameters.

2.2 Measurements with fluorescence

Fluorescence spectroscopy and time-resolved fluorescence are considered to be primary research tools in biochemistry and biophysics. However, it was not until the last 15 years that fluorescence spectroscopy was used in measuring the local glass transition temperature T_g of polymer thin films. In 2002, Ellison and Torkelson found that the pyrene dye could be used to measure the glass transition temperature of a polystyrene matrix.[10,11] Their initial papers were done by exciting doped pyrene in polymer thin films and collecting the emission signal at single wavelengths of 374 nm, 384 nm and 395 nm corresponding to the first, third and fourth peaks of the emission spectra of pyrene, as the temperature was dropped by 5°C in successive steps upon cooling. Later, they focused on integrating the full emission spectrum to reduce noise in the data. By doing this, they reproduced the T_g reduction behavior of a single layer PS film on silica substrate upon decreasing film thickness as first observed by Keddie, Jones and Cory using ellipsometry.[12] They attributed the sensitivity of pyrene to T_g as: fluorescence from the excited state of pyrene is in a constant competition with non-radiative decay processes. Pyrene in the excited electronic state also relaxes by non-radiative processes where excitation energy is not converted into photons like the radiative process, but is dissipated by thermal processes such as vibrational relaxations.[13] As the temperature decreases, a slightly denser environment reduces the non-radiative processes leading to increase in fluorescence signal. Superimposed on this is the

sensitivity to the local density of the nanoscale environment of pyrene, so the change in the temperature dependence of the fluorescence intensity at T_g is thus a result of the shift in the temperature dependence of sample density. Besides doping films with pyrene, Ellison et al. were able to chemically attach a 1-pyrenyl butyl methacrylate monomer to the backbone of PS during polymerization and measured the same T_g as previously reported.[1] This became the origin of using pyrene labeled polymer thin films to locally measure the glass transition temperature inside a polymer matrix.

In 2003, Ellison and Torkelson constructed bilayer PS films of a neat (polymer with no dye) 270 nm thick PS underlayer with a pyrene labeled PS layer on top.[1] Thermally annealing the sample to consolidate the two layers into one sample, they observed a T_g reduction starting at ~40 nm with decreasing labeled layer thickness. The substantially reduced T_g at the free surface indicates that the segmental mobility is significantly faster than in bulk PS, demonstrating that the origin of the T_g reduction in supported PS films comes from the free surface. Then they inserted a 14 nm thick pyrene labeled PS layer inside the PS matrix at different distances away from the free surface to measure the local glass transition temperature T_g, finding that bulk PS T_g is recovered at ~30-40 nm deep into the film.[1] They also inserted the labeled layer in the middle of the film and right next to the silica substrate demonstrating bulk PS T_g is recovered under both circumstances.[1] Applying the same idea of these experiments, over the last decade Torkelson's group has measured various physical properties of polymer systems under different confinements using fluorescence spectroscopy, investigating physical aging,[10,14,15] polymer blends,[16–18] and effects of plasticization.[19,20]

The experimental apparatus used to locally measure T_g in this dissertation is called a spectrofluorometer, as shown in Figure 2.3. A xenon arc lamp provides continues light output

from 250 nm to 700 nm, with a number of sharp lines occurring near 450 nm and above 800 nm. Then a dual grating monochromator picks out the desired excitation. A beam splitter separates the excitation light into two rays, one going to the reference cell and the other directly to the sample. The emitted fluorescence signal from the sample is passed to the detector through another monochromator, to a photomultiplier, and a photon counting device to record fluorescence intensity as a function of wavelength. At the first glance, it seems easy to perform fluorescence experiments. However, there are numerous factors that can compromise the data and invalidate the results. For example, photobleaching caused by adverse chemical reactions of the fluorophore in the presence of UV light, heat, and oxygen can permanently destroy some fraction of the dyes.[21] This occurs more readily at higher temperatures, which can limit the measurement range of the glass transition. To verify that my samples had remained stable during the course of the experiment and no photobleaching occurred, all samples were reheated to the starting temperature after each run to ensure that the same initial fluorescence intensity was recovered. Unlike the fluorescence apparatus from Torkelson's group, we add a neutral density (ND) filter to attenuate light before sending it to the sample.

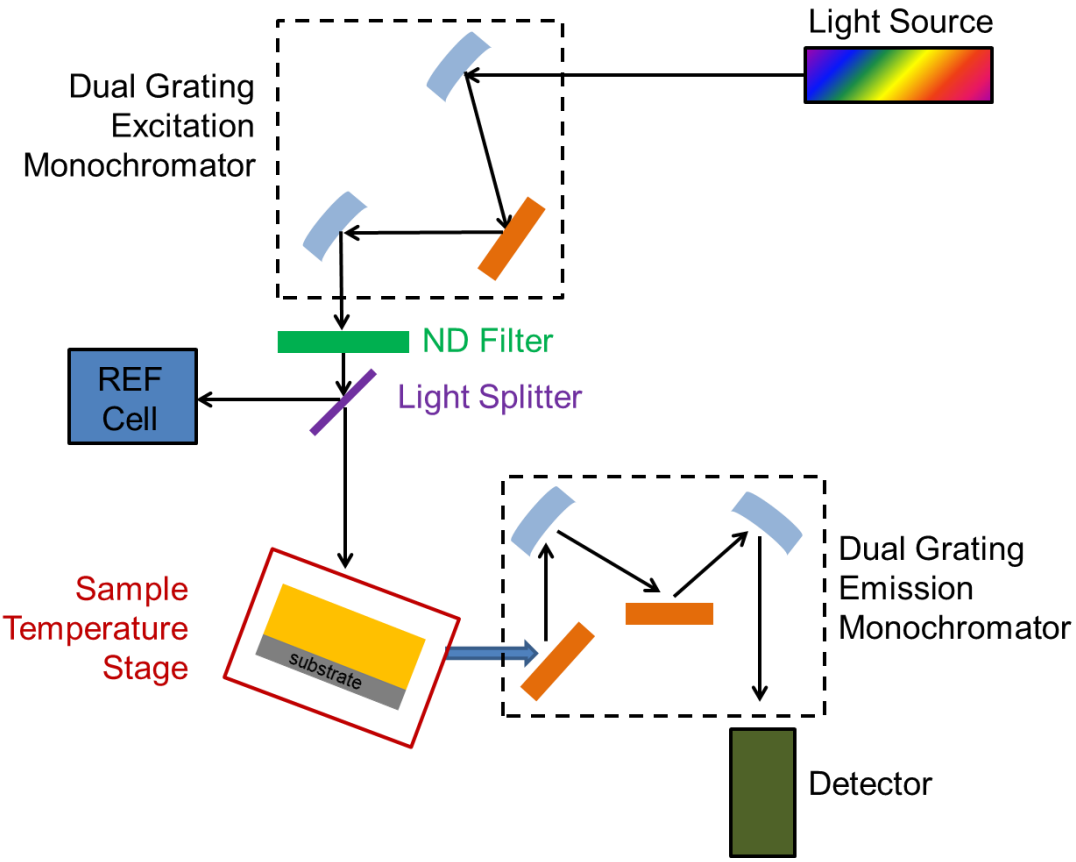

Fig. 2.3: A schematic of the spectrofluorometer from Photon Technology International (now HORIBA Instruments Inc.). The light source is a xenon arc lamp, which emits continuous light at wavelength from 250 nm to 700 nm. A dual grating monochromator picks out the specific excitation wavelength and sends it through a neutral density (ND) filter to attenuate light equally at all wavelengths. After passing the beam splitter, excitation light will shine directly onto the sample temperature stage. Finally, the emitted fluorescence signal goes through another dual grating monochromator before arriving at the detector.

There are mainly two different protocols that can be used to determine the glass transition temperature T_g using the intensity change of pyrene, as shown in Figure 2.4. Left

panel corresponds to the procedure I am using to determine T_g in Chapter 4 and Chapter 5, which is a method modified by our group by Rauscher et al.[22] Figure 2.4a plots fluorescence intensity at 379 nm as a function of temperature for a 196 nm thick PS single layer film labeled with 1-pyrenyl butyl methacrylate monomers. Initially, films were annealed at 130 °C for 20 minutes and then cooled at 1 °C/min while measuring the pyrene fluorescence intensity at 379 nm for 3 s every 30 s, using an excitation wavelength of 330 nm (band-pass 5-6 nm). Samples were reheated to the starting temperature to ensure no photobleaching occurred (< 5 %). The glass transition temperature T_g is defined as the intersection of extrapolated liquid and glassy lines. Compared to the original method developed by Torkelson's group,[1,11,23] our lab's modification of enabling temperature ramping has the advantages of increasing the number of data points collected, while still minimizing photobleaching by decreasing the time pyrene is exposed to excitation light. Right panel of Figure 2.4 shows the original method from Torkelson's group in measuring T_g using the same 1-pyrenyl butyl methacrylate monomers. Figure 2.4b plots the integrated fluorescence intensity as a function of temperature for 545 nm and 17 nm thick pyrene labeled PS films cooling from 135 °C.[1] First, the samples were heated to the starting temperature and allowed to equilibrate for at least 10 minutes. An excitation spectrum was recorded, and each subsequent spectrum was taken 5 minutes after the sample had cooled to the next temperature setting. By integrating the area underneath each spectrum and plotting the total fluorescence intensity as a function of temperature, they also identified T_g as the intersection of linear fits to the glassy and liquid regimes. Both of these two protocols measuring the T_g reduction with film thickness for single-layer PS films agree with the data previously reported.[12]

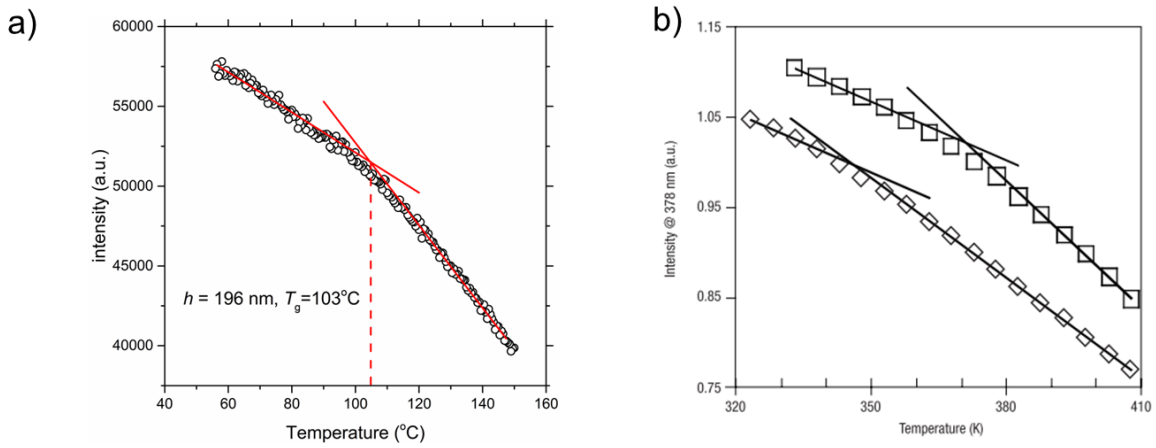

Fig. 2.4: Two main methods to determine T_g from fluorescence spectroscopy. a) Fluorescence intensity at 379 nm as a function of temperature upon cooling at 1 °C/min, while measuring the pyrene fluorescence intensity for 3 s every 30 s for a 196 nm thick PS labeled film. The glass transition temperature T_g is defined as the intersection of extrapolated liquid and glassy lines. b) Integrated fluorescence intensity as a function of temperature for a 545 nm bulk film (square) and a 17 nm thin film (diamond). Each excitation spectrum was taken after equilibrating at a given temperature for 5 minutes. T_g is also determined as the intersection of the linear fits of glassy and liquid regimes. (Figure reproduced from Ref. 1 with permission from Springer Nature: Nature Materials, The distribution of glass-transition temperatures in nanoscopically confined glass formers, C. J. Ellison and J. M. Torkelson, 2003)

2.3 Comparison of T_g values reported by ellipsometry and fluorescence

Both ellipsometry and fluorescence techniques agree well with each other quantitatively in measuring $T_g(h)$ of polymer films, however, there are still some minor differences. Figure 2.5

shows literature glass transition temperature T_g a function of film thickness measured by ellipsometry[8,12,24–26] and fluorescence spectroscopy.[1,10,11,19] T_g values reported by ellipsometry exhibit a spread for PS film thickness below ~40 nm, while fluorescence measurements show greater reduction in T_g with a much tighter data points compared to ellipsometry. A number of possible causes can be associated with the range in $T_g(h)$ reduction behavior in thin PS supported films. First, there may be investigator-to-investigator variation in the sample preparation and analysis methods used to define the average T_g of PS films. Also, different heating/cooling stages from various groups will naturally cause difference in reported T_g values. These are likely the main explanations for the spread in ellipsometry data. All the fluorescence T_g values only come from Torkelson's group. Furthermore, as mentioned in Chapter 1 the glass transition becomes broader and weaker with decreasing film thickness due to the increasing influence of the free surface.[8] Also the collected raw data inherently will be noisier because less material is being measured. As a result, thinner films inherently make it more difficult to accurately define a single T_g within a PS film, thereby leading to some variation of T_g values. Finally, there is the issue as to whether various experimental methods are reporting different average T_g values across a film because they might be more sensitive to one region to the film than another. Fluorescence measurements rely on the quantum yield of pyrene fluorophores inside the polymer matrix. However, the quantum yield of pyrene at the free surface is expected to be smaller than the quantum yield in the bulk since mobility is greater at the free boundary.[27] As film thickness decreases, the free surface dominates and the "average" T_g response as measured by the temperature dependence of fluorescence intensity or quantum yield may be slightly overweighed to the free surface layer with increasing levels of nanoconfinement. This could potentially explain why T_g values reported by fluorescence spectroscopy are smaller compared to

ellipsometry measurements. However, ellipsometry may also overweight the response from the free surface region as the thermal expansion of the liquid state is higher than that of the glass.

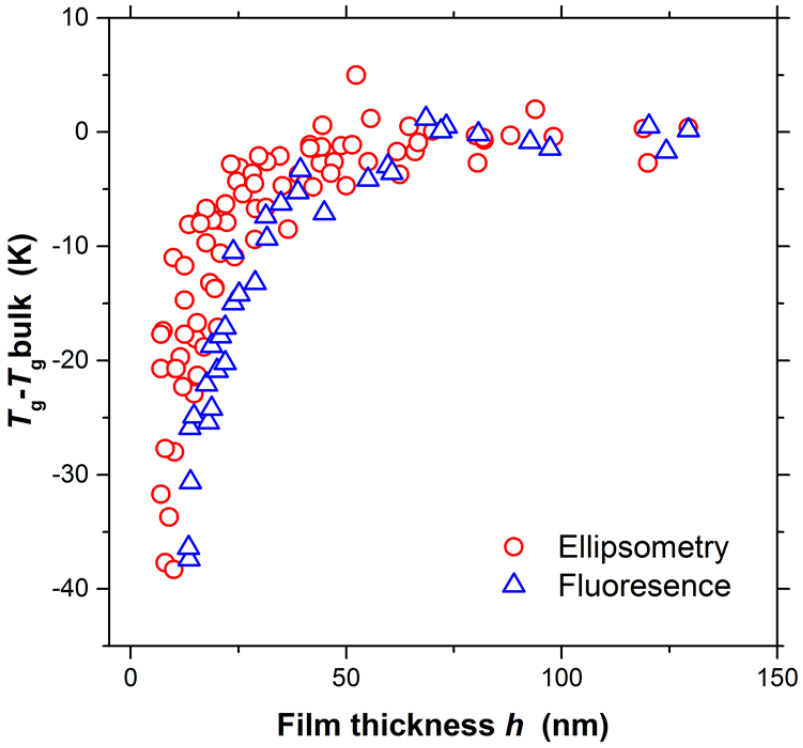

Fig. 2.5: T_g reduction as a function of film thickness for supported PS thin films reported by ellipsometry and fluorescence spectroscopy. Red circles correspond to literature data collected by ellipsometry by different research groups.[8,12,24–26] Blue triangles are the T_g values measured by fluorescence from Torkelson's group.[1,10,11,19]

Figure 2.6a plots the thermal expansion coefficient α as a function of temperature to quantify the breadth of the glass transition of a supported PS film.[27] This step in the $\alpha(T)$ data is fit using three straight lines. The two intersections of the fitted lines represent the onset and endpoint of the glass transition region and they are denoted as T_+ and T_-. Within this transition zone, Kim et al.[27] also defined the midpoint and the three-quarter point as T_{mid} and $T_{3/4}$. Figure

2.6b shows the thickness dependence of T_+ - T_+(bulk), T_- - T_-(bulk), T_{mid} - T_{mid}(bulk), and $T_{3/4}$ - $T_{3/4}$(bulk) of PS films as determined from ellipsometry measurements of the thermal expansivity and compares them to the best-fit curves obtained by Keddie et al. from ellipsometry[12] and Ellison et al. from fluorescence data.[10,28] It turns out that the fluorescence data from Ellison et al.[10,28] are most closely consistent with $T_{3/4}$ - $T_{3/4}$(bulk) data while the T_g - T_g(bulk) data from Keddie et al.[12] through ellipsometry are in closer agreement with T_{mid} - T_{mid}(bulk) data. This indicates that the difference between the ellipsometry and fluorescence data points from Figure 2.5 is more likely from two experimental methods reporting average T_g values at different locations within the broadening glass transition with decreasing thickness.

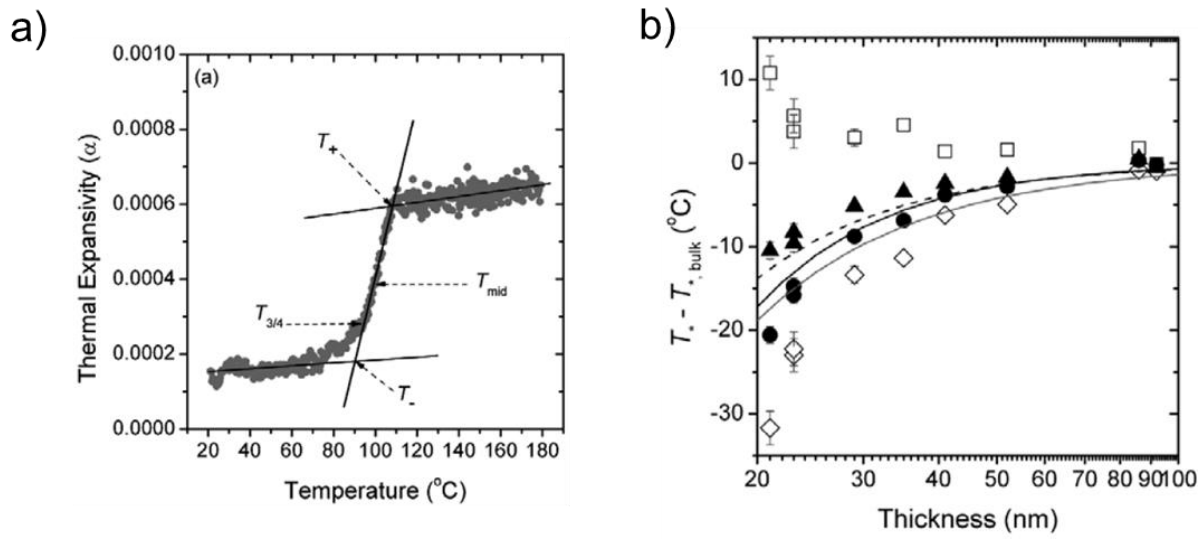

Fig. 2.6: a) Thermal expansion coefficient α as a function of temperature. By fitting the step like function with three straight lines, Kim et al. defined the intersections as the onset point (T_+) and endpoint (T_-) of the glass transition.[27] Also, T_{mid} and $T_{3/4}$ are denoted as the midpoint and three-quarter point on the curve. b) T_+ - T_+(bulk), T_- - T_-(bulk), T_{mid} - T_{mid}(bulk), $T_{3/4}$ - $T_{3/4}$(bulk) of PS films determined from ellipsometry measurements of thermal expansivity as a function of film thickness. Dashed curve is the best fit curve from Keddie et al.[12] by ellipsometry and it is in a

close agreement with the T_{mid} - T_{mid}(bulk) data. Both solid curves are the best fit of Ellison et al.'s [10,28] fluorescence data and they are more closely consistent with $T_{3/4}$ - $T_{3/4}$(bulk) data. (Figure reproduced from Ref. 27 with permission from Springer Nature: the European Physical Journal E: Soft Matter, Confinement effects on glass transition temperature, transition breadth, and expansivity: Comparison of ellipsometry and fluorescence measurements on polystyrene films, S. Kim, S. A. Hewlett, C. B. Roth, and J. M. Torkelson, 2009)

2.4 Reference

[1] C.J. Ellison and J.M. Torkelson, Nat. Mater. **2**, 695 (2003).

[2] H.G. Tompkins, *A User's Guide to Ellipsometry*, Dover Punlications, New York (1993)

[3] W. Spottiswoode, *Polarisation of Light*, Macmillan & Co., London (1891).

[4] P. Drude, *The Theory of Optics*, Longmans, Green & Co., New York (1901).

[5] A. Rothen, Rev. Sci. Instrum. **16**, 26 (1945).

[6] W. Boyle and G. Smith, patent number: US3792322A, United States Patent (1973).

[7] F.A Jenkins and H.E. White, *Fundamentals of Optics*, McGraw Hill, Boston (1957) .

[8] S. Kawana and R.A.L. Jones, Phys. Rev. E **63**, 021501 (2001).

[9] H. Fujiwara, *Spectroscopic Ellipsometry*, John Wiley and Sons, Ltd., Chichester, England (2007)

[10] C.J. Ellison, S.D. Kim, D.B. Hall, and J.M. Torkelson, Eur. Phys. J. E **8**, 155 (2002).

[11] C.J. Ellison and J.M. Torkelson, J. Polym. Sci. Part B Polym. Phys. **40**, 2745 (2002).

[12] J.L. Keddie, R.A.L. Jones, and R.A. Cory, Europhys. Lett. **27**, 59 (1994).

[13] J.R. Lakowicz, *Principles of Fluorensence Spectroscopy*, Springer Publications, New York (2016).

[14] R.D. Priestley, P. Rittigstein, L.J. Broadbelt, K. Fukao, and J.M. Torkelson, J. Phys. Condens. Matter **19**, 205120 (2007).

[15] R.D. Priestley, L.J. Broadbelt, and J.M. Torkelson, Macromolecules **38**, 654 (2005).

[16] K. Jin and J.M. Torkelson, Polym. **118**, 85 (2017).

[17] C.M. Evans and J.M. Torkelson, Polym. **53**, 6118 (2012).

[18] C.M. Evans, R.W. Sandoval, and J.M. Torkelson, Macromolecules **44**, 6645 (2011).

[19] C.J. Ellison, R.L. Ruszkowski, N.J. Fredin, and J.M. Torkelson, Phys. Rev. Lett. **92**, 119901 (2004).

[20] M.K. Mundra, C.J. Ellison, P. Rittigstein, and J.M. Torkelson, Eur. Phys. J. Spec. Top. **141**, 143 (2007).

[21] R.I. Ghauharali and G.J. Brakenhoff, J. Microsc. **198**, 88 (2000).

[22] P.M. Rauscher, J.E. Pye, R.R. Baglay, and C.B. Roth, Macromolecules **46**, 9806 (2013).

[23] C.B. Roth and J.M. Torkelson, Macromolecules **40**, 3328 (2007).

[24] J.L. Keddie and R.A.L. Jones, Israel J. Chem. **35**, 21 (1995).

[25] J.A. Forrest, K. Dalnoki-Veress, and J.R. Dutcher, Phys. Rev. E **56**, 5705 (1997).

[26] O.K.C. Tsui and H.F. Zhang, Macromolecules **34**, 9139 (2001).

[27] S. Kim, S.A. Hewlett, C.B. Roth, and J.M. Torkelson, Eur. Phys. J. E **30**, 83 (2009).

[28] C.J. Ellison, M.K. Mundra, and J.M. Torkelson, Macromolecules **38**, 1767 (2005).

Chapter 3

Changes in the Temperature-Dependent Specific Volume of Supported Polystyrene Films with Film Thickness

A version of this chapter was published as Xinru Huang and Connie B. Roth, *Journal of Chemical Physics 144*, 234903, 2016.

3.1 Synopsis

Recent studies have measured or predicted thickness-dependent shifts in density or specific volume of polymer films as a possible means of understanding changes in the glass transition temperature $T_g(h)$ with decreasing film thickness, with some experimental works claiming unrealistically large (25-30 %) increases in film density with decreasing thickness. Here we use ellipsometry to measure the temperature-dependent index of refraction of polystyrene (PS) films supported on silicon and investigate the validity of the commonly used Lorentz-Lorenz equation for inferring changes in density or specific volume from very thin films. We find that the density (specific volume) of these supported PS films do not vary by more than ± 0.4 % of the bulk value for film thicknesses above 30 nm, and that the small variations we do observe are uncorrelated with any free volume explanation for the $T_g(h)$ decrease exhibited by these films. We conclude that the derivation of the Lorentz-Lorenz equation becomes invalid for very thin films as the film thickness approaches ~20 nm, and that reports of large density changes greater than ± 1 % of bulk for films thinner than this likely suffer from breakdown in the

validity of this equation or in the difficulties associated with accurately measuring the index of refraction of such thin films. For larger film thicknesses, we do observed small variations in the effective specific volume of the films of 0.4 ± 0.2 %, outside of our experimental error. These shifts occur simultaneously in both the liquid and glassy regimes uniformly together starting at film thicknesses less than ~120 nm, but appear to be uncorrelated with $T_g(h)$ decreases; possible causes for these variations are discussed.

3.2 Introduction

The experimentally observed large changes in the glass transition temperature T_g of ultra-thin supported and free-standing polymer films with decreasing thickness h have puzzled the field for more than two decades.[1-15] Studies of local dynamics near the free surface[16-18] and local T_g within the film[19-21] have led to the understanding that decreases or increases in the average T_g of the film[2,6,22] are typically the result of competing dynamical perturbations from the interfaces. The free surface with its reduced number of intermolecular contacts tends to increase the local dynamics and reduced T_g, while the polymer-substrate interface can lead to a decrease in mobility and increase in T_g, especially if specific interactions such as hydrogen bonding are present.

An open question at present is what other material property changes occur in these thin films, and in particular which correspond to the large shifts in $T_g(h)$. To date, studies have looked at physical aging,[23-27] viscosity,[17,28,29] modulus,[30-33] and permeability.[34] Here, we investigate changes in the temperature-dependent specific volume (inverse density) with decreasing film thickness of polystyrene (PS) films supported on silicon using ellipsometry. It

has been extensively reported that such supported PS films show a large ~30 K decrease in average film T_g as the thickness is decreased below ~60 nm down towards ~10 nm.[1,5,19,35] Our work was motivated by recent theoretical efforts from White and Lipson[36] that predict a small (~0.5 %) increase in the liquid-line specific volume (decrease in density) with decreasing film thickness that may account for the observed $T_g(h)$ shifts. All previous experimental efforts measuring the density of thin films have only investigated the glassy regime with experimental errors of ± 1 %.[37-41] Although the focus of the present study is to comment on these measurements of the average film density and theoretical efforts to explain $T_g(h)$ shifts based on the predicted temperature dependence of the average film specific volume, we note that computer simulations have previously compared depth-dependent density profiles near free surface and substrate interfaces with local mobility, and generally find these quantities to be uncorrelated.[42-47] Less frequently commented on in these studies is whether the density of thin films is the same as bulk. One study by Baschnagel and coworkers[43] has shown that in computer simulations, even though the local density near interfaces varies considerably, the local density at the interior of the film is the same as bulk, provided that the film is sufficiently thick that bulk density can be recovered in the interior.[42]

Changes in mass density (or specific volume) in thin polymer films have been little studied. There was some early interest in the topic during the 1990s when $T_g(h)$ shifts were first observed. In 1998, Wallace et al.[37] used neutron reflectivity to investigate if the density of ultrathin PS films supported on silicon was reduced, as a possible explanation for the observed T_g reductions. Such an observation would correlate with the ideas behind the original free volume models of T_g,[48-51] although they have since been disproven.[52,53] Wallace et al. found no evidence

of density changes to within ± 1 % for PS films supported on silicon measured at room temperature down to film thicknesses of 6.5 nm.[37] This conclusion was corroborated by Forrest et al.[38] using Brillouin Light Scattering to measure the acoustic phonon velocities, related to the film's mass density and mechanical stiffness, finding them to be equivalent to the bulk glassy values within ± 1 % at room temperature for free-standing PS films down to film thicknesses of 29 nm. Given that these early studies saw no change in mass density to within ± 1 % with decreasing film thickness, and the experimental challenge with measuring such small changes within ultrathin films with small sample sizes, this issue has remained relatively dormant.

However, more recently a couple of studies have reported increases in density with decreasing film thickness below ~40 nm by as much as 30 % for ~5 nm thick films as measured by x-ray reflectivity,[39,40] or corresponding increases in index of refraction from ellipsometry.[39-41] Such large increases in density seem unrealistic given that so-called stable glasses that are slowly formed by physical vapor deposition to optimize molecular packing, obtaining material densities equivalent to glasses that have been aged for thousands or millions of years to reach equilibrium well below the typical glass transition temperature measured, still only show an increase in density of ~1 % relative to ordinarily cooled glasses.[54-56] Even samples of amber glass that have been aged for millions of years, the density increases are only ~2 %.[57,58] In particular, Vignaud et al.[39] measured supported PS films (M_w = 136 kg/mol) reporting an increase in mass density of the film of 26 % below 25 nm relative to bulk values that varied within ± 1 % between 30-140 nm thick films as measured by the electron density profile from x-ray reflectivity measurements. They also used spectroscopic ellipsometry (λ = 250-1700 nm) to measure the index of refraction of the PS films at 20 ^{o}C using three different angles of incidence (65^{o}, 70^{o}, and 75^{o}) and

determined the density of the PS films using the Lorentz-Lorenz equation, where values for the polarizability α were estimated by benchmarking the index values for bulk films to the known bulk density for PS. These ellipsometry data also reported an increase in density of 30 % below 40 nm relative to bulk values that varied within ± 1 % between 40-150 nm thick films. In support of these results, they cited work by Ata et al.[40] that reported similar measurements for supported PS films (M_w = 980 kg/mol) measured using x-ray reflectivity and ellipsometry, also analyzed using the Lorentz-Lorenz equation, as well as index of refraction values reported by Li et al.[41] for supported PS films (152 kg/mol and 590 kg/mol) showing an increase in index with decreasing thickness. To within experimental error, these studies report the same index of refraction despite the varying molecular weights used, while simultaneously suggesting that the film's thickness relative to the polymer's radius of gyration R_g and chain distortion (and hence molecular weight) may be important factors. We also note that all these studies report only on the density or index of refraction at room temperature in the non-equilibrium glassy state.

Recently, White and Lipson[36] have used a thermodynamic lattice model to predict the temperature-dependent specific volume for the liquid state of thin free-standing PS films. This equation-of-state model uses bulk pressure-volume-temperature (PVT) data for PS (literature data for a molecular weight of 110 kg/mol was used[36]) to determine the relevant model parameters: nearest neighbor non-bonded segment interaction energy, lattice site volume, and number of segments per chain. In addition, data for the temperature dependence of surface tension is used to define an additional surface parameter *f* representing the fraction of missing contacts or interactions at the free surface. With these model parameters so defined, predictions for temperature-dependent material properties in thin films can be made with no further

adjustable parameters. The core foundation of this thermodynamic model has been shown to work well describing the miscibility and phase behavior of polymer blends,[59-62] and bulk glass transition values across different polymers.[63] The 2011 work on free-standing PS films uses this thermodynamic model to predict the temperature-dependent specific volume for the equilibrium liquid-line above T_g.[36] The model's equation-of-state predicts an increase in the specific volume liquid-line with decreasing thickness of about 0.3 % for 30 nm and 0.8 % for 10 nm thick films of free-standing PS relative to the bulk value. In the model, this film expansion with decreasing thickness arises from a reduction in the attractive energy between polymer segments due to missing contacts at the free surface. The study then goes on to estimate an anticipated $T_g(h)$ for the films by determining the intersection point of this predicted specific volume liquid-line from the model with a glassy-line. As the equilibrium thermodynamic model is unable to make predictions about the non-equilibrium thermodynamic glassy state, the authors simply assumed that the glassy line remains fixed at the bulk value obtained from PVT data. Given the lack of any other information at the time, this was as reasonable an assumption as any. Thus, based on the small predicted increase in specific volume of the liquid-line, the intersection temperature with the assumed bulk glassy-line was identified as $T_g(h)$ and found to decrease by ~40 K with decreasing film thickness in remarkable agreement[36] with experimental data for low molecular weight free-standing PS films from the literature[64] given that the theory had no adjustable parameters. More recently, they have also expanded this model to incorporate substrate interactions and treat supported polymer films.[65] To clarify, the thermodynamic model, which has a strong theoretical foundation and proven record in blends and bulk systems, predicts a driving force for film expansion (increase in specific volume) with decreasing film thickness. However, the subsequent prediction of a corresponding decrease in $T_g(h)$ is less theoretically

sound because it relies on the untested assumption that the glassy-line specific volume remains the same as bulk.

Here, we test the predictions of this thermodynamic model by using ellipsometry to measure the temperature dependence of the index of refraction and calculate the Lorentz-Lorenz parameter as a proxy for film density in order to compare the relative specific volume between thin and thick films. Because of the experimental challenges with measuring ultrathin free-standing films, we focus here on PS films supported on silicon with a 1.25-nm native silicon oxide layer. It has been previously demonstrated that the PS/silicon-oxide interface is neutral when it comes to T_g perturbations; the local T_g of a thin PS layer next to a silicon-oxide interface reports the bulk value.[19] In addition, the $T_g(h)$ behavior of low molecular weight free-standing PS films has the same $T_g(h)$ functional form as that for PS films supported on silicon, but with the magnitude of the T_g reduction at a given film thickness h being twice as large.[64] This is consistent with the free surface being the source of the enhanced mobility leading to the $T_g(h)$ reduction with free-standing PS films (two free surfaces) having a $T_g(h)$ value in agreement with supported PS films (one free surface) of half the thickness, $T_g(h/2)$.[66] Thus, supported PS films should exhibit the same phenomenon as free-standing PS films, if only weaker by a factor of two.

From our investigation, we find that both the liquid and glassy lines of specific volume show equivalent shifts with decreasing thickness in supported PS films, negating the assumption made by White and Lipson[36] to explain the $T_g(h)$ decrease that the glassy-line specific volume remains unshifted and the same as bulk. Yet, for film thicknesses of ~120 to 65 nm, we do observe an increase in specific volume (decrease in density) of 0.4 ± 0.2 % consistent in magnitude with the film expansion, shifted specific volume liquid-line prediction of White and

Lipson based on their detailed thermodynamic model.[36] But then, for film thicknesses below 65 nm, where the $T_g(h)$ decrease is observed, we find that the specific volume decreases returning back to the bulk value at ~40 nm suggesting that if the film expansion prediction from the thermodynamic model is correct, some additional factor acts to counteract the effect for very thin films where the $T_g(h)$ decrease is observed. Below ~30 nm, we observe a large unrealistic increase in apparent film density (~5 % increase for a 10 nm thick film), consistent with some of the more recent reports.[39-41] We believe such unrealistic values in apparent film density likely arise from difficulties in measuring the index of refraction of very thin films and breakdown in validity of the Lorentz-Lorenz formula (a continuum approach assuming an isotropic medium[67]) as the film thickness is no longer 'large' relative to the monomer size. Also of note, in agreement with previous reports,[68-70] we find that the slope of the liquid-line (thermal expansion coefficient) remains constant upon confinement, and the $T_g(h)$ decrease is accompanied by a broadening of the transition and a small increase in the glassy-line thermal expansion, consistent with a larger fraction of the sample remaining liquid to lower temperatures.

3.3 Experimental Methods

Films were made by dissolving monodisperse, weight average molecular weight M_w = 650 kg/mol, M_w/M_n = 1.06 (Pressure Chemical) polystyrene in toluene and spin coating onto 2 cm × 2 cm silicon wafers with 1.25 nm native oxide layers (Wafernet). All samples were annealed under vacuum at 120 ^oC for at least 16 h to evaporate residual solvent and allow the chains to relax, and then cooled to room temperature. Ellipsometry measurements of the temperature-dependent film thickness $h(T)$ and index of refraction $n(T)$ were initiated by

increasing the temperature of the sample from room temperature to 130 ^{o}C over a span of 10 min, and equilibrating the film at 130 ^{o}C for 30 min. A second alignment of the sample was then performed at 130 ^{o}C immediately before beginning the 1 ^{o}C/min cooling run.

Ellipsometry measurements were performed on a J.A. Woollam M-2000D rotating compensator instrument that measures the change in polarization state (all four Stokes parameters) of the light reflected off the sample. The raw data are expressed as $\Psi(\lambda)$ and $\Delta(\lambda)$ data representing the amplitude ratio and phase shift of the *p*- to *s*- polarized light. Although this was varied as described in detail below, typically measurements were taken at an angle of incidence of 65^{o} every 10 s on cooling at 1 ^{o}C/min. The PS film thickness h and index of refraction $n(\lambda)$ were determined by fitting the transparent PS film with a Cauchy layer over the wavelength range of 400-1000 nm atop a semi-infinite temperature-dependent silicon substrate containing a 1.25-nm native oxide layer. Unless otherwise noted, the index of refraction values reported are those at a wavelength of $\lambda = 632.8$ nm (corresponding to a HeNe laser) obtained by evaluating the best fit Cauchy parameters at $n(\lambda = 632.8 \text{ nm})$.

3.4 Results and Discussion

3.4.1 Temperature-dependence of film thickness and index of refraction

Measurements of the temperature-dependent film thickness $h(T)$ and index of refraction $n(T)$ were collected by ellipsometry on cooling at a rate of 1 ^{o}C/min for PS films of different thicknesses supported on silicon. Figure 3.1 graphs the PS film thickness as a function of temperature for four different thicknesses: 977, 330, 65, and 31 nm. In order to compare the shape of the $h(T)$ data for the different film thicknesses, the datasets have been normalized by the

film thickness at 110 °C, evaluated based on a linear fit to the liquid-line data from 105-125 °C. From the data, we can clearly see that the liquid-line thermal expansion is the same for all film thicknesses, as has been reported previously by other studies,[68-71] along with an overall broadening of the transition. As the glass transition temperature T_g decreases with decreasing film thickness, it is the glassy line that deviates. The 65-nm data show a slightly reduced T_g value, but the glassy-line slope is essentially parallel to the thick (bulk) films. In contrast, the 31-nm data show a larger slope in the glassy line, at least down to 30 °C, consistent with a significant fraction of this film remaining liquid-like to lower temperatures.

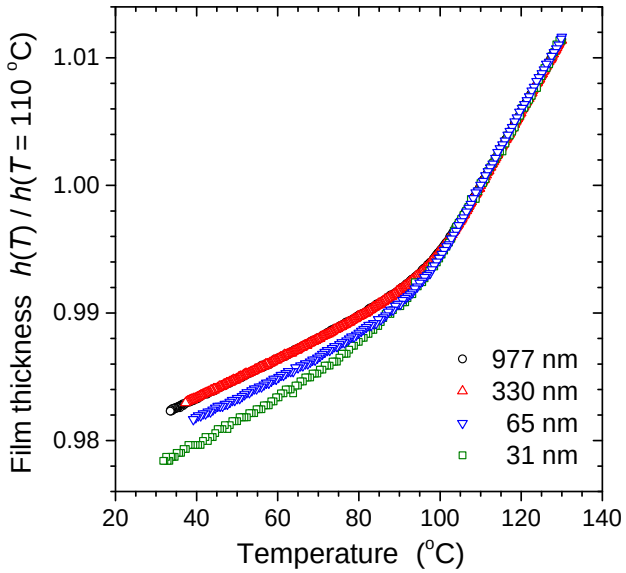

Fig. 3.1: Temperature-dependent film thickness $h(T)$ measured by ellipsometry on cooling at 1 °C/min for supported PS (M_w = 650 kg/mol, M_w/M_n = 1.06) films on silicon. Data for four different film thicknesses (977, 330, 65, and 31 nm) have been superimposed at 110 °C to demonstrate that the slope of the equilibrium liquid-line is the same for all thicknesses, while it is the glassy thermal expansion that deviates for thinner films as the glass transition decreases and broadens.

We have determined $T_g(h)$ values from the $h(T)$ data in the usual manner by determining the intersection of linear fits to the liquid and glassy regions of the data.[1,5,70] The corresponding fit ranges used, 40-80 ^oC (glassy) and 105-125 ^oC (liquid), come from consideration of fitting the data away from the transition. For consistency, the film thickness values reported for the corresponding $T_g(h)$ values were all evaluated at 30 ^oC from a linear fit to the glassy-line data, to closely match the room temperature thickness values typically reported in such studies. Figure 3.2 plots our measured $T_g(h)$ values from the present work, along with data from previous literature studies[1,69,72-74] (data collated in the review by Roth and Dutcher[5]), showing our data are in excellent agreement with existing studies. The *y*-axis has been graphed relative to T_g^{bulk}, the T_g value reported for thick films in each study, in order to accommodate small differences in T_g^{bulk} values between different studies. Based on an average of films thicker than 200 nm, the T_g^{bulk} for our samples is 95.8 ^oC, typical for ellipsometry measurements. The data clearly show that below ~60 nm in film thickness the average glass transition temperature $T_g(h)$ of the film begins to decrease quite substantially. The reported decrease in $T_g(h)$ for 10-15 nm thick films vary considerably from -10 K to greater than -35 K, which likely reflects the broadening of the transition in thin films as shown in Fig. 3.1.

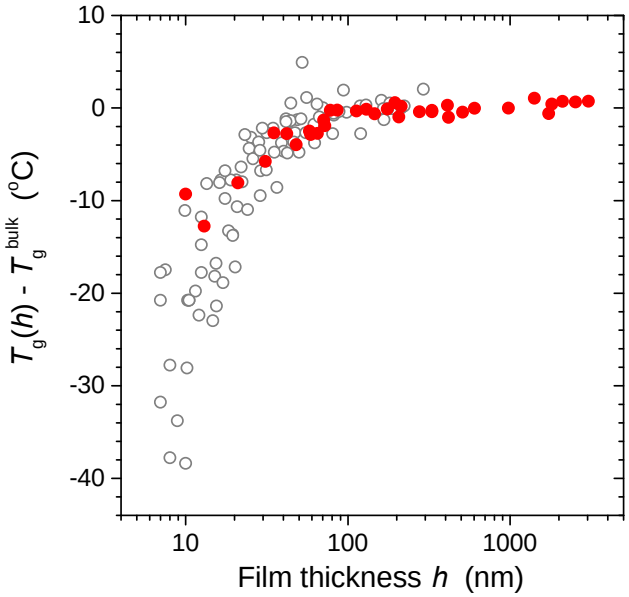

Fig. 3.2: Film thickness h dependence of the average glass transition temperature $T_g(h)$ for PS films supported on silicon as measured by ellipsometry (solid symbols). The $T_g(h)$ data are plotted relative to their bulk value T_g^{bulk} measured for thick films to facilitate comparison between different studies. Literature data (open symbols) measured by ellipsometry are from Refs. [1,69,72-74].

Figure 3.3 graphs the temperature-dependence of the index of refraction $n(T)$ for the PS layer (at $\lambda = 632.8$ nm), for the same four films as the thicknesses shown in Fig. 3.1. Surprisingly, we find that the absolute values of the index of refraction at any given temperature in both the liquid and glassy regimes are not constant, but vary with film thickness in a non-monotonic manner. Multiple measurements on different samples find this non-monotonic trend to be very reproducible with comparable film thicknesses giving similar absolute values in refractive index, as shown in Fig. 3.3. The $n(T)$ slopes of the liquid-line are all similar as would be expected for an equilibrium liquid; in contrast, the slopes in the glassy region vary slightly

with film thickness indicating differences in how the films fall out of equilibrium on cooling.

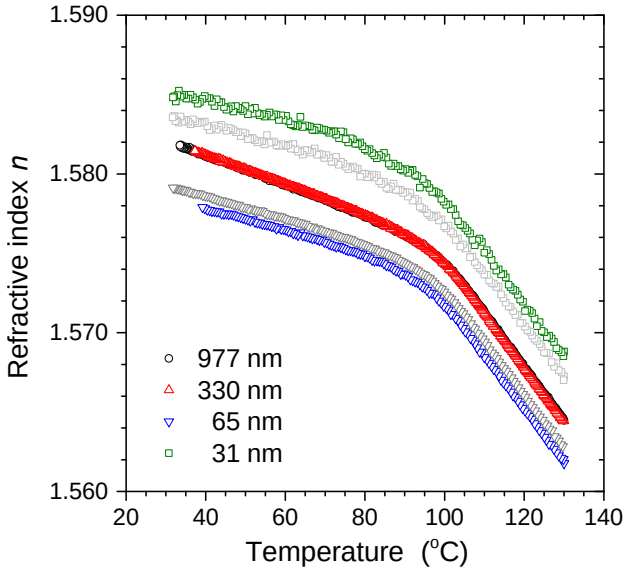

Fig. 3.3: Temperature dependence of the index of refraction $n(T)$ measured by ellipsometry on cooling at 1 °C/min for supported PS (M_w = 650 kg/mol, M_w/M_n = 1.06) films on silicon. Data for four different film thicknesses (977, 330, 65, and 31 nm, the same films as shown in Fig. 3.1) demonstrate that the absolute refractive index varies non-monotonically with film thickness. Data for comparable film thicknesses (71 nm gray triangles and 35 nm gray squares) give similar values of refractive index demonstrating reproducibility of the non-monotonic behavior.

To characterize the small vertical shifts in the $n(T)$ data with film thickness, we have evaluated the index of refraction at 110 °C and 50 °C, in the liquid and glassy regimes, respectively, by taking a linear fit of the $n(T)$ data between 105-125 °C and 40-80 °C, and evaluating the best fit parameters at $n(T = 110\ ^oC)$ and $n(T = 50\ ^oC)$. These refractive index values are plotted in Figure 3.4 as a function of film thickness, in the liquid regime at $n(T = 110\ ^oC)$ and the glassy regime at $n(T = 50\ ^oC)$. We find the same small vertical shifts in the absolute

value of the refractive index for both the liquid and glassy regimes. At film thicknesses above 200 nm, the film's index of refraction remains constant at 1.5712 ± 0.0007 in the liquid regime and 1.5801 ± 0.0008 in the glassy regime. Below 200 nm, the refractive index decreases until a minimum is reached at 65 nm before increasing again. In both the liquid and glassy regimes, the minimum in refractive index at 65 nm, 1.5685 in the liquid state and 1.5772 in the glassy state, is more than three times bigger than the variability observed for bulk films (h > 200 nm). Below this minimum in refractive index at 65 nm, the data increase again returning to the bulk index value for thicknesses of ~30 nm. Below 20 nm, the measured index of refraction is observed to apparently increase substantially, consistent with recent reports in the literature.[39-41]

3.4.2 Ellipsometry data fitting

Before proceeding any further, we should consider the accuracy of the index of refraction values obtained from fitting of the ellipsometry Ψ(λ) and Δ(λ) data, defined as:

$$\rho \equiv \frac{r_p}{r_s} = \tan\Psi \, e^{i\Delta} \quad , \qquad (1)$$

where r_p and r_s are the reflection coefficients for the *p*- and *s*- polarizations.[75] Formally, there is no generally accepted method to quantify the measurement accuracy of ellipsometry, primarily because the sensitivity of modern ellipsometers has exceeded the accuracy with which known reference samples can be created.[76] Thus, the most reasonable measure of the error for our results, especially given we are primarily interested in relative differences between bulk and thin films, is the sample-to-sample variability in the index of refraction data for nominally identical bulk films, which we have found to be less than ± 0.001 for films thicker than 200 nm. Even for

the thinner films ~65 nm where we observe the decrease in refractive index, the sample-to-sample variability remains less than ± 0.001. For comparison, the variability in the refractive index data for repeated measurements of a single sample is much less (± 0.0002), even for the thinnest films, indicating stability of the films over time. (Note, no evidence of dewetting was observed for these high molecular weight films, even after multiple temperature ramps of the thinnest films, as determined by atomic force microscopy.) However, this all assumes we are accurately fitting the Ψ(λ) and Δ(λ) data with a valid layer model, and that the fits remain robust as the film thickness is decreased.

The common method of fitting ellipsometry data for transparent polymer films is to model the wavelength dependence of the index of refraction of the polymer layer using a Cauchy model:

$$n(\lambda) = A + \frac{B}{\lambda^2} + \frac{C}{\lambda^4} + \cdots \quad , \qquad (2)$$

where the absorption term of the index is taken to be zero. Eq. (2) represents an expansion of the Sellmeier model,

$$n^2(\lambda) = 1 + \sum_i \frac{A_i \lambda^2}{\lambda^2 - \lambda_i^2} \quad , \qquad (3)$$

which can be derived from the Lorentz model where the absorption frequencies $\nu_i = \frac{c}{\lambda_i}$ of the material are approximated by a simple spring-bonded electron model.[77] Far from the characteristic absorption wavelengths λ_i of the material, the Cauchy and Sellmeier models are identical. We have fit some of the data at representative thicknesses treating the index of the PS film with the Sellmeier model (taking only a single term in the sum of Eq. (3)) and found there to

be no difference in fitted index values to within the reproducibility of the measurement, as expected for wavelengths λ = 400-1000 nm where PS has no characteristic absorptions.

The layer model we use is comprised of air, the PS film modeled as a Cauchy layer, and a silicon substrate with a 1.25 nm native oxide layer. The known index values for the silicon and native oxide layer, including the temperature dependence for the index of silicon $N(\lambda) \equiv n(\lambda) - ik(\lambda)$ are taken from the literature,[78] and provided as part of the Woollam software. When using the Cauchy model for the PS layer, employing the standard three parameters (*A*, *B*, and *C*) provides the best fit. However, we have found that for film thicknesses less than 300 nm, the third parameter *C* is not well defined during fitting; when it is allowed to vary in thin films, additional noise is introduced into the *B* parameter to compensate random fluctuations in *C*. These wavelength-dependent fitting parameters become less robust for thinner films because, as the film thickness and hence path length of the light through the film decreases, more of the ellipsometry signal comes from the interface and less from the dispersion (wavelength dependence) in the material. To be consistent with all the data presented in this manuscript, we have chosen to fit only the two parameters, *A* and *B* in Eq. (2), while holding the parameter *C* = 0.00038, a value determined from the average of bulk films with thicknesses greater than 800 nm.[79] Other ellipsometry studies have also reduced the number fitting parameters when modeling very thin films.[71] (We have verified that the small shifts in refractive index with film thickness discussed in Fig. 3.4 do not change if a different value of *C* is used.) For these very thick films, we have also included an additional non-uniformity parameter into the fitting to account for small variations in film thickness across the measurement spot size common in films greater than a micron in thickness. The silicon oxide layer was held fixed at 1.25 nm, a value

determined from many measurements of bare silicon wafers. Analysis of the data using a different value for the SiOx layer thickness (e.g., 2.0 nm) does not change the results appreciably (by less than 0.3 % even for the thinnest PS films of 10 nm in thickness), and that the same film-thickness dependent trends in PS index are observed.

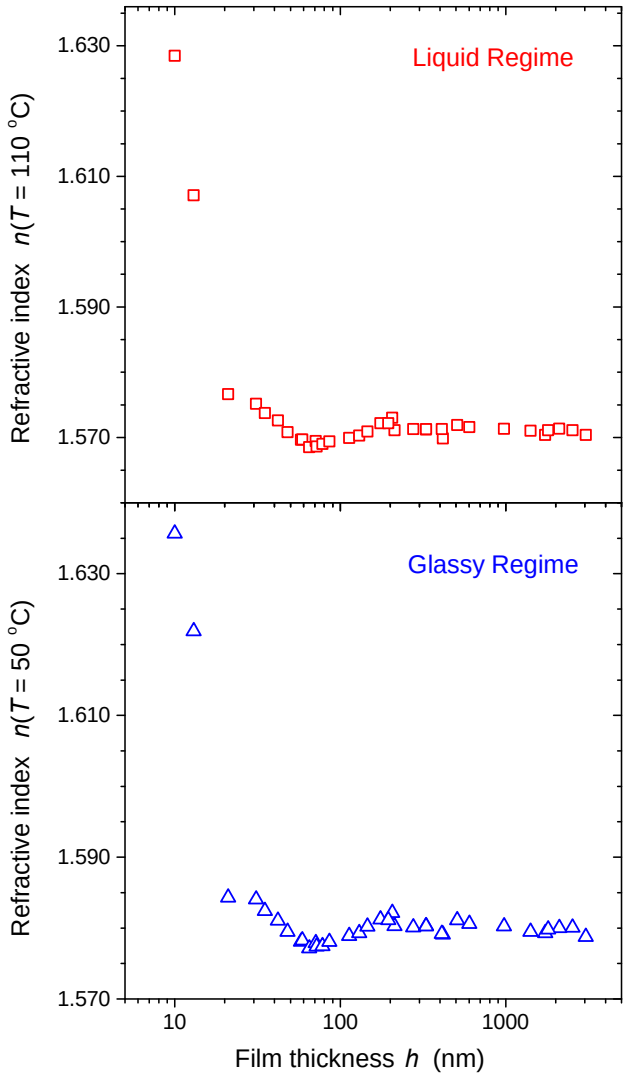

Fig. 3.4. Refractive index evaluated in the liquid regime (top) at $n(T = 110\ ^{o}C)$ and the glassy regime (bottom) at $n(T = 50\ ^{o}C)$ as a function of film thickness. We observe a minimum in refractive index at 65 nm in thickness that is more than three times larger than the standard

deviation in values observed for bulk films (h > 200 nm), while the large increase in index observed for the thinnest films of 10 and 13 nm have been reported previously.[39-41] Note that the error associated with multiple measurements on a single sample are less than the symbol size, while the noise in the data represent the sample-to-sample variability.

Figure 3.5 graphs experimental data of Ψ(λ) and Δ(λ) collected for PS supported on silicon at 110 ^{o}C for representative film thicknesses (977, 330, 65, and 31 nm), where the experimental data are shown as symbols and the best fit values as curves. For all film thicknesses, excellent fits to the experimental data are obtained, with the exception of the thinnest films as described below. Nominally we fit all of the Ψ(λ) and Δ(λ) data between λ = 400-1000 nm; however, we also varied this wavelength range to be 400-700 nm, 700-1000 nm, or 450-950 nm with no significant change in the observed results. Accuracy of Ψ(λ) and Δ(λ) data fits within the Woollam measurement and analysis software are characterized by the mean squared error (MSE), a biased estimator that is weighted by measurement error:[80,81]

$$\mathrm{MSE}^2 = \frac{1}{2n-m}\sum_{i=1}^{n}\left[\left(\frac{\Psi_i^{\mathrm{mod}}-\Psi_i^{\mathrm{exp}}}{\sigma_{\Psi,i}^{\mathrm{exp}}}\right)^2 + \left(\frac{\Delta_i^{\mathrm{mod}}-\Delta_i^{\mathrm{exp}}}{\sigma_{\Delta,i}^{\mathrm{exp}}}\right)^2\right] \quad , \qquad (4)$$

where $\sigma_{\Psi}^{\mathrm{exp}}$ and $\sigma_{\Delta}^{\mathrm{exp}}$ are the measurements errors for Ψ and Δ, n is the total number of (Ψ, Δ) data pairs being fit and m is the number of fitting parameters (typically 3 = h_{PS}, A and B). Values of MSE provide a quantitative measure of the difference between the experimental data (Ψ^{exp}, Δ^{exp}) and model fit (Ψ^{mod}, Δ^{mod}). Note formally within the Woollam CompleteEASE software for the M-2000 ellipsometer, the experimental parameters being measured[82] are $N = \cos(2\Psi)$, $C = \sin(2\Psi)\cos(\Delta)$, and $S = \sin(2\Psi)\sin(\Delta)$, such that the MSE is actually calculated as:

$$\mathrm{MSE} = \sqrt{\frac{1}{3n-m}\sum_{i=1}^{n}\left[\left(\mathrm{N}_i^{\mathrm{mod}} - \mathrm{N}_i^{\mathrm{exp}}\right)^2 + \left(\mathrm{C}_i^{\mathrm{mod}} - \mathrm{C}_i^{\mathrm{exp}}\right)^2 + \left(\mathrm{S}_i^{\mathrm{mod}} - \mathrm{S}_i^{\mathrm{exp}}\right)^2\right]} \times 1000 \quad (5)$$

The MSE values function as a χ^2 parameter that can be used to verify that a well-defined and robust global minimum is being found during fitting by plotting values of MSE as a function of a given fitting parameter to visualize the shape and depth of the minimum. Figure 3.6 graphs the shape of the MSE function at the best fit minimum for each of our three fitting parameters (h_{PS}, *A* and *B*) for many different film thicknesses that were measured. As can be seen from the plots, film thickness values larger than 30 nm have sharp, well-defined minima for each of the fitting parameters, which includes the 65 nm samples where the unusual minimum in index of refraction is observed in Fig. 3.4. For the thinnest films, 21, 13, and 10 nm, the shape of the MSE minima become progressively flatter making the fitting less robust. The 21 nm thick film shows MSE minima that should still be sufficiently well defined, but the 13 and 10 nm thick films have very flat and ill-defined minima, especially for the *B* parameter, that the resulting best fit values should be suspect. It is well known and described in ellipsometry texts[75,83] that ellipsometry is unable to reliably measure the index of refraction of very thin films, ~10 nm or less. This ambiguity in index arises because the $\Psi(\lambda)$ and $\Delta(\lambda)$ trajectories (graphs such as Fig. 3.8) for films with different indices all merge to a single point at zero film thickness, called the film-free point ($h_{PS} = 0$).[75,83] Even data measured at different wavelengths merge to this single point at $h_{PS} = 0$ such that enlarging the spectroscopic range does not resolve the problem. Thus, we conclude that the unusually large values of the index of refraction for the thinnest films (10 and 13 nm) plotted in Fig. 3.4 are unreliable because of fitting uncertainty in the $\Psi(\lambda)$ and $\Delta(\lambda)$ data.

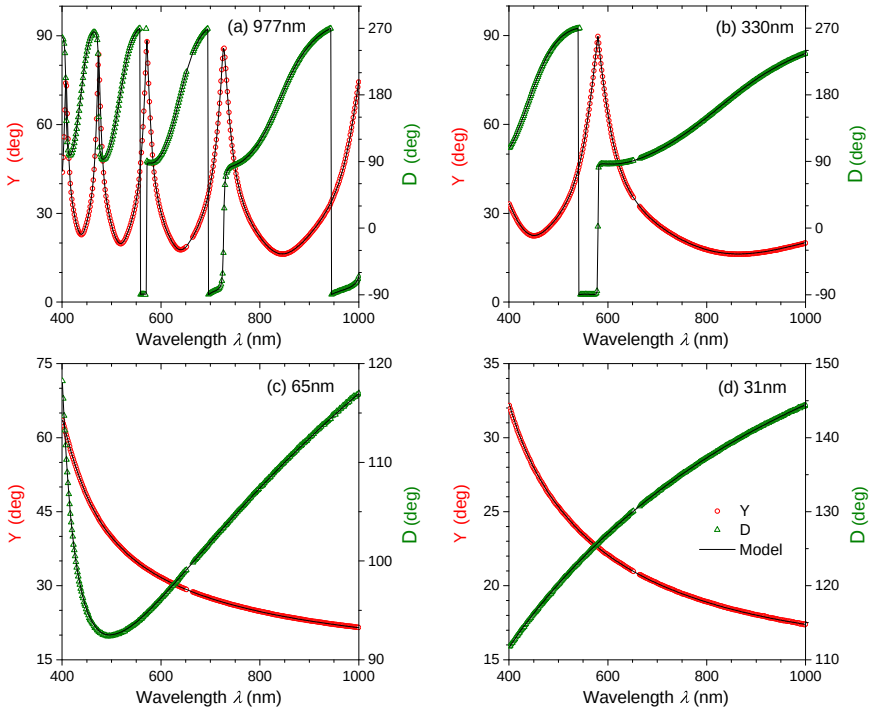

Fig. 3.5: Raw Ψ(λ) and Δ(λ) data collected of PS supported on silicon at 110 ^{o}C for representative film thicknesses: (a) 977 nm, (b) 330 nm, (c) 65 nm, and (d) 31 nm, are plotted for the wavelength range of λ = 400-1000 nm. Curves represent fits to the layer model: PS film modeled as Cauchy layer $n(\lambda) = A + \frac{B}{\lambda^2} + \frac{0.00038}{\lambda^4}$, 1.25 nm native SiOx layer, Si substrate.

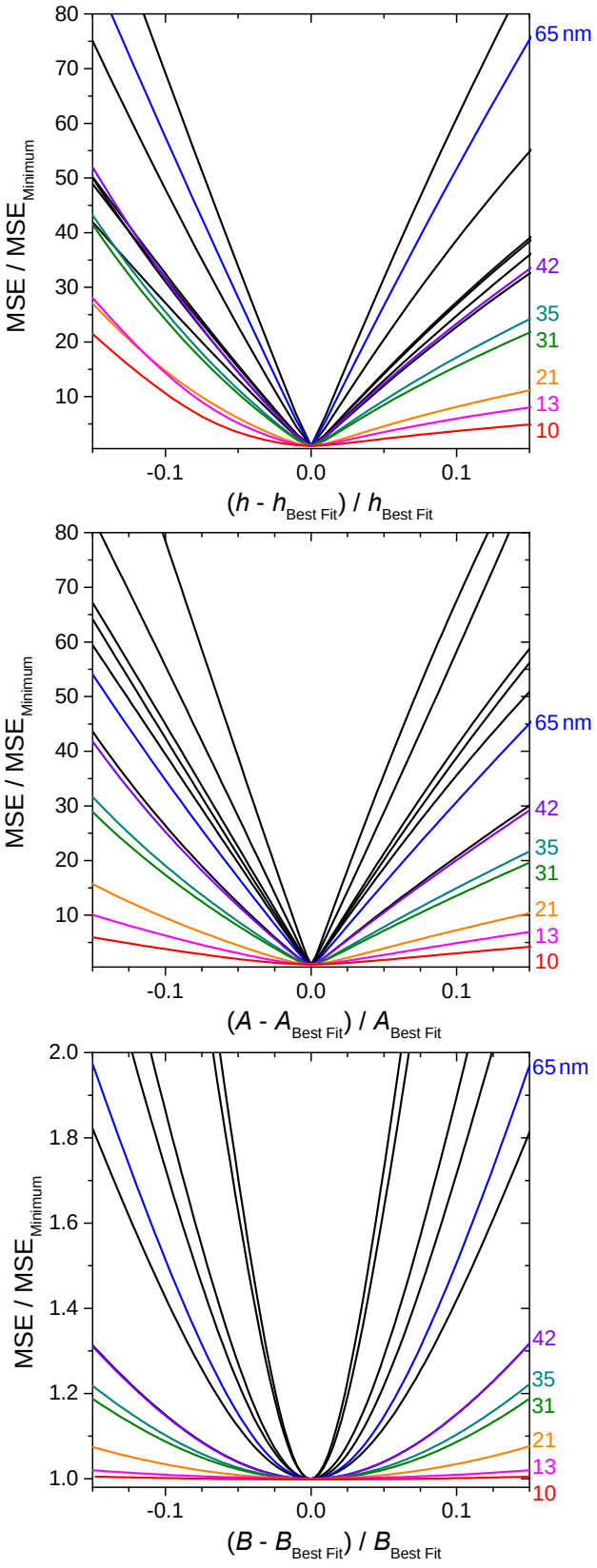
MSE / MSE_Minimum
(h - h_Best Fit) / h_Best Fit
65 nm
42
35
31
21
13
10
(A - A_Best Fit) / A_Best Fit
(B - B_Best Fit) / B_Best Fit

Fig. 3.6: Shape of MSE function, normalized to the minimum MSE value, about the best fit values for each of the three fitting parameters: *h*, *A* and *B*. The black curves represent various film thicknesses between 48 and 603 nm, while specifically labeled thin films are shown in color. Notice how for almost all film thicknesses, including at 65 nm, the minima are sharp and well defined. However, for the thinnest films at 13 and 10 nm, the shape of the MSE minima, especially for the *B* parameter, become very flat and ill-defined making the fitting less robust and thus suspect.

Figure 3.7 graphs the best fit parameters *A* and *B* as a function of film thickness. As expected the *A* parameter follows the same trend shown in Fig. 3.4 for the index of refraction at λ = 632.8 nm demonstrating that the results do not depend on the specific choice of wavelength. (In addition, we also evaluated the index at λ = 900 nm (data not shown) and found the same trend.) Interestingly, the *B* parameter is primarily constant for films greater than ~20 nm except for an unusual hump in the data between 70 and 200 nm, with a peak at ~120 nm. The *B* parameter accounts for the wavelength-dependent dispersion of the index of refraction, suggesting some change in the material is occurring. Even if we let the third *C* parameter vary in the Cauchy model fit, the hump in the *B* parameter data is still present.

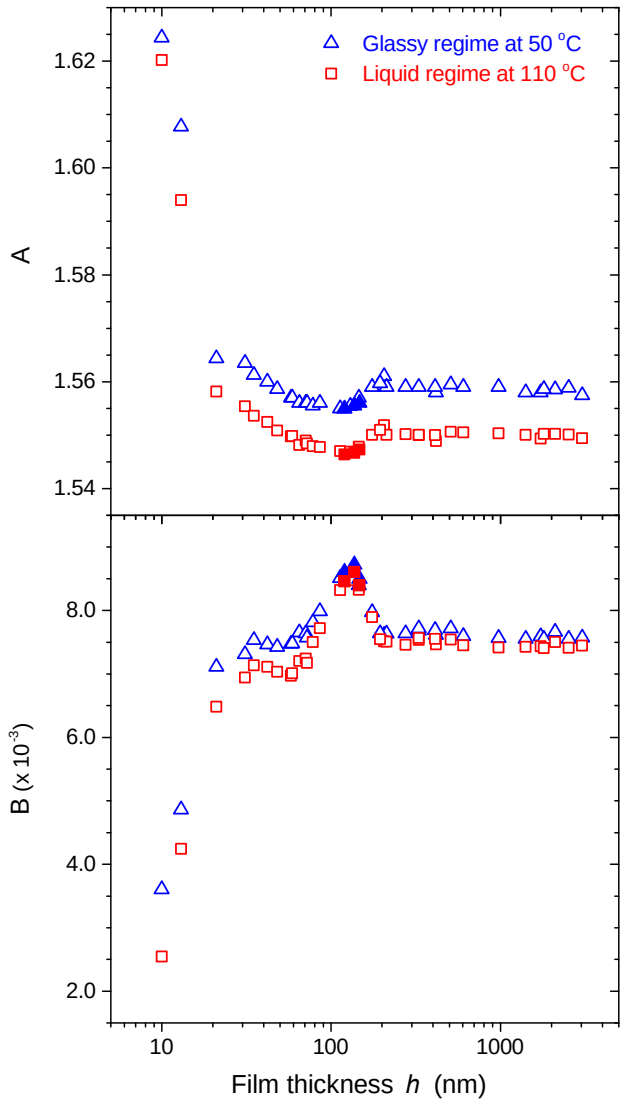

Fig. 3.7: Best fit parameters *A* and *B* from Cauchy model fit to PS layer, representing the PS index of refraction $n(\lambda) = A + \frac{B}{\lambda^2} + \frac{0.00038}{\lambda^4}$, as a function of PS film thickness. Nominally, all the data shown have been collected at an angle of incidence of 65°; however, some additional data collected at 58° angle of incidence are also shown here as solid symbols demonstrating that the results are independent of the specific angle used for the measurement. Note that the errors associated with multiple measurements on a single sample are less than the symbol size, while the noise in the data represents the sample-to-sample variability.

The robustness and uniqueness of fitting ellipsometry data can be visualized by plotting Ψ–Δ trajectories.[75] For a given layer model, expected (Ψ, Δ) values can be calculated for increasing PS film thickness showing how the Δ vs. Ψ trajectory circles counter-clockwise as the optical path length cycles through $\lambda/2$. In Figure 3.8, we plot the expected Δ vs. Ψ data evaluated at λ = 632.8 nm for PS films supported on silicon calculated using values from our layer model: $n(T = 110\ ^{o}\mathrm{C}) = 1.5712$ for PS, $n = 1.7338$ for native SiOx, and $N = 3.9091 - 0.001308i$ for Si.[78] Figure 3.8 graphs Ψ–Δ trajectories for two different angles of incidence, 65° and 58°, where data were collected. (Note the Ψ–Δ trajectory for 65° appears discontinuous because a value of Δ = 0 is equivalent to Δ = 360.) The measured experimental (Ψ, Δ) values are also plotted demonstrating excellent agreement with the calculated curves, regardless of where in the trajectories the data falls. In addition, we have highlighted in orange a 20 nm region about 65 nm where the dip in index of refraction occurs in Fig. 3.4 and about 120 nm where the hump in the *B* parameter occurs in Fig. 3.7. In ellipsometry fitting, the part of the trajectory that is particularly hard to fit unambiguously is the region near the film-free point ($h = 0$) and the period-point when the trajectory returns to the same point as $h = 0$ due to destructive interference (for λ = 632.8 nm in Fig. 3.8, the period points are $h = 245$ nm for 65° and $h = 237$ nm for 58°).[83] Here, trajectories for different values of the index of refraction merge and this is the primary reason why it is hard to measure the refractive index of very thin films (~10 nm) with ellipsometry as described above.[75,83] In reality, we are simultaneously fitting the entire range of wavelengths λ = 400-1000 nm at a single angle of incidence (nominally 65°) such that the period points range between 155-387 nm. The purpose of Fig. 3.8 is to note that neither of the regions where we observe variations in the index of refraction in Fig. 3.4 or hump in the *B* parameter in

Fig. 3.7, occur near the period-point that is hard to fit. We conclude that the index of refraction data presented in Fig. 3.4 are a robust measure, independent of the fitting details, with the exception of the two thinnest films at 10 and 13 nm. Thus, we continue with our analysis below focusing only on the films with thicknesses of 20 nm and larger.

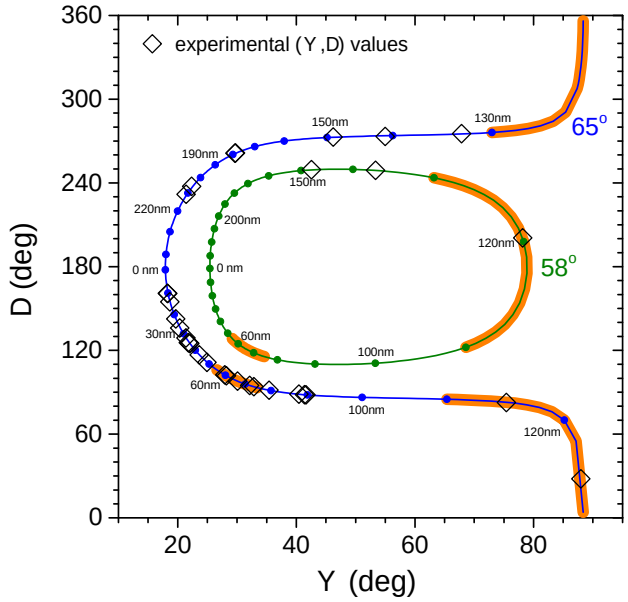

Fig. 3.8: Ψ vs. Δ trajectories calculated at λ = 632.8 nm for PS films supported on silicon using values from our layer model, $n(T = 110\ ^{o}C) = 1.5712$ for PS, $n = 1.7338$ for native SiOx, and $N = 3.9091 - 0.001308i$ for Si, for angles of incidence of 65° (blue) and 58° (green) where the dots indicate increments in PS film thickness every 10 nm. Highlighted in orange are 20 nm regions about 65 nm where the dip in index of refraction occurs in Fig. 3.4 and about 120 nm where the hump in the *B* parameter occurs in Fig. 3.7. Measured experimental (Ψ, Δ) values (diamonds) plotted demonstrate excellent agreement with the calculated curves regardless of location within the trajectories.

3.4.3 Lorentz-Lorenz equation as a measure of density and specific volume

The Lorentz-Lorenz equation, Eq. (6), relates the index of refraction, a macroscopic (continuum) quantity, to the microscopic polarizability of the material. As this inherently depends on the number of molecular dipoles per unit volume, which can be written in terms of the material's mass density, the Lorentz-Lorenz equation has been frequently used as a measure of density.[54,84-87] For common solids and liquids the Lorentz-Lorenz relation gives accurate values of the density to within a few percent (typically 1-2 %);[84,85,88] the largest discrepancies are for dense gases with large density fluctuations[88,89] or highly polar compounds.[84] We consider here what limitations may exist in the validity of this equation for very thin films based on the assumptions made in its derivation.

The derivation of the Lorentz-Lorenz relation is typically done by considering separately the electric field contribution from inside and outside an arbitrary small spherical cavity.[67,90] The size of the cavity must be large with respect to the molecular dipoles such that the local microscopic electric field at the center of the cavity can be replaced by the macroscopic field contribution from those charges residing outside the cavity, $\vec{E}^{\text{macro}}_{\text{outside}}(\vec{r})$. This macroscopic field outside the cavity can then be written in terms of the total macroscopic electric field, $\vec{E}^{\text{macro}}_{\text{total}}(\vec{r}) \equiv \vec{E}(\vec{r})$, minus the macroscopic field inside the cavity: $\vec{E}^{\text{macro}}_{\text{outside}}(\vec{r}) = \vec{E}(\vec{r}) - \vec{E}^{\text{macro}}_{\text{inside}}(\vec{r})$. For a spherical cavity with uniform polarization, i.e., negligible spatial variation in the molecular dipoles, this macroscopic field inside the cavity can be easily calculated[90,91] giving $\vec{E}^{\text{macro}}_{\text{inside}}(\vec{r}) = -\frac{1}{3\epsilon_0}\vec{P}$, where $\vec{P}$ is the polarization density equal to the number density of molecular dipoles inside the cavity, $\vec{P} = \frac{N}{v}\vec{p}$. The remaining quantity needed is the microscopic local electric field

inside the cavity $\vec{E}^{\text{local}}_{\text{inside}}(\vec{r})$, which has been shown to explicitly sum to zero for a uniform spatial distribution of dipoles having either a cubic lattice or random distribution.[67,90] Combining all of these, we have for the total local (or effective) electric field:

$$\vec{E}^{\text{local}}_{\text{total}}(\vec{r}) = \vec{E}^{\text{local}}_{\text{inside}}(\vec{r}) + \vec{E}^{\text{macro}}_{\text{outside}}(\vec{r})$$

$$= 0 + \vec{E}(\vec{r}) - \vec{E}^{\text{macro}}_{\text{inside}}(\vec{r})$$

$$= \vec{E}(\vec{r}) + \frac{1}{3\epsilon_0}\vec{P} \ ,$$

which is the standard Lorentz relation. At the microscopic level, the induced molecular dipole moment $\vec{p}$ at a given location is the molecular polarizability α times this total local electric field:

$$\vec{p} = \alpha \, \vec{E}^{\text{local}}_{\text{total}}(\vec{r}) \ .$$

At the macroscopic level, the polarization density $\vec{P}$ is defined in terms of the total macroscopic electric field $\vec{E}(\vec{r})$ and the dielectric constant $\kappa = \frac{\epsilon}{\epsilon_0}$ of the material as $\vec{P} = \epsilon_0(\kappa - 1)\vec{E}(\vec{r})$, where ϵ_0 is the permittivity of free space. By merging the microscopic and macroscopic definitions of $\vec{P}$ one arrives at the classic Clausius-Mossotti relation:

$$\frac{\kappa-1}{\kappa+2} = \frac{\alpha}{3\epsilon_0}\frac{N}{v} \ .$$

For optical frequencies, the dielectric constant is usually written in terms of the index of refraction $n = \sqrt{\kappa}$. In addition, the number density of molecular dipoles $\frac{N}{v}$ is often replaced with the material's mass density ρ by using Avogadro's number N_A and the molar mass of the molecular dipole unit, which for polymers is typically taken to be the molar mass of the

monomer M_0.[40,86] Thus, $\frac{N}{v} = \rho \frac{N_A}{M_0}$ leads us to the commonly used form of the Lorentz-Lorenz equation:[39-41,84-86]

$$\frac{n^2-1}{n^2+2} = \frac{\alpha N_A}{3\epsilon_0 M_0}\rho \quad , \qquad (6)$$

where the quantity $\frac{n^2-1}{n^2+2}$ is often defined as L. (Note this has been written in SI units, whereas much of the literature is historically in Gaussian units where $\vec{P} = \frac{(\epsilon-1)}{4\pi}\vec{E}(\vec{r})$ and $\epsilon_0 = 1$.)

We can see that two key assumptions were made in the derivation of Eq. (6) that are relevant and potentially a concern when applying the Lorentz-Lorenz relation to very thin films: (1) An arbitrarily sized cavity must fit inside the film, but still be large relative to the molecular dipole unit, the monomer, and (2) these molecular dipoles need to have a uniform spatial distribution inside the cavity for their contribution to the microscopic local electric field to sum to zero. First we consider what the minimum size for this arbitrary cavity is in the derivation of the Lorentz-Lorenz relation. For PS, although the main polarizing unit is the large phenyl ring, the relevant size is that of the entire molecular dipole unit, the monomer. The PS monomer size has been estimated at ~0.7 nm.[92] Within the derivation of the Lorentz-Lorenz relation, the radius of the cavity should be large (at least an order of magnitude) relative to the interparticle spacing of the molecular dipoles, i.e., at least $r \approx 7$ nm or larger.[90] Meaning a cavity of at least ~14 nm in diameter or larger should fit inside the film. Second, we should consider if the molecular dipoles are uniformly randomly oriented across this arbitrary cavity. Experimental studies primarily with second harmonic generation indicate alignment of the phenyl rings locally at the free surface and substrate interface of PS films typically to a depth ~1 nm.[93-96] As the film thickness

is decreased and the cavity size starts to span the entire thickness of the film, the non-random spatial orientation of the molecular dipoles at the interfaces may also invalidate assumptions in the derivation. Thus, we can certainly see that there will come a point in decreasing the film thickness where the Lorentz-Lorenz relation must fail because the film can no longer be accurately approximated as a continuum material. Based on the above discussion we conclude that a cavity of at least ~14 nm in diameter must fit inside the film, excluding a couple of nanometers at either interface where molecular orientation occurs, meaning that we anticipate the Lorentz-Lorenz relation, Eq. (6), to only be valid for film thicknesses larger than ~20 nm.

The temperature dependence of the density and index of refraction have often been used as a stringent test of the validity of the Lorentz-Lorenz formula.[54,84,85] The reasoning being that the molecular polarizability α at optical wavelengths is primarily determined by the electronic quantum states, which have a very weak temperature dependence.[85] Thus, the refractive index *n* should only vary with temperature through density, implying that, according to Eq. (6),

$$\frac{1}{\rho}\left(\frac{n^2-1}{n^2+2}\right) = \frac{N_A \alpha}{3\epsilon_0 M_0} \qquad (7)$$

should be a constant, independent of temperature. For a polymer film supported on silicon, the thermal expansion and hence volume change will occur entirely in the thickness direction.[97] As such, the film thickness *h* can be used to represent the change in density = sample mass / volume with temperature. We find that the quantity $h\left(\frac{n^2-1}{n^2+2}\right)$ for PS films on silicon is independent of temperature to within ± 0.1 % for film thicknesses greater than 150 nm, within ± 0.2 % for *h* = 50-150 nm, and within ± 0.3 % for *h* = 30-50 nm. Below 30 nm, the deviations in the temperature dependence of $h\left(\frac{n^2-1}{n^2+2}\right)$ begins to increase substantially, varying by ± 0.4 % for

films 12-30 nm thick and exceeding 0.9 % for 10 nm thick films. This is consistent with our conclusion above that the Lorentz-Lorenz equation should become invalid for thin films as the thickness approaches ~20 nm.

As an interesting historical note, in 1965, Looyenga proposed a different quantity $\left(n^{2/3}-1\right)$ to replace the $\left(\frac{n^2-1}{n^2+2}\right)$ term in the Lorentz-Lorenz equation.[98] Looyenga's expression was based on a previous formula he had derived to describe the dielectric constant of heterogeneous media incorporating the volume fraction of each component.[99] Looyenga argued that the same formula could be adapted to homogeneous media by treating it as a mixture where one component was vacuum,[98] leading to Looyenga's replacement for the Lorentz-Lorenz formula:

$$n^{2/3}-1=\frac{\alpha N_A}{3\epsilon_0 M_0}\rho \quad . \qquad (8)$$

Although Looyenga's expression for heterogeneous mixtures is routinely used, the formula $\left(n^{2/3}-1\right)$ replacing that of Lorentz-Lorenz's has received little attention, despite both Looyenga[98] and others[85] demonstrating that the temperature dependence of Looyenga's expression is superior. For gases, Looyenga's $\left(n^{2/3}-1\right)$ expression is nearly identical to Lorentz-Lorenz's $\left(\frac{n^2-1}{n^2+2}\right)$, as they have the same expansion in $(n-1)$ to second order.[85,100] However, for organic liquids with $n \approx 1.3$-1.5, the $(n-1)^3$ cubic and higher order terms give rise to small differences of 2-4 %.[85] For completeness and out of curiosity, we evaluated the quantity $h\left(n^{2/3}-1\right)$ as a function of temperature for our PS films on silicon. Consistent with previous observations,[85,98] we find Looyenga's expression, Eq. (8), to show smaller deviations

with temperature then that of Lorentz-Lorenz, Eq. (6). The temperature dependence of $h\left(n^{2/3}-1\right)$ is constant to within ± 0.1 % for film thicknesses down to 50 nm, and show deviations to within only ± 0.2 % for h = 30-50 nm, before increasing for thinner films below 30 nm. Below we continue our discussion by using the more commonly accepted Lorentz-Lorenz expression, Eq. (6), to comment on the relative change in specific volume and density of PS films as a function of film thickness; however, we note that the same deviations from bulk as that shown in Fig. 3.10 are observed to within experimental error if Looyenga's expression, Eq. (8), is used instead.

3.4.4 Changes in specific volume and density with decreasing film thickness

Here we proceed in our data analysis assuming the Lorentz-Lorenz equation is valid for sufficiently thick films with the understanding that the continuum approximation will breakdown for thin films as the thickness approaches ~20 nm. Using the Lorentz-Lorenz equation, Eq. (6), we can define an effective specific volume v_{sp}, equivalent to the inverse density, from the Lorentz-Lorenz parameter $L = \frac{n^2-1}{n^2+2}$, recognizing that the remaining terms $\frac{\alpha N_A}{3\epsilon_0 M_0}$ are constants independent of temperature and film thickness:

$$v_{sp} = \frac{1}{\rho} \propto \frac{n^2+2}{n^2-1} \quad . \tag{9}$$

Following White and Lipson,[36] we plot curves of effective specific volume $v_{sp}(T)$ in Figure 3.9 for several different film thicknesses. We find supported PS films of bulk thickness (977 and 330 nm) trace out the same $v_{sp}(T)$ curve, while thinner films (65 nm) are shifted to larger $v_{sp}(T)$

values by 0.4 % relative to bulk. This magnitude for the increase in specific volume is comparable to that predicted by the White and Lipson model suggesting it may result from a natural driving force for film expansion as missing contacts at the interface lead to a reduction in the attractive energy between polymer segments.[36,65] However, the thinnest films (31 nm in Fig. 3.9) show a shift in $v_{sp}(T)$ in the opposite direction to smaller values relative to bulk. In Fig. 3.9, for reference, the datasets have been normalized to the bulk $v_{sp}(T)$ value at T = 110 ^{o}C, as measured for film thicknesses greater than 200 nm. It is also clear from the $v_{sp}(T)$ data in Fig. 3.9 that both the liquid and glassy lines shift uniformly with film thickness. As the films are cooled from the equilibrium liquid state along a shifted $v_{sp}(T)$ curve, the film falls out of equilibrium into a glass along a similarly shifted $v_{sp}(T)$ curve. The glass transition does not occur at the same specific volume (i.e., total free volume) for different film thicknesses, in contradiction with ideas behind the original free volume models for the glass transition.[48-51]

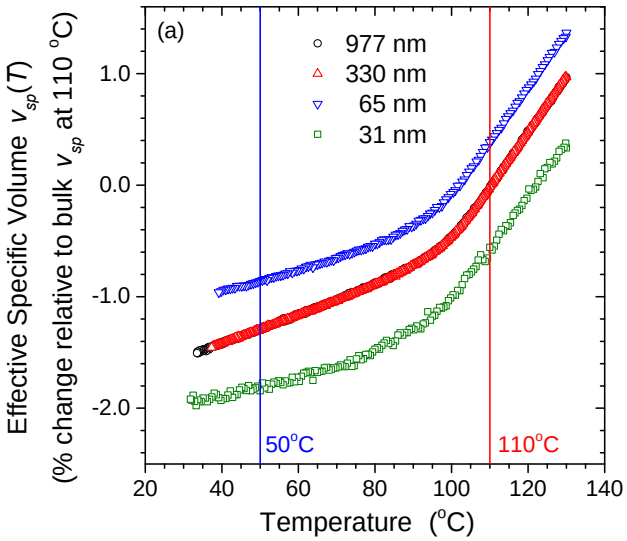

Fig. 3.9: Measure of the effective specific volume, $v_{sp} = \frac{1}{\rho} \propto \frac{n^2+2}{n^2-1}$ based on the Lorentz-Lorenz equation Eq. (6), as a function of temperature for supported PS films on silicon. $v_{sp}(T)$ curves

for bulk films (977 and 330 nm) sit atop each other, but thinner films have $v_{sp}(T)$ curves shifted in correspondence to the $n(T)$ data shown in Fig. 3.3. For comparison, the datasets have all been normalized to the bulk $v_{sp}(T)$ value at T = 110 ^{o}C (based on films > 200 nm). The $v_{sp}(T)$ curve for 65 nm thick films shows a shift to larger values by 0.4 %, while 31 nm thick films are shifted to smaller values relative to bulk. In all cases, both the liquid and glassy lines are shifted uniformly.

To study the film thickness dependent shifts in $v_{sp}(T)$ in more detail, in Figure 3.10 we plot the effective specific volume $v_{sp}(T)$ values in the liquid (T = 110 ^{o}C) and glassy (T = 50 ^{o}C) regimes as a function of film thickness. The data clearly show that these small shifts in the effective specific volume of the film are consistently the same for the liquid and glassy regimes. Fig. 3.10a with a logarithmic thickness scale shows that for bulk films between 200-3100 nm, the liquid and glassy $v_{sp}(T)$ values are independent of film thickness to within a standard deviation of ± 0.11 %. In Fig. 3.10b, we focus on the unusual non-monotonic behavior of the data for films below ~200 nm that varies outside this range, where we have highlighted the variation in the bulk values with horizontal lines. Below ~120 nm, the effective specific volume increases to a peak value of 0.4 ± 0.2 % at a film thickness of 65 nm, an increase in $v_{sp}(T)$ of more than three times larger than the variation in the bulk data. However below this peak at 65 nm, conspicuously around the thickness where the $T_g(h)$ decrease begin in Fig. 3.2, the effective specific volume decreases again back to the bulk value at ~40 nm before continuing to decrease further for much thinner films. We do not show data below 20 nm because as we argued above, the ellipsometry fitting is unreliable for very thin films ~10-13 nm. However, we do note that if

values for film thicknesses less than 20 nm were plotted, the values would be off the scale showing an ~5 % increase in density for a 10 nm thick film consistent with recent literature reports.[39,40] Also as described above, the approximations made to derive the Lorentz-Lorenz equation breakdown as the film thickness approaches ~20 nm, making the trends in the data shown in Fig. 3.10 for the very thinnest films somewhat suspect. Note that all the variations in $v_{sp}(T)$ plotted in Fig. 3.10 are within the ± 1 % experimental error of previous studies reporting no changes in density with film thickness.[37,38]

To further demonstrate that these data in Figure 3.10 are representative of the properties of the polymer film and not some systematic artifact of the data collection and analysis procedure, we have made a handful of additional measurements of PS films on silicon substrates that contain an added 23.5 ± 0.8 nm aluminum oxide (AlOx) layer (nominal index of 1.64) creating a strong uniform index contrast with PS. Bare silicon wafers were sputtered with AlOx and then subsequently characterized by ellipsometry fitting the sputtered AlOx film thickness and index characteristics $n(\lambda)$ with a Cauchy layer. These characterized AlOx substrates were then spin-coated with PS and further measurements of the PS specific volume $v_{sp}(T)$ were done. Figure 3.10a plots as gray data these additional measurements of $v_{sp}(T)$ for PS on the AlOx coated substrates at 50 and 110 ^{o}C. To within reasonable accuracy, these measurements agree with those collected on bare silicon wafers clearly showing the same film thickness dependent features. Thus, we conclude that the data shown in Figure 3.10 are accurately reflecting the properties of the thin PS films.

We have labeled the *y*-axes of Fig. 3.10 as the effective specific volume $v_{sp}(T)$ because,

according to Eq. (6), density $\rho = \frac{1}{v_{sp}}$ seems like the most reasonable parameter to vary with film thickness within the Lorentz-Lorenz expression. However, we do note there is another potential variable within the Lorentz-Lorenz expression, Eq. (6), the molecular polarizability α. It seems unlikely that such a local property would vary with film thickness at such large length scales, as α is not even expected to vary much with temperature. However, within the Lorentz-Lorenz derivation, the polarizability is assumed to be uniformly isotropic. One could imagine that as the film thickness is reduced and polymer chain segments must orient more within the plane of the film that the polarizability could become slightly anisotropic leading to deviations from the expected Lorentz-Lorenz expression. Perhaps the non-monotonic behavior in the *y*-axes of Fig. 3.10, formally $\frac{1}{L} = \frac{n^2+2}{n^2-1}$, occurs because of some film thickness change in density coupled with some film thickness change in the isotropic polarizability. Future work will investigate such a possibility.

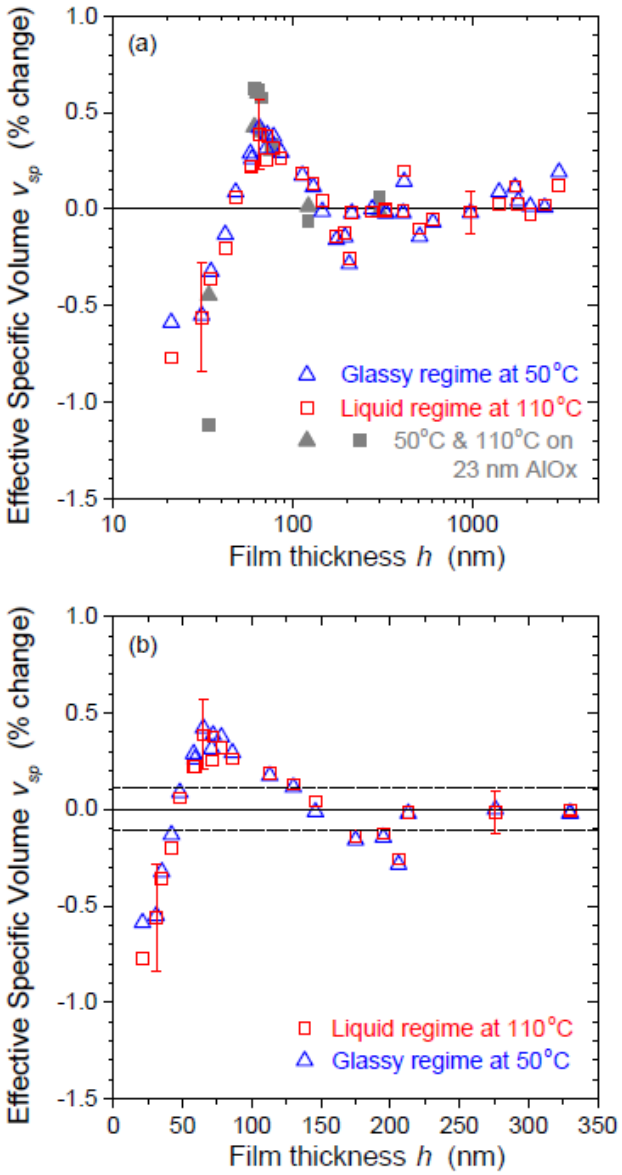

Fig. 3.10: Film thickness dependence of the effective specific volume v_{sp} in the liquid (T = 110 °C) and glassy (T = 50 °C) regimes. (a) All data plotted on a semi-log scale showing that v_{sp} values for bulk films (h = 200-3100 nm) only vary within ± 0.11 %, but then exhibit larger, reproducible deviations in v_{sp} from bulk for smaller film thicknesses. These deviations are all within the ± 1 % experimental error of previous studies. Gray data represent measurements done on substrates that were coated with 23.5 ± 0.8 nm aluminum oxide (AlOx), see text for details.

(b) Films thinner than 350 nm plotted on a linear scale, where the standard deviation in the bulk data (h > 200 nm) has been represented by dashed-dotted lines. The peak in v_{sp} at 65 nm of 0.4 ± 0.2 % is roughly three times larger then the variability in the bulk data. Note we have not plotted data for less than 20 nm because of concerns with the reliability of the ellipsometry fitting; the error associated with multiple measurements on a single sample are less than the symbol size, while the noise in the data represent the sample-to-sample variability; representative error bars have been added for the different regions of the data.

Although we can only comment on the validity of ellipsometry measurements, we do note that Wallace et al.[37] previously questioned the reliability of reflectivity measurements on very thin films. To avoid some of these concerns for their own neutron reflectivity measurements, Wallace et al.[37] used a "twin" reflectivity technique that collected data of the critical angle for reflection from both the free surface side and substrate side of the PS film on silicon samples. A data reduction scheme was then used to identify the crossover point in the momentum transfer vector to account for the unknown tilt of the sample. This allowed for reliable determination of the film's density to within ± 1 %. Wallace et al.[37] called into question previous neutron and x-ray reflectivity works[101,102] on thin polymer films that had claimed density changes of ~5 % with decreasing film thickness because they had not accounted for interfacial roughness or other confounding factors inherent in fitting reflectivity curves. In their careful study, Wallace et al.[37] found the mass density of PS films to be consistent with the bulk value within ± 1 % down to film thicknesses of 6.5 nm. Perhaps it is also worth considering how unrealistic ~5 % increase in density really is. One can use PVT data for PS from handbooks[103] to

estimate what equivalent pressure increase would be required for such an isothermal increase in density. For PS in the melt state at 115 ^{o}C (the lowest temperature for which such data are available), pressures in excess of 100 MPa would be needed for ~5 % density increase, and in excess of 4 GPa of pressure would be required for ~30 % increase in density (glassy materials with larger bulk moduli values would require even greater pressures). Also as noted in the introduction, stable glasses carefully formed by physical vapor deposition to optimize molecular packing only show increases in material density of ~1 % relative to ordinary glasses.[54,55] Thus, given the unrealistic value of 5 or 30 % increases in density, it seems likely that the recent x-ray reflectivity results[39,40] may suffer from similar uncertainties in fitting of reflectivity curves as expressed by Wallace et al.[37]

3.5 Conclusions

We have used ellipsometry to measure the temperature dependence of the index of refraction $n(T)$ for PS films supported on silicon and explored the validity of the Lorentz-Lorenz relation in very thin films. We find that the specific volume (density) of supported PS films do not vary by more than ± 0.4 % of the bulk value for film thicknesses above 30 nm, and that the small variations we do observe are uncorrelated with the $T_g(h)$ reductions exhibited by these films. Based on the assumptions made in its derivation, we conclude that the Lorentz-Lorenz equation is not valid for very thin films, breaking down as the thickness approaches ~20 nm. We believe that the large increase in index of refraction and apparent density (~5 % for a 10 nm thick film) we observe, consistent with recent experimental reports,[39-41] are an experimental artifact because ellipsometry is known to be unreliable in accurately measuring the index of refraction of

very thin films, ~10 nm or less,[75,83] and that such density increases would be unrealistic given stable glasses with optimum, equilibrium packing only show increases in density of ~1 % relative to ordinary glasses.[54,55]

We have also tested recent theoretical predictions and assumptions made by White and Lipson.[36,65] Their thermodynamic model predicts a driving force for film expansion with decreasing film thickness in thin films, caused by the missing interactions at the free surface, that should result in a small increase of the liquid-line specific volume $v_{sp}(T)$ of less than 1%. Based on this prediction, they suppose that such a shift in $v_{sp}(T)$ of the liquid line could explain the observed $T_g(h)$ decreases exhibited by these films, assuming that the glassy-line specific volume remains the same as bulk. Experimentally we observed that both the liquid and glassy specific volume $v_{sp}(T)$ shift consistently together such that the glass transition does not occur at the same specific volume for different film thicknesses. In the thickness regime where we believe the Lorentz-Lorenz equation is valid (h > ~ 20 nm), we do observe a small increase in specific volume $v_{sp}(T)$ of 0.4 ± 0.2 % relative to bulk for film thicknesses between ~120 to 65 nm. However, below ~60 nm where the $T_g(h)$ reductions begin, the effective specific volume is observed to decrease again returning the bulk value at ~40 nm. We speculate that the non-monotonic changes in index of refraction with film thickness we observe for film thicknesses greater than 20 nm may result from small competing changes in film density (specific volume) and uniform polarizability.

3.6 References

[1] J.L. Keddie, R.A.L. Jones, and R.A. Cory, Europhys Lett **27**, 59 (1994).

[2] J.L. Keddie, R.A.L. Jones, and R.A. Cory, Faraday Discuss **98**, 219 (1994).

[3] J.A. Forrest, K. Dalnoki-Veress, J.R. Stevens, and J.R. Dutcher, Phys Rev Lett **77**, 2002 (1996).

[4] J.A. Forrest and K. Dalnoki-Veress, Adv Colloid Interfac **94**, 167 (2001).

[5] C.B. Roth and J.R. Dutcher, J Electroanal Chem **13**, 584 (2005).

[6] C.B. Roth, K.L. McNerny, W.F. Jager, and J.M. Torkelson, Macromolecules **40**, 2568 (2007).

[7] J.E. Pye and C.B. Roth, Phys Rev Lett **107**, 235701 (2011).

[8] J.E. Pye and C.B. Roth, J Polym Sci, Part B: Polym Phys **53**, 64 (2015).

[9] P.M. Rauscher, J.E. Pye, R.R. Baglay, and C.B. Roth, Macromolecules **46**, 9806 (2013).

[10] J. Wang and G.B. McKenna, Macromolecules **46**, 2485 (2013).

[11] J. Wang and G.B. McKenna, J Polym Sci, Part B: Polym Phys **51**, 1343 (2013).

[12] K. Paeng, S.F. Swallen, and M.D. Ediger, J Am Chem Soc **133**, 8444 (2011).

[13] K. Paeng and M.D. Ediger, Macromolecules **44**, 7034 (2011).

[14] K. Paeng, R. Richert, and M.D. Ediger, Soft Matter **8**, 819 (2012).

[15] H. Yoon and G.B. McKenna, Macromolecules **47**, 8808 (2014).

[16] Z. Fakhraai and J.A. Forrest, Science **319**, 600 (2008).

[17] Z. Yang, Y. Fujii, F.K. Lee, C.-H. Lam, and O.K.C. Tsui, Science **328**, 1676 (2010).

[18] M.D. Ediger and J.A. Forrest, Macromolecules **47**, 471 (2014).

[19] C.J. Ellison and J.M. Torkelson, Nature Materials **2**, 695 (2003).

[20] R.D. Priestley, M.K. Mundra, N.J. Barnett, L.J. Broadbelt, and J.M. Torkelson, Aust J Chem **60**, 765 (2007).

[21] R.R. Baglay and C.B. Roth, J Chem Phys **143**, 111101 (2015).

[22] J.S. Sharp and J.A. Forrest, Phys Rev Lett **91**, 235701 (2003).

[23] S. Kawana and R.A.L. Jones, Eur Phys J E **10**, 223 (2003).

[24] R.D. Priestley, C.J. Ellison, L.J. Broadbelt, and J.M. Torkelson, Science **309**, 456 (2005).

[25] R.D. Priestley, L.J. Broadbelt, and J.M. Torkelson, Macromolecules **38**, 654 (2005).

[26] J.E. Pye, K.A. Rohald, E.A. Baker, and C.B. Roth, Macromolecules **43**, 8296 (2010).

[27] B. Frieberg, E. Glynos, and P.F. Green, Phys Rev Lett **108**, 268304 (2012).

[28] C.B. Roth and J.R. Dutcher, Phys Rev E **72**, 021803 (2005).

[29] C.B. Roth and J.R. Dutcher, J Polym Sci, Part B: Polym Phys **44**, 3011 (2006).

[30] C.M. Stafford, B.D. Vogt, C. Harrison, D. Julthongpiput, and R. Huang, Macromolecules **39**, 5095 (2006).

[31] J.M. Torres, C.M. Stafford, and B.D. Vogt, ACS Nano **3**, 2677 (2009).

[32] T.B. Karim and G.B. McKenna, Polymer **54**, 5928 (2013).

[33] T.B. Karim and G.B. McKenna, Macromolecules **45**, 9697 (2012).

[34] B.W. Rowe, B.D. Freeman, and D.R. Paul, Polymer **50**, 5565 (2009).

[35] C.J. Ellison, M.K. Mundra, and J.M. Torkelson, Macromolecules **38**, 1767 (2005).

[36] R.P. White and J.E.G. Lipson, Phys Rev E **84**, 041801 (2011).

[37] W.E. Wallace, N.C.B. Tan, W.L. Wu, and S. Satija, J Chem Phys **108**, 3798 (1998).

[38] J.A. Forrest, K. Dalnoki-Veress, and J.R. Dutcher, Phys Rev E **58**, 6109 (1998).

[39] G. Vignaud, M.S. Chebil, J.K. Bal, N. Delorme, T. Beuvier, Y. Grohens, and A. Gibaud, Langmuir **30**, 11599 (2014).

[40] S. Ata, K. Kuboyama, K. Ito, Y. Kobayashi, and T. Ougizawa, Polymer **53**, 1028 (2012).

[41] Y. Li, J.Q. Pham, K.P. Johnston, and P.F. Green, Langmuir **23**, 9785 (2007).

[42] J. Baschnagel and F. Varnik, J Phys: Condens Matter **17**, R851 (2005).

[43] F. Varnik, J. Baschnagel, and K. Binder, Phys Rev E **65**, 021507 (2002).

[44] A. Shavit and R.A. Riggleman, Macromolecules **46**, 5044 (2013).

[45] A. Shavit and R.A. Riggleman, J Phys Chem B **118**, 9096 (2014).

[46] P.Z. Hanakata, J.F. Douglas, and F.W. Starr, J Chem Phys **137**, 244901 (2012).

[47] P.Z. Hanakata, B.A. Pazmiño Betancourt, J.F. Douglas, and F.W. Starr, J Chem Phys **142**, 234907 (2015).

[48] M.H. Cohen and D. Turnbull, J Chem Phys **31**, 1164 (1959).

[49] D. Turnbull and M.H. Cohen, J Chem Phys **34**, 120 (1961).

[50] M.H. Cohen and G.S. Grest, Phys Rev B **20**, 1077 (1979).

[51] M.H. Cohen and G.S. Grest, Ann Ny Acad Sci **371**, 199 (1981).

[52] J.C. Dyre, J Non-Cryst Solids **142**, 235-237 (1998).

[53] J.C. Dyre, Rev Mod Phys **78**, 953 (2006).

[54] S.S. Dalal and M.D. Ediger, J Phys Chem Lett 3, 1229 (2012).

[55] S.F. Swallen, K.L. Kearns, M.K. Mapes, Y.S. Kim, R.J. McMahon, M.D. Ediger, T. Wu, L. Yu, and S. Satija, Science **315**, 353 (2007).

[56] T. Liu, K. Cheng, E. Salami-Ranjbaran, F. Gao, C. Li, X. Tong, Y.-C. Lin, Y. Zhang, W. Zhang, L. Klinge, P.J. Walsh, and Z. Fakhraai, J Chem Phys **143**, 084506 (2015).

[57] J. Zhao, S.L. Simon, and G.B. McKenna, Nat Commun **4**, 1783 (2013).

[58] T. Pérez-Castañeda, R.J. Jiménez-Riobóo, and M.A. Ramos, Phys Rev Lett **112**, 165901 (2014).

[59] R.P. White, J.E.G. Lipson, and J.S. Higgins, Macromolecules **45**, 1076 (2012).

[60] R.P. White, J.E.G. Lipson, and J.S. Higgins, Macromolecules **45**, 8861 (2012).

[61] J.E.G. Lipson and R.P. White, J. Chem. Eng. Data **59**, 3289 (2014).

[62] R.P. White and J.E.G. Lipson, Macromolecules **47**, 3959 (2014).

[63] R.P. White and J.E.G. Lipson, ACS Macro Lett. **4**, 588 (2015).

[64] J. Mattsson, J.A. Forrest, and L. Borjesson, Phys Rev E **62**, 5187 (2000).

[65] R.P. White, C.C. Price, and J.E.G. Lipson, Macromolecules **48**, 4132 (2015).

[66] J.A. Forrest and J. Mattsson, Phys Rev E **61**, R53 (2000).

[67] M. Born and E. Wolf, Principles of Optics, 7 ed. (Cambridge University Press, New York, 2006).

[68] R. Seemann, K. Jacobs, K. Landfester, and S. Herminghaus, J Polym Sci, Part B: Polym Phys **44**, 2968 (2006).

[69] S. Kawana and R.A.L. Jones, Phys Rev E **63**, 021501 (2001).

[70] S. Kim, S.A. Hewlett, C.B. Roth, and J.M. Torkelson, Eur Phys J E **30**, 83 (2009).

[71] E.C. Glor and Z. Fakhraai, J Chem Phys **141**, 194505 (2014).

[72] J.L. Keddie and R.A.L. Jones, Israel J Chem **35**, 21 (1995).

[73] J.A. Forrest, K. Dalnoki-Veress, and J.R. Dutcher, Phys Rev E **56**, 5705 (1997).

[74] O.K.C. Tsui and H.F. Zhang, Macromolecules **34**, 9139 (2001).

[75] H. Fujiwara, Spectroscopic Ellipsometry: Principles and Applications (John Wiley & Sons, Ltd., West Sussex, England, 2007).

[76] B. Johs and C.M. Herzinger, Phys. Stat. Sol. (C) **5**, 1031 (2008).

[77] F.A. Jenkins and H.E. White, Fundamentals of Optics, 2nd ed. (McGraw-Hill Book Company, New York, 1950).

[78] C.M. Herzinger, B. Johs, W.A. McGahan, J.A. Woollam, and W. Paulson, J Appl Phys **83**, 3323 (1998).

[79] Note that the values of *A*, *B*, and *C* for the Cauchy equation are typically quoted with the wavelength λ in Eq. (2) calculated in microns, and we have followed this common convention used within the Woollam software.

[80] C.M. Herzinger, P.G. Snyder, F.G. Celii, Y.C. Kao, D. Chow, B. Johs, and J.A. Woollam, J Appl Phys **79**, 2663 (1996).

[81] J.N. Hilfiker, N. Singh, T. Tiwald, D. Convey, S.M. Smith, J.H. Baker, and H.G. Tompkins, Thin Solid Films **516,** 7979 (2008).

[82] G.E. Jellison Jr, Thin Solid Films 313-314, **33** (1998).

[83] H.G. Tompkins, A User's Guide to Ellipsometry (Academic Press, Inc., San Diego, CA, 1993).

[84] D. Beysens and P. Calmettes, J Chem Phys **66**, 766 (1977).

[85] W.B. Li, P.N. Segre, R.W. Gammon, J.V. Sengers, and M. Lamvik, J Chem Phys **101**, 5058 (1994).

[86] E.A. Baker, P. Rittigstein, J.M. Torkelson, and C.B. Roth, J Polym Sci, Part B: Polym Phys **47**, 2509 (2009).

[87] R.K. Krishnaswamy and J. Janzen, Polymer Testing **24**, 762 (2005).

[88] S.Y. Larsen, R.D. Mountain, and R. Zwanzig, J Chem Phys **42**, 2187 (1965).

[89] J.G. Kirkwood, J Chem Phys **4**, 592 (1936).

[90] N.W. Ashcroft and N.D. Mermin, Solid State Physics (Saunders College Publishing, 1976).

[91] D.J. Griffiths, Introduction to Electrodynamics, 3rd ed. (Prentice Hall, New Jersey, 1999).

[92] H.B. Eitouni and N.P. Balsara, in Physical Properties of Polymers Handbook, edited by J.E. Mark, 2nd ed. (Springer, New York, 2007), pp. 339–356.

[93] K.S. Gautam, A.D. Schwab, A. Dhinojwala, D. Zhang, S.M. Dougal, and M.S. Yeganeh, Phys Rev Lett **85**, 3854 (2000).

[94] A.D. Curtis, S.B. Reynolds, A.R. Calchera, and J.E. Patterson, J Phys Chem Lett **1**, 2435 (2010).

[95] A.D. Curtis, A.R. Calchera, M.C. Asplund, and J.E. Patterson, Vibrational Spectroscopy **68**, 71 (2013).

[96] J.L. Lenhart, D.A. Fischer, T.L. Chantawansri, and J.W. Andzelm, Langmuir **28**, 15713 (2012).

[97] J.E. Pye and C.B. Roth, Macromolecules **46**, 9455 (2013).

[98] H. Looyenga, Molecular Physics **9**, 501 (1965).

[99] H. Looyenga, Physica **31**, 401 (1965).

[100] H. Looyenga, Journal of Polymer Science: Polymer Physics Edition 11, 1331 (1973).

[101] M.L. Fernandez, J.S. Higgins, J. Penfold, and C.S. Shackleton, Polym Commun **31**, 124 (1990).

[102] G. Reiter, Europhys Lett **23**, 579 (1993).

[103] J. Brandrup, E.H. Immergut, E.A. Grulke, A. Abe, and D.H. Bloch, editors, Polymer Handbook, 4 ed. (Wiley: New York, 1999).

Chapter 4

Optimizing the Grafting Density of Tethered Chains to Alter the Local Glass Transition Temperature of Polystyrene near Silica Substrates: the Advantage of Mushrooms over Brushes

A version of this chapter was published as Xinru Huang and Connie B. Roth, *ACS Macro Letters* **7**, 269 - 274, 2018.

4.1 Synopsis

We measured the local glass transition temperature $T_g(z)$ of polystyrene (PS) as a function of distance z from a silica substrate with end-grafted chains using fluorescence, where competing effects from the free surface have been avoided to focus only on the influence of the tethered interface. The local $T_g(z)$ increase next to the chain-grafted substrate is found to exhibit a maximum increase of 49 ± 2 K relative to bulk at an optimum grafting density that corresponds to the mushroom-to-brush transition regime. This perturbation to the local $T_g(z)$ dynamics of the matrix is observed to persist out to a distance $z \approx 100 - 125$ nm for this optimum grafting density before bulk T_g is recovered, a distance comparable to that previously observed by Baglay and Roth [*J. Chem. Phys.* **2017**, *146*, 203307] for PS next to the higher-T_g polymer polysulfone.

4.2 Introduction

Direct interrogation of how end-tethered chains affect the local properties of a neighboring polymer matrix has been little studied but widely utilized to alter adhesion and lubrication, and improve matrix reinforcement in polymer nanocomposites.[1-7] There are few local experimental techniques that can interrogate material properties next to such buried interfaces, usually leaving local properties to be inferred from global macroscopic measurements or investigated by theoretical and simulation methods.[2,8,9] The influence tethered chains can have on the neighboring matrix is complicated by various interconnected parameters such as grafting density, surface coverage, tethered-chain length, matrix interpenetration, and substrate curvature, with the macroscopic properties of nanocomposites being further affected by the filler content and dispersion.[6,7] Studies on thin films provide an accessible planar geometry where the grafting density can be well controlled, serving as a simplified system to mimic polymer nanocomposites.[10-12] However, most thin-film studies investigating substrates with grafted chains are additionally affected by the competing effects of the free surface.[13-21] Here, we purposely avoid such competing effects of the free surface and experimentally map the local glass transition temperature $T_g(z)$ as a function of distance from a tethered-chain interface using a localized fluorescence method.

Studies of the average glass transition temperature $T_g(h)$ of thin polystyrene (PS) films with substrate-grafted chains date back to Keddie and Jones in 1995.[13] Over the years studies have reported both increases[14,15,18] and decreases[16] in the average $T_g(h)$ value relative to films of equivalent thickness h with no grafted chains. Generally, these changes are only observed for

very thin films $h \lesssim 30$ nm and can be sufficiently small to appear as effectively no change.[19] Recently, Hénot et al.[19] have made great efforts to compare and correlate different studies based on the grafting density and ratio of matrix-to-grafted chain lengths, ultimately concluding that the grafted chains have little to no effect on the measured average film $T_g(h)$. However, such measurements are complicated by the presence of a strong, and potentially dominating, free surface effect. Lan and Torkelson used fluorescence to measure the local T_g of grafted chains within a thin film, finding large variations in local T_g within the films with increases as high as ~35 K near the substrate, while the near free surface region was reduced by ~15 K.[17] This large variation in local T_g within the film suggests there is strong competition between free surface and chain-tethered substrate effects such that much benefit would be gained from isolating only the impact of the chain-tethered substrates.

4.3 Experimental Methods

In the present work, we have created a sample geometry that allows us to measure the local glass transition temperature $T_g(z)$ as a function of distance from an end-grafted PS substrate. End-grafted polystyrene substrates were created by spin-coating a film of monocarboxy-terminated polystyrene (PS-COOH) (M_w = 101.8 kg/mol, M_w/M_n = 1.03) onto either silicon wafers or silica substrates cleaned by washing in ~10 vol% hydrochloric acid for 20 s. These films were annealed under vacuum at 170 ^oC for 1.5 h to establish covalent bonding between PS-COOH and Si-OH, and then washed in a 90 ^oC toluene bath for 20 min to remove any ungrafted chains and subsequently rinsed in acetone and DI water, dried with nitrogen gas, and annealed overnight in a vacuum oven at room temperature, a procedure following previous works.[13-15]

The final dry-brush thickness h_{brush} was measured by ellipsometry (Woollam M-2000) for those samples made on silicon wafers modeling the PS layer with a standard Cauchy model $n(\lambda) = A + B/\lambda^2 + C/\lambda^4$, fitting A and B with C held at the bulk value, and including a 1.25 nm native oxide layer for the silicon substrate.[22] The grafting density σ was calculated as $\sigma = \frac{\rho N_A h_{brush}}{M_n}$,[23] where ρ = 1.045 g/cm^3 was taken to be the bulk density of PS;[24] N_A is Avogadro's number; and M_n is the PS-COOH number-average molecular weight.

Multilayer samples as depicted in Figures 4.1 and 4.3 were then assembled by floating on additional PS layers of known thickness made from either neat PS (M_w = 1920 kg/mol, M_w/M_n = 1.26) or pyrene-labeled PS (M_w = 672 kg/mol, M_w/M_n = 1.3, with 1.4 mol% pyrene[25,26]). The dry-brush layer and first PS layer floated atop were annealed separately at 170 ^oC for 2 h to ensure good interpenetration of the tethered chains with the neighboring PS matrix.[27,28] Prior to the fluorescence measurements, the entire multilayer stack was annealed at 170 ^oC for 20 min to consolidate the stack into a single material but keep the pyrene-labeled layer localized, as well as remove thermal history of the sample before $T_g(z)$ was measured. In some samples, the PS-pyrene layer was also lightly cross-linked using UV light to limit diffusion at such high temperatures (see Appendix of Chapter 4). Following our previous works,[25,26,29] pyrene fluorescence emission at 379 nm was monitored on cooling at 1 ^oC/min for 3 s every 27 s while exciting at 330 nm (band passes 5-6 nm). The local $T_g(z)$ was determined by the change in slope of the temperature-dependence of the fluorescence intensity, as established by Torkelson and co-workers,[30-32] a value that has been shown to agree well with the change in thermal expansion coefficient by ellipsometry and differential scanning calorimetry (DSC) in bulk.

4.4 Results and Discussion

Figure 4.1 compares the local $T_g(z = 0)$ next to end-tethered substrates as a function of grafting density σ. The multilayer samples assembled for this place the 12 ± 1 nm pyrene-labeled layer directly next to the dry-brush layer, which were then separately annealed together such that the pyrene-labeled chains become well intermixed with the tethered chains. A 590 ± 5 nm bulk neat PS layer is then added to avoid competing effects from the free surface. Thus, the $T_g(z = 0)$ value being reported here is for a (12 nm + h_{brush}) layer next to the silica substrate. When no chains are grafted to the substrate, the 12-nm pyrene-labeled layer reports a $T_g(z = 0)$ = 101 ± 2 ^oC, equal to the bulk value for PS and in agreement with that previously measured by Ellison and Torkelson.[30] In contrast, with the addition of end-tethered chains to the substrate, the local $T_g(z = 0)$ is increased dramatically: for σ = 0.011 chains/nm^2 (h_{brush} = 1.7 ± 0.2 nm), $T_g(z = 0)$ = 150 ± 2 ^oC; σ = 0.042 chains/nm^2 (h_{brush} = 6.6 ± 0.2 nm), $T_g(z = 0)$ = 143 ± 2 ^oC; where these values represent the average of multiple samples. These increases in local $T_g(z = 0)$ appear large given previous reports on end-grafted PS films,[13-16,18,19] but in those studies competing free surface effects were also present. In the current study, the addition of the top bulk neat PS layer allows us to isolate only the effect of the end-tethered substrate.

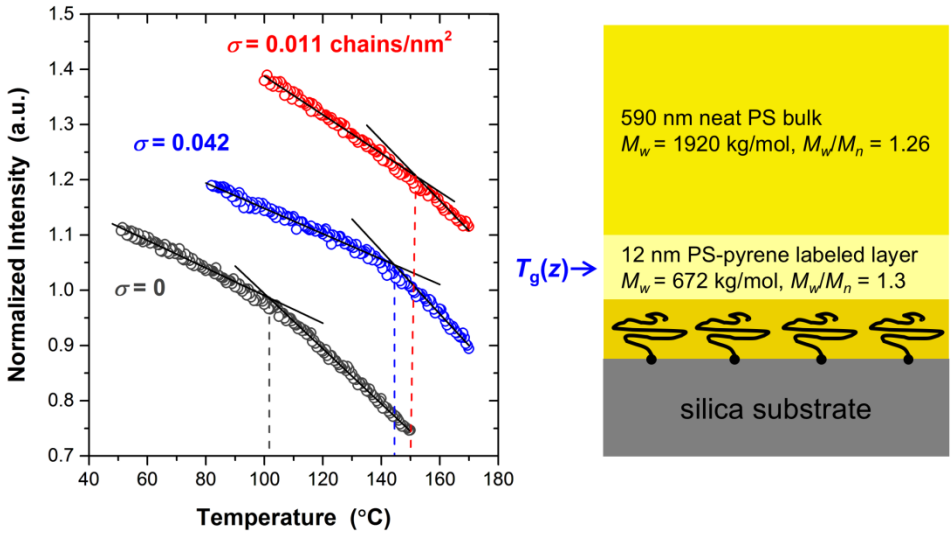

Figure 4.1. Sample geometry used to measure the local $T_g(z = 0)$ next to end-tethered substrates with different grafting densities σ, where the temperature-dependent fluorescence intensity curves show large increases in this local T_g value.

In Figure 4.2, we plot this $T_g(z = 0)$ value measured next to end-tethered substrates as a function of grafting density. We observe a maximum $T_g(z = 0)$ increase at σ = 0.011 chains/nm^2 (h_{brush} = 1.7 ± 0.2 nm) suggesting an optimum grafting density exists for greatest T_g reinforcement of the PS matrix. This result may seem surprising initially but makes sense if one considers the limits at low and high grafting density. Clearly at σ = 0, we must recover bulk T_g of PS, as has been previously demonstrated[30] for this noninteracting substrate. At extremely high grafting densities, the tight chain packing of the tethered chains in the true brush regime will limit interpenetration of the free (untethered) matrix chains,[33,34] resulting in a decrease in the measured $T_g(z)$ of the neighboring PS matrix as the two become decoupled. For example, the recent study by Lan and Torkelson[17] measured the local T_g of pyrene-labeled PS brushes made by a "grafting from" technique that results in much higher grafting densities. Their closest

measurement to our current study is the local T_g of an 11-nm thick brush with $\sigma = 0.3$ chains/nm^2 covered with a 101-nm thick neat PS overlayer resulting in a local $T_g \approx 126$ ^oC for the brush chains next to the silica substrate. This value is consistent with our data presented in Figure. 4.2a if we were to extrapolate an estimate out to this value of σ that is an order of magnitude larger than our largest σ.

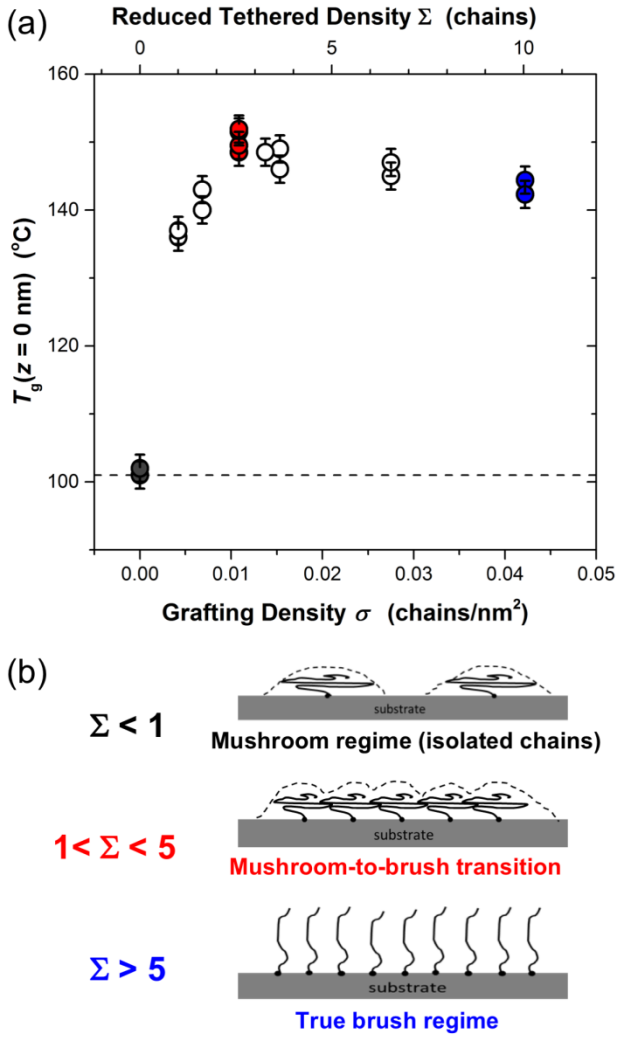

Figure 4.2. (a) Local $T_g(z = 0)$ measured next to end-tethered substrates as a function of grafting density σ (bottom axis) and reduced tethered density Σ (top axis). (b) Cartoon illustrating the

three different regimes associated with increasing Σ as the tethered chains go from isolated mushrooms to highly stretched brushes.

A better measure of how much end-tethered chains cover a substrate is the reduced tethered density $\Sigma = \pi R_g^2 \sigma$,[23,35,36] which multiplies the grafting density σ (chains/nm^2) by the projected area of the surface (πR_g^2) each tethered chain nominally covers, where the radius of gyration R_g = 8.7 nm for our molecular weight.[37] This enables characterization of the grafted surface into different regimes. Values of Σ < 1 refer to the "mushroom" regime where the chains are still predominately isolated, while the "true brush" regime where the grafting density is high enough for chains to become highly stretched is generally observed for Σ > 5.[23,35] The mushroom-to-brush transition regime where the conformations of neighboring chains begin overlapping happens between 1 < Σ < 5, the precise onset of which can vary somewhat from system to system.[23,35,36] Interestingly, we observe that the optimum grafting density σ = 0.011 chains/nm^2 that shows the maximum $T_g(z = 0)$ increase occurs at a value of Σ = 2.6, near the middle of the mushroom-to-brush transition (well within the "wet" brush regime $\sigma\sqrt{N} < 1$).[38,39] It is worth noting that nearly all previous studies that have investigated T_g changes in thin films due to grafted chains are very close to or well within the true brush regime, $\Sigma \gtrsim 5$,[13-19] with the general belief being that higher grafting density should lead to larger effects.[19] Our results suggest more is not necessarily better and that a lower grafting density can lead to a higher T_g increase. However, we caution that blindly applying this reasoning to polymer nanocomposites may cause additional complications, as low grafting densities often lead to increased nanoparticle aggregation.[6]

The extent to which end-tethered chains can interpenetrate into a matrix depends not only on the grafting density but also on the relative difference in molecular weight between the tethered and matrix chains. For the case of a polymer melt where the brush is chemically identical to the matrix, the scaling behavior of the penetration length L over which the end-tethered chains extend from the substrate has been well studied.[33,34] For our case where the matrix chain length P is larger than the tethered chain length N, the tethered chains retain their ideal conformation from the mushroom regime all the way up to the beginning of the true brush regime such that $L \sim N^{1/2}$. This means that within the mushroom-to-brush transition regime, as the grafting density increases, the number of matrix chains P that interpenetrate into the brush region L decreases continuously, while the tethered chains retain their ideal conformation. Finally at the start of the true brush regime, little interpenetration will occur when the tethered chains must finally stretch beyond their ideal chain conformations to accommodate further increases in grafting density. We can estimate the amount of chain interpenetration present for our optimum grafting density $\sigma = 0.011$ chains/nm^2 by comparing the initial dry brush thickness ($h_{\text{brush}} = 1.7 \pm 0.2$ nm) to the penetration length L. For an ideal chain conformation, we estimate $L \approx 2R_g \approx 17$ nm, giving a volume fraction $\phi = \frac{h_{\text{brush}}}{L} \approx 0.1$ for the tethered chains within this layer L near the substrate. This estimate for L is consistent with theoretical calculations by Matsen and Gardiner[38] where an extrapolation down to our grafting density gives a value of ≈ 18 nm. In addition, neutron reflectivity profiles by Clarke[27] for deuterated PS-COOH tethered chains (M_w = 79.8 kg/mol) with grafting density $\sigma \approx 0.074$ chains/nm^2 in a hydrogenated PS matrix (M_w = 500.8 kg/mol or 8000 kg/mol) show the volume fraction depth profile for the grafted chains extending out to ≈ 18-20 nm.

What seems surprising is that the observed maximum increase in $T_g(z = 0)$ occurs when only ~10% of this near substrate region is comprised of tethered chains. Little is known about how tethered chains would cause an increase in T_g. The closest theoretical efforts are those that have tried to account for attractive substrate interactions. For example, Long and Lequeux[40] developed a percolation model of the glass transition that defined T_g based on when dynamically slow regions percolate across the sample, envisioning that attractive substrate interactions increased the fraction of slow regions. Lipson and Milner[41] developed this idea into a more detailed picture of how a profile in local $T_g(z)$ increase would look near substrates with attractive interactions, a prediction that is qualitatively consistent with our experimental observations shown below. Within such a framework one could imagine how a few extra slow domains that included segments of chains tethered to the substrate could have a large influence on such a percolation rigidity transition. However, chain connectivity is not typically associated with the glass transition. The molecular weight dependence of $T_g(M_n)$ saturates to ≈100 ^oC for PS at $M_n \approx$ 20 kg/mol,[42,43] which has been correlated with when chain dynamics asymptotically display Gaussian behavior,[44,45] as local chain flexibility near free chain ends is different. This suggests that tethered chain ends may in a similar fashion alter local mobility of the chain influencing local T_g. Experimentally, recent studies by Foster et al.[46,47] have shown that substrate tethered chains can significantly slow surface relaxation times of PS films, even when films include substantial amounts of untethered matrix chains, which likely results from the increased entropic penalty to stretch tethered chains.[48,49]

Figure 4.3 addresses how far this strong perturbation to local T_g near the end-tethered substrate propagates into the neighboring polymer matrix. To locally measure $T_g(z)$ as a function

of distance from the substrate, we insert a high molecular weight neat PS spacer layer of thickness $z = 0 – 250$ nm between the dry brush and 12-nm thick pyrene-labeled PS layer. Again to ensure good interpenetration of the grafted chains with the PS matrix, while still avoiding diffusion of the pyrene-labeled layer, the PS z-layer and dry brush were separately annealed at 170 ^{o}C for 2 h prior to floating on the remaining layers. Figure 4.3 plots the local $T_g(z)$ measured as a function of distance from the end-tethered substrate for the optimum and maximum grafting densities shown in Figure 4.2. We also include data for $T_g(z)$ with zero grafting density that confirms no T_g increase is observed for PS next to bare silica. To accommodate the slight differences in dry brush thickness h_{brush} with increasing grafting density, we defined the distance from the interface (x-axis of Figure 4.3) as $z + h_{brush}$, although this correction is minor on the scale of Figure 4.3. For both grafting densities shown, the $T_g(z)$ perturbation is observed to propagate far from the interface ($z \sim 100$ nm) before bulk T_g is recovered, a distance much larger than the end-tethered chains extend from the substrate, $L \approx 2\ R_g \approx 17$ nm. Interestingly, the $T_g(z)$ perturbation for the optimum grafting density $\sigma = 0.011$ chains/nm^2, which gave the maximum $T_g(z = 0)$ in Figure 4.2, appears to influence the PS matrix out to a somewhat greater distance ($z \approx 100$-125 nm) from the interface, compared with that ($z \approx 75$-100 nm) for the higher grafting density of $\sigma = 0.042$ chains/nm^2.

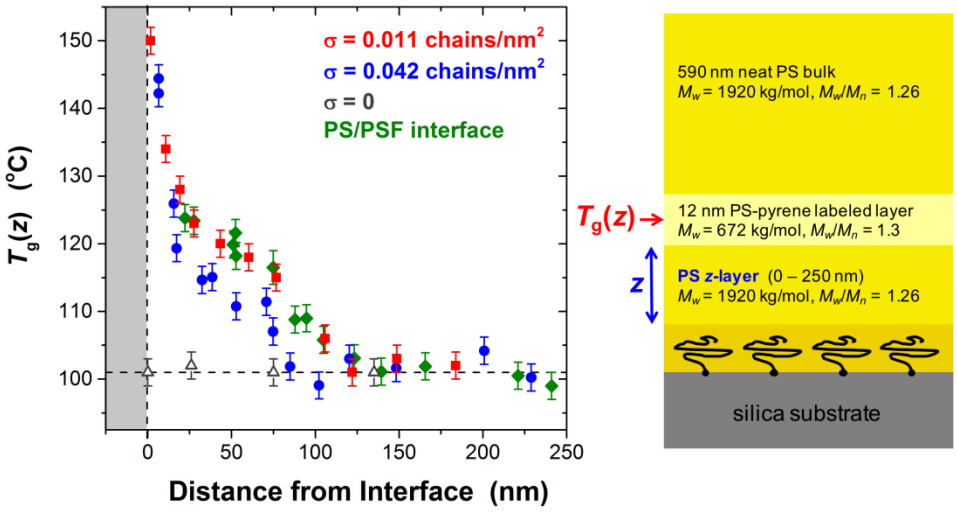

Figure 4.3. Local $T_g(z)$ profiles extending from end-tethered substrates for grafting densities σ = 0.011 chains/nm^2 (red squares) and σ = 0.042 chains/nm^2 (blue circles), as well as for substrates with no grafted chains (σ = 0, gray triangles). For comparison, data from Baglay and Roth[26] for the $T_g(z)$ profile in PS next to polysulfone (PSF, T_g^{PSF} = 186 °C) are shown as green diamonds.

For comparison, Figure 4.3 also includes data from Baglay and Roth[26] for the $T_g(z)$ profile measured in PS next to a polymer-polymer interface with polysulfone (PSF). As the bulk T_g of PSF (T_g^{PSF} = 186 °C) is much higher than that of PS, this polymer-polymer interface is somewhat analogous to that of the end-tethered silica interface studied in the present work. Figure 4.3 shows that the $T_g(z)$ profile in PS next to the PS/PSF interface is comparable to that observed in PS next to the end-tethered silica substrate at the optimum grafting density of σ = 0.011 chains/nm^2. In their paper, Baglay and Roth[26] discussed three possible differences for why dissimilar polymer-polymer interfaces may show such long-range $T_g(z)$ perturbations, in contrast to a polymer-free surface: increased breadth of the interfacial width, chain connectivity across the interface, and increased interfacial roughness. The results of the present study suggest that

chain connectivity may play the dominant role in causing such long-ranged $T_g(z)$ perturbations, with factors such as interfacial breadth[50] and substrate roughness[51,52] having more limited effects.

4.5 References

[1] S.T. Milner, Science **251**, 905 (1991).

[2] L.S. Schadler, S.K. Kumar, B.C. Benicewicz, S.L. Lewis, and S.E. Harton, MRS Bull. **32**, 335 (2007).

[3] A. Bansal, H. Yang, C. Li, R.C. Benicewicz, S.K. Kumar, and L.S. Schadler, J. Polym. Sci. Part B Polym. Phys. **44**, 2944 (2006).

[4] H. Oh and P.F. Green, Nat. Mater. **8**, 139 (2009).

[5] D. Maillard, S.K. Kumar, B. Fragneaud, J.W. Kysar, A. Rungta, B.C. Benicewicz, H. Deng, L.C. Brinson, and J.F. Douglas, Nano Lett. **12**, 3909 (2012).

[6] S.K. Kumar, N. Jouault, B. Benicewicz, and T. Neely, Macromolecules **46**, 3199 (2013).

[7] S.K. Kumar, V. Ganesan, and R. A. Riggleman, J. Chem. Phys. **147**, 020901 (2017).

[8] A.P. Holt, V. Bocharova, S. Cheng, A.M. Kisliuk, B.T. White, T. Saito, D. Uhrig, J.P. Mahalik, R. Kumar, A.E. Imel, T. Etampawala, H. Martin, N. Sikes, B.G. Sumpter, M.D. Dadmun, and A.P. Sokolov, ACS Nano **10**, 6843 (2016).

[9] L.M. Hall, A. Jayaraman, and K.S. Schweizer, Curr. Opin. Solid State Mater. Sci. **14**, 38 (2010).

[10] A. Bansal, H.C. Yang, C.Z. Li, K.W. Cho, B.C. Benicewicz, S.K. Kumar, and L.S. Schadler, Nat. Mater. **4**, 693 (2005).

[11] P. Rittigstein, R.D. Priestley, L.J. Broadbelt, and J.M. Torkelson, Nat. Mater. **6**, 278 (2007).

[12] J.M. Kropka, V. Pryamitsyn, and V. Ganesan, Phys. Rev. Lett. **101**, 075702 (2008).

[13] J.L. Keddie and R.A.L. Jones, Isr. J. Chem. **35**, 21 (1995).

[14] R.S. Tate, D.S. Fryer, S. Paqualini, M.F. Montague, J.J. De Pablo, and P.F. Nealey, J. Chem. Phys. **115**, 9982 (2001).

[15] A. Clough, D. Peng, Z. Yang, and O.K.C. Tsui, Macromolecules **44**, 1649 (2011).

[16] H. Lee, H. Ahn, S. Naidu, B.S. Seong, D.Y. Ryu, D.M. Trombly, and V. Ganesan, Macromolecules **43**, 9892 (2010).

[17] T. Lan and J.M. Torkelson, Polym. **64**, 183 (2015).

[18] B. Zuo, S. Zhang, C. Niu, H. Zhou, S. Sun, and X. Wang, Soft Matter **13**, 2426 (2017).

[19] M. Hénot, A. Chennevière, E. Drockenmuller, K. Shull, L. Léger, and F. Restagno, Eur. Phys. J. E **40**, 11 (2017).

[20] O.K.C. Tsui, T.P. Russell, and C.J. Hawker, Macromolecules **34**, 5535 (2001).

[21] N. Neubauer, R. Winkler, M. Tress, P. Uhlmann, M. Reiche, W.K. Kipnusu, and F. Kremer, Soft Matter **11**, 3062 (2015).

[22] X. Huang and C.B. Roth, J. Chem. Phys. **144**, 234903 (2016).

[23] W.J. Brittain and S. Minko, J. Polym. Sci. Part A Polym. Chem. **45**, 3505 (2007).

[24] R.A. Orwoll, Densities, *Coefficients of Thermal Expansion, and Compressibilities of Amorphous Polymers*, Physical Properties of Polymers Handbook, J.E. Mark, Springer, New York (2007).

[25] R.R. Baglay and C.B. Roth, J. Chem. Phys. **143**, 111101 (2015).

[26] R.R. Baglay and C.B. Roth, J. Chem. Phys. **146**, 203307 (2017).

[27] C.J. Clarke, Polym. **37**, 4747 (1996).

[28] K.P. O'Connor and T.C.B. McLeish, Macromolecules **26**, 7322 (1993).

[29] P.M. Rauscher, J.E. Pye, R.R. Baglay, and C.B. Roth, Macromolecules **46**, 9806 (2013).

[30] C.J. Ellison and J.M. Torkelson, Nat. Mater. **2**, 695 (2003).

[31] C.J. Ellison, M.K. Mundra, and J.M. Torkelson, Macromolecules **38**, 1767 (2005).

[32] S. Kim, S. A. Hewlett, C.B. Roth, and J.M. Torkelson, Eur. Phys. J. E **30**, 83 (2009).

[33] M. Aubouy, G.H. Fredrickson, P. Pincus, and E. Raphael, Macromolecules **28**, 2979 (1995).

[34] R.A.L Jones and R.W. Richards, *Polymer at Surfaces and Interfaces*, Cambridge University Press (1999).

[35] M.S. Kent, Macromol. Rapid Commun. **21**, 243 (2000).

[36] S.Z.D. Cheng, *Phase Transitions in Polymers: the Role of Metastable States*, Elsevier Science, Oxford, UK (2008).

[37] L.J. Fetters, N. Hadjichristidis, J.S. Lindner, and J.W. Mays, J. Phys. Chem. Ref. Data, **23**, 619 (1994).

[38] M.W. Matsen and J.M. Gardiner, J. Chem. Phys. **115**, 2794 (2001).

[39] Note, Σ is an experimental parameter whose definition is based on the theoretical scaling that mushrooms begin to overlap when the average distance between grafting sites $\sigma^{-½} \approx R_g$.[1,33,34] This is in contrast to other definitions of normalized grafting density[15] more commonly used in the theoretical literature that scale σ about the transition point from a "wet" screened (unstretched) brush to a "dry" (stretched) "true" brush at $\sigma \approx N^{-½}$.[33,34] According to self-consistent field theory calculations by Matsen and Gardiner,[38] our largest grafting density σ = 0.042 chains/nm^2 should still be within the "wet" brush regime with $\frac{\sigma N^{½}}{a\,\rho_0} \leq 0.32$.

[40] D. Long and F. Lequeux, Eur. Phys. J. E **4**, 371 (2001).

[41] J.E.G. Lipson and S.T. Milner, Eur. Phys. J. B **72**, 133 (2009).

[42] P.G. Santangelo and C.M. Roland, Macromolecules **31**, 4581 (1998).

[43] T.G. Fox and P.J. Flory, J. Polym. Sci. **14**, 315 (1954).

[44] Y. Ding, A. Kisliuk, and A.P. Sokolov, Macromolecules **37**, 161 (2004).

[45] S. Mirigian and K.S. Schweizer, Macromolecules **48**, 1901 (2015).

[46] G. Uğur, B. Akgun, Z. Jiang, S. Narayanan, S. Satija, and M.D. Foster, Soft Matter **12**, 5372 (2016).

[47] B. Akgun, G. Uğur, Z. Jiang, S. Narayanan, S. Song, H. Lee, W.J. Brittain, H. Kim, S.K. Sinha, and M.D. Foster, Macromolecules **42**, 737 (2009).

[48] G.H. Fredrickson, A. Ajdari, L. Leibler, and J.P. Carton, Macromolecules **25**, 2882 (1992).

[49] H. Xi and S.T. Milner, Macromolecules **29**, 4772 (1996).

[50] S. Mirigian and K.S. Schweizer, J. Chem. Phys. **146**, 203301 (2017).

[51] P.Z. Hanakata, J.F. Douglas, and F.W. Starr, Nat. Commun. **5**, 4163 (2014).

[52] P.Z. Hanakata, B.A. Pazmiño Betancourt, J.F. Douglas, and F.W. Starr, J. Chem. Phys. **142**, 234907 (2015).

Appendix of Chapter 4

Sample Preparation and Measurement Details

Following procedures previously established in the literature,[1-3] monocarboxy-terminated polystyrene (PS-COOH) (M_w = 101.8 kg/mol, M_w/M_n = 1.03, Scientific Polymer Products) was end-grafted to silicon wafers or silica substrates by spin-coating PS-COOH films from toluene and annealing them under vacuum at 170 ^oC for 1.5 h. The grafting process should be the same for these two types of substrates as their surfaces are both terminated with SiO_x. Prior to grafting, the substrates were cleaned in ~10 vol% hydrochloric acid for 20 s to remove any impurities. After annealing, samples were bathed in 90 ^oC toluene for 20 min to wash off ungrafted chains, and subsequently rinsed with acetone and DI water, while being blown dry with nitrogen gas after each step. A final drying step was done by placing the grafted substrates in the vacuum oven overnight at room temperature. Samples with different grafting densities were produced by decreasing the initial film thickness of the spin-coated PS-COOH films and mixing with neat polystyrene (PS) (M_w = 101.3 kg/mol, M_w/M_n = 1.04, Scientific Polymer Products). The final dry-bush thickness h_{brush} was measured by ellipsometry (Woollam M-2000) for those samples made on silicon wafers. There is insufficient contrast in the index of refraction between PS and silica to accurately measure such thin films directly on the silica substrates used for fluorescence. Ellipsometer data fitting was done using a standard layer model with the PS film treated as a Cauchy layer $n(\lambda) = A + B/\lambda^2 + C/\lambda^4$, and the underlying silicon wafer having a 1.25 nm native oxide layer. Following our previous work, such thin films were fit to the PS film thickness, A and B, while holding the Cauchy parameter C fixed at the bulk value 0.00038.[4] The

grafting density σ was calculated using $\sigma = \frac{\rho N_A h_{brush}}{M_n}$,[5] where the number average molecular weight M_n = 98.8 kg/mol for the PS-COOH, and the density ρ = 1.045 g/cm^3 was taken as the bulk value for PS.[6] Measured dry brush thicknesses h_{brush} varied from 0.7 to 6.6 nm giving grafting densities σ from 0.004 to 0.042 chains/nm^2 (Σ = 1.0 to 10).

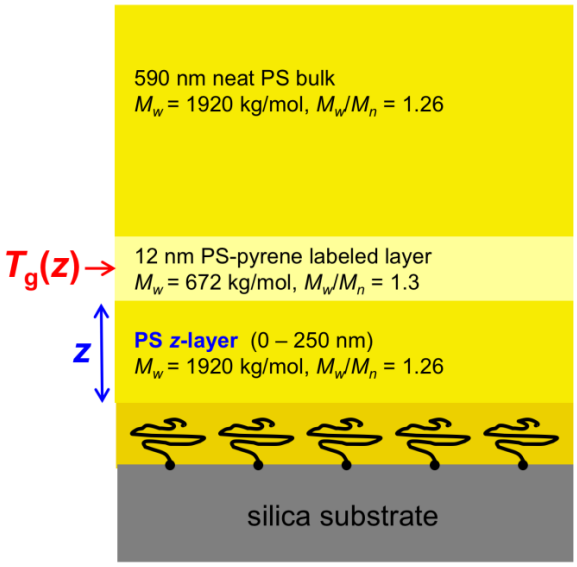

Figure 4.S1. Schematic of multilayer sample geometry assembled for fluorescence measurements of the localized glass transition temperature $T_g(z)$ as a function of distance z from end-tethered substrates.

Neat PS (M_w = 1920 kg/mol, M_w/M_n = 1.26, Pressure Chemical) of variable thickness z = 0 to 250 nm, and bulk 590 ± 5 nm thick, or 12 ± 1 nm thick pyrene-labeled PS (M_w = 672 kg/mol, M_w/M_n = 1.3, with 1.4 mol% pyrene[7,8]) films were spin-coated from toluene onto freshly-cleaved mica. All such layers were independently annealed overnight at 120 °C under vacuum prior to floating. Multilayer sample structures, as depicted in Figure 4.S1, were

assembled by first floating the neat PS layer of desired thickness *z* atop the PS-COOH end-grafted silica substrates. This bilayer was then annealed under vacuum at 170 ^{o}C for 2 h to ensure good interpenetration of the tethered chains with the neighboring PS matrix. O'Connor and McLeish[9] argued that for relatively low grafting densities, isolated tethered chains can rapidly penetrate into high molecular weight matrices (or even cross-linked elastomers) via Rouse mode and "breathing" mode (chain-end) relaxations. This was experimentally confirmed by Clarke[10] using neutron reflectivity to measure the interpenetration of deuterated PS-COOH (M_w = 79.8 kg/mol, M_w/M_n = 1.04) end-tethered chains into matrices of high molecular weight protonated PS of M_w = 500.8 kg/mol (M_w/M_n = 1.06) or M_w = 8,000 kg/mol (M_w/M_n < 1.07). For grafting densities of σ = 0.074 chains/nm^2, even 15 min of annealing at 150 ^{o}C was sufficient to obtain a depth profile for the dPS-COOH chains that did not change substantially with further annealing up to 23 h. After this initial annealing step of the bilayer structure, the 12-nm pyrene-labeled PS layer and neat bulk PS layer were subsequently floated on, allowing the sample to thoroughly dry between each successive floating step.

Fluorescence measurements were carried out using a Photon Technology International QuantaMaster spectrofluorometer with samples mounted in an Instec HCS402 heater. Samples were heated from room temperature to 170 ^{o}C and equilibrated for 20 min. This allows the assembled multilayer samples to form a consolidated material with sufficient interdiffusion at the floated interfaces to remove any air gaps. The pyrene fluorescence emission is then monitored on cooling at 1 ^{o}C/min for 3 s every 27 s at an emission wavelength of 379 nm, while exciting at 330 nm (with band passes kept between 5-6 nm). All samples were reheated to the starting temperature after each run to ensure that the same initial fluorescence intensity was recovered,

verifying that the sample had remained stable during the course of the experiment and no photobleaching occurred. The local $T_g(z)$ is then determined from the temperature-dependent fluorescence intensity by fitting straight lines to the slope of the intensity data above and below the transition to identify the intersection of the two fits. Data collected on multiple samples allows us to determine the local $T_g(z = 0)$ value next to the substrate for different grafting densities, as well as the $T_g(z)$ profile as a function of distance from the substrate. Figure 4.S2 plots such temperature-dependent fluorescence intensity data for three different samples all with the same grafting density of $\sigma = 0.042$ chains/nm^2, where the thickness of the z-layer spacer was varied to determine the local $T_g(z)$ value at different distances from the substrate: $T_g(z = 0) = 144 \pm 2$ ^oC, $T_g(z = 32$ nm$) = 115 \pm 2$ ^oC, and $T_g(z = 222$ nm$) = 100 \pm 2$ ^oC. Figure 4.S3 shows the $T_g(z)$ profile for $\sigma = 0.042$ chains/nm^2 constructed from measurements on multiple samples. To accommodate the dry-brush thickness $h_{brush} = 6.6$ nm for $\sigma = 0.042$ chains/nm^2, the distance from the grafted substrate (x-axis of Fig. S3) was taken to be equal to the thickness of the z spacer layer plus 6.6 nm.

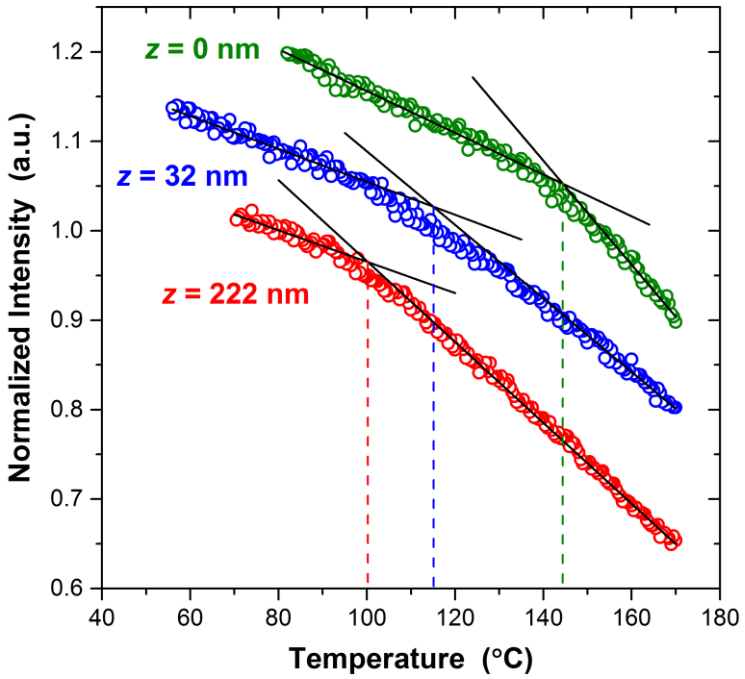

Figure 4.S2. Fluorescence intensity versus temperature measured on cooling at 1 ^{o}C/min for three samples with a grafting density of $\sigma = 0.042$ chains/nm^2, where the pyrene-labeled layer was placed at different distances $z = 0$, 32, and 222 nm.

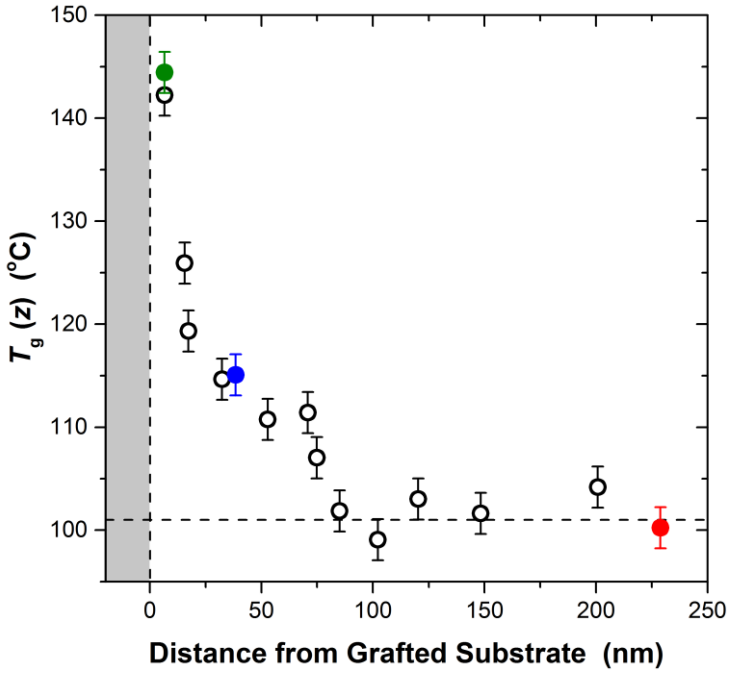

Figure 4.S3. Local $T_g(z)$ profile measured for end-tethered substrates with a grafting density of $\sigma = 0.042$ chains/nm^2. The distance from the substrate (x-axis) was taken to be $z + 6.6$ nm to accommodate the thickness of the dry brush. The three colored data points correspond to the datasets shown in Figure 4.S2.

One of the keys to making these localized fluorescence measurements is the use of high molecular weight polymers to limit the diffusion of the pyrene-labeled probe layer during the course of the measurement. Sufficient annealing needs to be done initially to weld the various interfaces of the assembled layers together to create a single consolidated material without any air gaps. This occurs quickly via Rouse modes with interfacial widths of a few nanometers easily formed after a few minutes; further diffusion and growth of the interface is then limited by the reptation time.[11-13] Typically, the amount of time necessary to collect data at elevated temperatures above T_g is sufficiently small such that simply the use of high molecular weight polymers adequately limits the diffusion of the thin pyrene-labeled layer away from its localized position.[7,8,14] However, for the present study, we measured elevated local $T_g(z)$ values around 140-150 ^oC, necessitating data collection far enough above the transition to accurately identify the slope of the liquid regime. Given the strong temperature dependence of polymer reptation times, we decided to lightly crosslink the pyrene-labeled PS layer to further ensure that it would remain localized even at these elevated temperatures. Very few crosslinks would be necessary to arrest diffusion, which can be accomplished at a level of crosslink density much less than the entanglement density, and as such have no impact on the glass transition of the material.

The use of ultra-violet (UV) light to crosslink polystyrene has been employed frequently in the literature. Commonly a UV-ozone treatment is done that utilizes two UV wavelengths,

185 nm that dissociates molecular oxygen leading to the generation of ozone and 254 nm that is absorbed directly by the phenyl ring of PS.[15,16] The oxygen reaction with the phenyl rings of PS occurs rapidly (<5 min) resulting in the formation of a more polar surface containing carbonyl and carboxyl species, but its effects are generally limited to the near surface region (≈5 nm) because of the limited ability of oxygen to penetrate into the film.[15-17] In contrast, crosslinking by only the 254 nm UV light is a much slower process that can take several hours and penetrates much deeper into the film (~1 μm).[17-19] To minimize chemical changes, we use only the 254 nm UV wavelength for a time and intensity that enacts a minimum of crosslinks. Solvent swelling tests were used to confirm that the 254 nm UV exposure did lead to a crosslinked film, while several control measurements described below were carried out with fluorescence to ensure that the UV exposure did not harm the pyrene dye and affect the accuracy of the T_g fluorescence measurement. The 254 nm wavelength is close the absorption maximum for the phenyl ring of PS,[15] while pyrene primarily absorbs at longer wavelengths because of its larger resonance structure. Thus, predominantly only a handful of PS phenyl rings are being affected by this UV process.

During the sample preparation described above, the 12-nm pyrene-labeled layer was lightly crosslinked by exposing it to a UV lamp (UVP compact UV lamp, model UVG-11) with a 254 nm wavelength prior to floating off the mica surface. A UV exposure of 10 min with the lamp located at a distance of 16 mm from the film's surface was found to be sufficient to prevent diffusion and stabilize the pyrene-labeled PS layer to extended annealing times at 170 ^{o}C. The pyrene fluorescence emission spectrum is generally unaffected by this UV treatment. There is some photobleaching that occurs indicating loss of some dye, but this does not impact the

fluorescence measurement of the glass transition provided that no further photobleaching occurs during the course of the measurement, something which is verified after each measurement. We now describe the various tests we conducted to ensure that this UV treatment to lightly crosslink the pyrene-labeled layer does not affect the measured glass transition by fluorescence.

We verified that the 10 min of UV exposure at 254 nm does not alter the ability of the pyrene-labeled PS layer to measure the glass transition by directly comparing measurements on identical samples with and without this added crosslinking step of the pyrene-labeled probe layer. Following the work of Ellison and Torkelson,[14] we constructed samples with a 24 ± 2 nm thick pyrene-labeled PS layer atop a bulk, 270 ± 5 nm underlayer. The local T_g was measured by heating the samples to 130 ^oC, equilibrating for 20 min, and then measuring the fluorescence intensity on cooling at 1 ^oC/min as described above. Figure 4.S4 shows the temperature-dependent intensity curves for two samples, one where the pyrene-labeled layer was lightly crosslinked with 10 min of UV light exposure at 254 nm and another where the sample was traditionally made with no crosslinking. Both samples report at local T_g for the 24 nm thick PS free surface layer of 80 ± 2 ^oC. Repeated measurements on multiple nominally identical samples give, for the average and standard deviation of four separate measurements each: 82.5 ± 3.6 ^oC for the UV crosslinked and 82.5 ± 4.0 ^oC for the traditionally made samples. These values are in reasonably good agreement with those measured by Ellison and Torkelson[14] on similar multilayer samples.

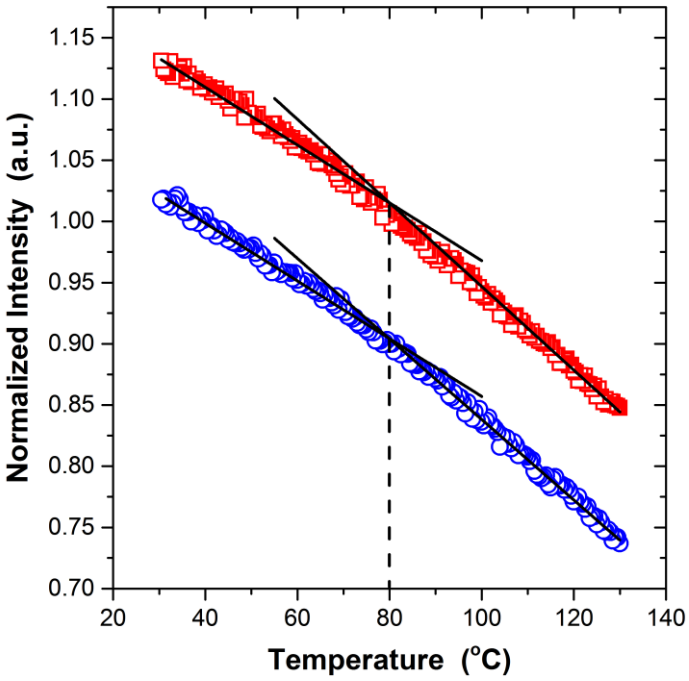

Figure 4.S4. Temperature-dependent fluorescence intensity data for a 24 nm thick pyrene-labeled PS free surface layer atop a bulk PS underlayer for a sample where the pyrene-labeled probe layer had been lightly crosslinked using UV light (blue circles) and a traditionally made sample without UV crosslinking (red squares). Data have been vertically offset for clarity.

To ensure that this additional crosslinking step adequately limits diffusion of the pyrene-labeled probe layer even with extended annealing at elevated temperatures, we used a series of samples with a 24 ± 2 nm thick pyrene-labeled PS layer atop a bulk, 270 ± 5 nm underlayer to measure the local T_g value of this free surface layer as a function of annealing time at 170 ^oC. Figure 4.S5 shows that for the samples whose pyrene-labeled layer had been lightly crosslinked with 10 min of UV light at 254 nm, the measured local T_g value is stable to annealing at 170 ^oC for up to 18 h, while the traditionally made samples without crosslinking eventually show the measured T_g value increasing from the initial locally reduced T_g value of the free surface layer to

a value closer to that of bulk PS as the 24-nm thick pyrene-labeled PS layer at the free surface diffuses throughout the bulk PS film. Thus, we can conclude that the light crosslinking of the pyrene-labeled layer by UV light does not affect the measured T_g value and we do not need to be concerned with the diffusion of the labeled layer during the course of our experiments where the sample spends ~1 h at temperatures between 130-170 ^{o}C.

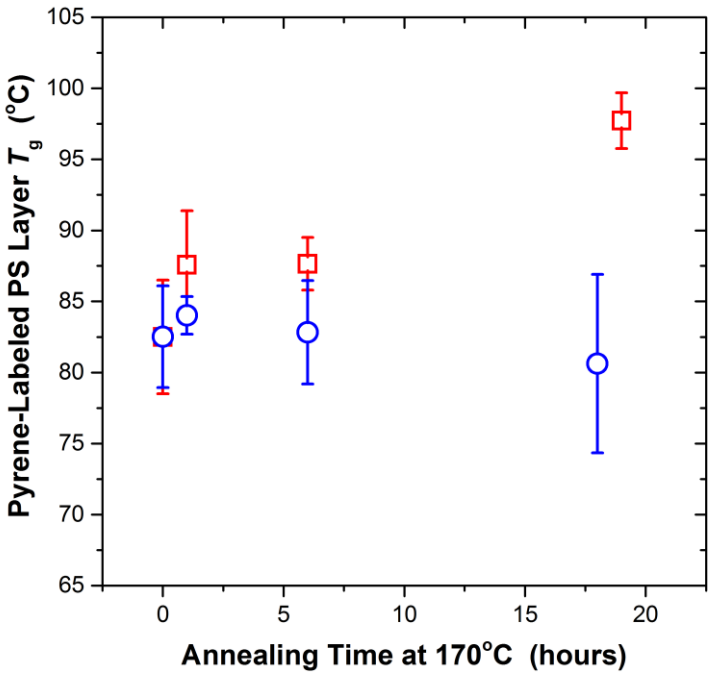

Figure 4.S5. Local T_g measured for a 24 nm thick PS free surface layer as a function of annealing time at 170 ^{o}C under vacuum for samples with (blue circles) and without (red squares) 10 min of UV treatment at 254 nm wavelength to lightly crosslink the pyrene-labeled PS layer. Each data point represents the average and standard deviation from measurements on four different nominally identical samples.

References

[1] J.L. Keddie and R.A.L. Jones, Isreal J. Chem. **35**, 21 (1995).

[2] R.S. Tate, D.S. Fryer, S. Paqualini, M.F. Montague, J.J. De Pablo, and P.F. Nealey, J. Chem. Phys. **115**, 9982 (2001).

[3] A. Clough, D. Peng, Z. Yang, and O.K.C. Tsui, Macromolecules **44**, 1649 (2011).

[4] X. Huang and C.B. Roth, J. Chem. Phys. **144**, 234903 (2016).

[5] W.J. Brittain and S. Minko, J. Polym. Sci. Part A Polym. Chem. **45**, 3505 (2007).

[6] R.A. Orwoll, Densities, *Coefficients of Thermal Expansion, and Compressibilities of Amorphous Polymers*, Physical Properties of Polymers Handbook, J.E. Mark, Springer, New York (2007).

[7] R.R. Baglay and C.B. Roth, J. Chem. Phys. **143**, 111101 (2015).

[8] R.R. Baglay and C.B. Roth, J. Chem. Phys. **146**, 203307 (2017).

[9] K.P. O'Connor and T.C.B. McLeish, Macromolecules **26**, 7322 (1993).

[10] C.J. Clarke, Polym. **37**, 4747 (1996).

[11] R.A.L Jones and R.W. Richards, *Polymer at Surfaces and Interfaces*, Cambridge University Press (1999).

[12] A. Karim, A. Mansour, G.P. Felcher, and T.P. Russell, Phys. Rev. B, **42**, 6846 (1990).

[13] M. Stamm, S. Huttenbach, G. Reiter, and T. Springer, Europhys. Lett. **14**, 451 (1991).

[14] C.J. Ellison and J.M. Torkelson, Nat. Mater. **2**, 695 (2003).

[15] R.J. Klein, D.A. Fischer, and J.L. Lenhart, Langmuir **24**, 8187 (2008).

[16] K. Efimenko, W.E. Wallace, and J. Genzer, J. Colloid Interface Sci. **254**, 306 (2002).

[17] D. Zhang, S.M. Dougal, and M.S. Yeganeh, Langmuir **16**, 4528 (2000).

[18] E.P. Otocka, S. Curran, and R.S. Porter, J. Appl. Polym. Sci. **28**, 3227 (1983).

[19] R. Zhang, T. Cherdhirankorn, K. Graf, K. Koynov, and R. Berger, Microelectron. Eng. **85**, 1261 (2008).

Chapter 5

Experimental Study of Substrate Roughness on the Local Glass Transition of Polystyrene

A version of this chapter is prepared as a paper ready to submit to *Journal of Chemical Physics* by Xinru Huang, Michael F. Thees, William B. Size and Connie B. Roth

5.1 Synopsis

Numerous computer simulations have shown that local dynamics associated with the glass transition can be slower next to rough interfaces compared with smooth interfaces. However, experimentally no such study has been published to date on a real molecular system. Using a hydrogen fluoride (HF) vapor treatment, we created silica substrates with increasing roughness that left the surface chemistry unchanged. The local glass transition temperature T_gs near silica substrates with increasing roughness were measured using fluorescence finding an increase in local T_g of 10 ± 2 K with increasing root-mean-square roughness R_{rms} from 0.5 to 10.9 nm. Characterization of the substrate roughness needed to create an experimental change in the local T_g was found to be quite large leaving the mechanism for this observed behavior uncertain. We explored one possible cause associated with polymer chains being more readily able to adsorb to roughened interfaces.

5.2 Introduction

The glass transition in thin films has been studied for more than two decades as a means of trying to better understand cooperative motion, finite size effects on dynamic heterogeneities, and material properties at nanoscale dimensions.[1-11] However, such confined systems are strongly influenced by the details of the interface. In computer simulations, where the specifics of the boundary are defined explicitly, it has been demonstrated that strong qualitative differences in local dynamics are observed between smooth and rough boundaries.[6,7,12-18] Smooth walls, which can allow lateral sliding of particles, generally result in locally faster dynamics,[15,16] while rough walls, which suppress such a possibility, typically result in locally slower dynamics.[7,12,14,17] Wall roughness in computer simulations has been modeled as particles in a frozen liquid structure,[12,13,18] missing particles or particles of different sizes,[18] and particles in a crystalline lattice.[6,14,17,18] Although particle layering and local density variations are common near such boundaries, Starr and coworkers have demonstrated that perturbations to the local dynamics caused by smooth versus rough walls are independent of local density changes.[16,17] In molecular dynamics (MD) simulations of bead-spring polymers, Starr et al. have shown that profiles of the local alpha relaxation time $\tau(z)$, local glass transition temperature $T_g(z)$, and local changes in fragility $m(z)$ are independent of any local changes in density $\rho(z)$. In these simulations, rough walls were modeled as a triangular, crystalline lattice, while smooth walls had no lateral (x,y) features.

Although stark differences in local glass transition dynamics between smooth and rough walls have been reported in computer simulations for many years,[6,7,12-18] an experimental comparison of interface roughness in a real molecular system has not been done. The one experimental study published to date compares the aging dynamics of a bidisperse colloidal glass

finding strong differences in the local gradient in dynamics near a boundary with a rough or smooth wall.[19] To experimentally investigate the influence of surface roughness in a real molecular system not composed of beads, several challenges need to be addressed. First is the important question of what is an appropriate roughness scale to perturb local glass transition dynamics and how to meaningfully quantify the surface roughness beyond simply typical root-mean-square (RMS) roughness values? Smooth walls in computer simulations are devoid of any lateral (x,y) features, which we would designate as 'artificial computer smooth', a smoothness which is actually not attainable experimentally. In contrast, rough walls in computer simulations were actually intended to better mimic real experimental systems with molecular scale roughness.[6,15] This would likely be akin to a typical experimentally smooth substrate. An experimentally rough interface would likely be quite challenging to simulate because the roughness scale could easily be larger than a computationally viable simulation volume. This would suggest that making such a comparison between experiments and computer simulations is futile. However, frequently comparing basic trends between experiments and computer simulations are extremely illuminating even if time scales or length scales are decades apart. Thus, with this caveat stated, we proceed with trying to experimentally test the basic trend observed in numerous computer simulations that rougher walls lead to slower local glass transition dynamics.

The next challenges to address are experimental in nature. How to reliably create different surface roughnesses without changing the surface chemistry or substrate compliance? Both these additional factors are known to exert their own influence on local dynamics.[7,17,20-23] Here we reliably alter the surface roughness of glass by vapor etching using hydrogen fluoride

(HF) for different lengths of time. This process results in the glass surface retaining its same SiO_2 surface chemistry,[24,25] while progressively increasing the surface roughness from root-mean-square (RMS) values of R_{rms} = 0.5 to 10.9 nm. We will more rigorously characterize the resulting surface roughness below, but identify here for easy reference this commonly used surface roughness parameter. Using a localized fluorescence method,[8,26-29] we measure the local T_g value of a bottom 12-nm layer of polystyrene (PS) next to the roughened glass interface. Flat SiO_2 substrates have been shown to have a neutral, unperturbing influence to local T_g in PS.[8,29] Atop the measured bottom 12-nm layer, a thick (590 nm) bulk layer of PS is added to avoid any competing perturbations by the free surface. Care has been taken in the annealing procedure to ensure that the bottom polymer layer is fully immersed into the valleys of the roughened substrate, while still limiting its diffusion away from the wall. Consistent with the basic trend in computer simulations, we observe an increase in local T_g next to the substrate with increasing roughness. The local T_g increases from the anticipated 101 ± 2 ^oC bulk T_g of PS next to a flat SiO_2 substrate (R_{rms} = 0.5 nm) to a local T_g = 111 ± 2 ^oC next to rough SiO_2 substrate with R_{rms} = 10.9 nm. We present characterization of the surface roughness needed to cause these changes in local T_g and discuss possible influencing factors.

5.3 Experimental Methods

5.3.1 Roughening silica substrates without changing surface chemistry

Silica substrates with different roughnesses were created by exposure to hydrogen fluoride (HF) vapor for various lengths of time. Hydrofluoric acid (48 wt%) is used to half fill a shallow groove (40 mm × 22 mm × 6 mm) in a wax box (depicted in Fig. 5.1a) with the flat

silica substrate placed face down across this groove partially covering the opening for the desired etching time. The aqueous HF solution generates a mixture of HF and H_2O vapor that form "clouds" reacting with the SiO_2 surface etching away material into a roughened geometry. The etching mechanism is believed to occur in several steps[24,30] with HF first being ionized by the water molecules on the SiO_2 surface

$$2HF + H_2O \leftrightarrow H_3O^+ + HF_2^- \quad . \qquad (1)$$

It is primarily the HF_2^- ions that rapidly react with SiO_2 to generate gaseous SiF_4

$$SiO_2 + 2H_3O^+ + 2HF_2^- \leftrightarrow SiF_4\,(gas) + 4H_2O \quad , \qquad (2)$$

with SiF_4 being quickly hydrated limiting the back reaction

$$SiF_4 + H_3O^+ + HF_2^- + H_2O \rightarrow 2H_3O^+ + SiF_6^{2-} \quad . \qquad (3)$$

The final products are water soluble and easily removed by sonicating the now roughened silica substrates in deionized (DI) water for 5 min, leaving behind a typical silica interface with its surface chemistry unchanged.[25] Compared to traditional wet HF etching in liquid, HF vapor etching from an aqueous HF solution introduces less contamination with a more controllable and flexible etching environment,[31] while still giving similar etching rates.[24]

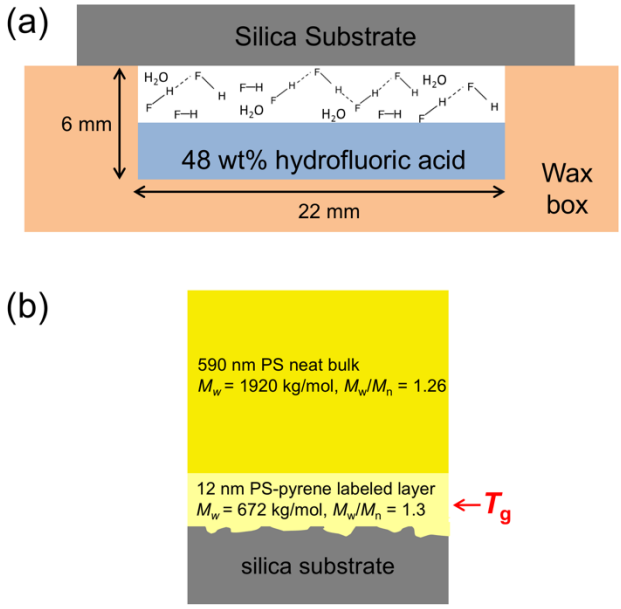

Fig. 5.1. (a) A side view of the setup used to chemically etch flat silica substrates with HF vapor. Hydrofluoric acid (48 wt%) is poured half way into a shallow groove in a wax block. By placing the flat silica substrate face down partially covering the groove, HF and H_2O vapor "clouds" coming off the acid react with SiO_2, leaving a rough silica substrate after rinsing without changing the surface chemistry. (b) Multilayer sample assembled on the rough substrate containing at 12-nm thick pyrene-labeled probe layer next to the substrate covered with a bulk PS layer to eliminate competing free surface effects.

Atomic force microscopy (AFM) images of the roughened silica substrates were collected using a Veeco Dimension 5000 AFM in tapping mode. AFM tips were purchased from NanoandMore GmbH with spring constants of 5.4-16 N/m and resonance frequencies of 150-300 kHz. The radius of AFM tips is 8 nm, resulting in good lateral resolution. For each rough substrate, at least three randomly spots on the surface were chosen for scans with 256 × 256 pixel resolution on 3 μm × 3 μm, 5 μm × 5 μm or 10 μm × 10 μm areas at 0.25 Hz scanning rate. The

resulting 3D images were then corrected by removing both a background tilt and second order polynomial to account for the bow of the piezoelectric tube scanner.

5.3.2 Sample preparation and fluorescence measure of local $T_g(z = 0)$ next to rough substrate

Polystyrene films were spin-coated from toluene onto freshly-cleaved mica using either neat PS (M_w = 1920 kg/mol, M_w/M_n = 1.26, Pressure Chemical) for the bulk 590 ± 5 nm thick top layer or pyrene-labeled PS (M_w = 672 kg/mol, M_w/M_n = 1.3, with 1.4 mol% pyrene, styrene free radically polymerized with 1-pyrenylbutyl methacrylate monomer[27-29]) for the 12 ± 1 nm thick probe layer placed next to the substrate. All such layers were independently annealed overnight at 120 ^oC under vacuum prior to floating. In some samples, the PS-pyrene layer was also lightly crosslinked using UV light (UVP compact UV lamp, model UVG-11) to limit diffusion at high temperatures.[29] Bilayer sample structures as depicted in Figure 5.1b were assembled by first floating the 12-nm pyrene-labeled PS layer onto the rough silica substrates and annealing under vacuum at 170 ^oC for 2 h. At such temperatures, capillary forces readily pull the polymer melt into the irregular surface features of the roughened substrate.[32,33] The 590 nm thick top bulk PS layer was then floated on and allowed to dry. Immediately prior to the fluorescence measurements, the sample was equilibrated at 170 ^oC for 20 min allowing the assembled multilayer stack to form a consolidated material without any air gaps.[29] Film thicknesses were measured using ellipsometry (Woollam M-2000) where PS films on silicon were fit to a standard layer model treating the PS layer with a Cauchy model $n(\lambda) = A + B/\lambda^2 + C/\lambda^4$, fitting A and B

with *C* held at the bulk value, and including a 1.25 nm native oxide layer atop the underlying silicon substrate.[34]

Fluorescence measurements were carried out using a Photon Technology International QuantaMaster spectrofluorometer with samples mounted in an Instec HCS402 heater. Pyrene fluorescence emission was monitored on cooling at 1 ^{o}C/min for 3 s every 27 s at an emission wavelength of 379 nm, while exciting at 330 nm with band passes kept between 5-6 nm.[26-29] After each cooling run, the samples were reheated to the starting temperature to ensure that the same initial fluorescence intensity was recovered, verifying that the sample had remained stable during the course of the experiment and limited photobleaching occurred. The local $T_g(z)$ was determined from the temperature-dependent fluorescence intensity by fitting straight lines to the slope of the intensity data above and below the transition to identify the intersection of the two fits.[27-29]

The influence of flat silica substrates with physically adsorbed PS chains on the local T_g next to the substrate interface were also investigated. For such samples, physically adsorbed layers were made by spin-coating 2.5 wt% PS (M_w = 400 kg/mol, M_w/M_n = 1.06, Pressure Chemical) toluene solutions onto silica substrates or silicon wafers that were pre-cleaned with 33 vol% hydrogen chloride (HCl) acid for 20 min before rinsing with DI water resulting in film thicknesses of 206 ± 2 nm. These films were then annealed at 150 ^{o}C under vacuum for different lengths of time to create adsorbed layers. Free chains were removed immediately after annealing by immersing the samples in 50 ml of toluene for 30 min. The resulting residual layers were dried under vacuum at room temperature overnight before measurement of the residual thickness h_{ads} using ellipsometry on those samples made on the silicon wafers. For these very thin films

(h_{ads} < 10 nm), only the film thickness was fit while holding all Cauchy parameters for the index of refraction to bulk values (A = 1.5627, B = 0.00788, C = 0.00038). Multilayer samples, similar to that described above, were then assembled for fluorescence measurements by floating a 12 ± 1 nm pyrene-labeled PS layer directly next to the adsorbed layer, which were then annealed together at 170 ^{o}C for 2 hours, such that the pyrene-labeled chains become well intermixed with the adsorbed chains.[29,35,36] A 590 ± 5 nm bulk neat PS layer was then added to eliminate competing effects from the free surface, forming a sample configuration similar to that used in our recent study to measure the local T_g next to substrates with end-tethered chains.[29] Prior to the T_g fluorescence measurements, as described above, the complete multilayer stack was equilibrated at 170 ^{o}C for 20 min to consolidate the layers into a single material.

5.4 Results and Discussion

5.4.1 Local increases in T_g next to roughened substrates

By exposing silica substrates to HF vapor for different lengths of time, different substrate roughnesses were created without changing the SiO_2 surface chemistry [24,25] Without knowing a priori what roughness scale was necessary to experimentally cause a change in the local T_g, a series of different samples exposed to the HF vapor treatment for increasing lengths of time were created until a change in local T_g was observed. Figure 5.2 plots the measured fluorescence intensity at 379 nm on cooling at 1 ^{o}C/min for four different samples representing the different exposure times to HF vapor. The local T_g next to the silica substrates were determined from the change in slope of the temperature dependence of the fluorescence intensity following the method developed previously.[8,26-29] The change in slope arises from the transition

in the local thermal expansion around the pyrene dye that occurs at T_g.[8,29,37] The data in Fig. 5.2 shows that 5 min of exposure to the HF vapor does not lead to a local T_g change outside of experimental error relative to that for a flat substrate, while 10 min of exposure does. Zero minutes represents the typical flat silica substrate giving a local T_g = 100 ± 2 °C next to the silica substrate consistent with the bulk value of T_g^{bulk} = 101 ± 2 °C for PS, in agreement with previous observations.[8,29] The data for the 5 min HF exposure time shown in Fig. 5.2 has a local T_g = 102 ± 2 °C, while the 10 and 12 min exposure times give local T_g values of 110 ± 2 °C and 112 ± 2 °C, respectively.

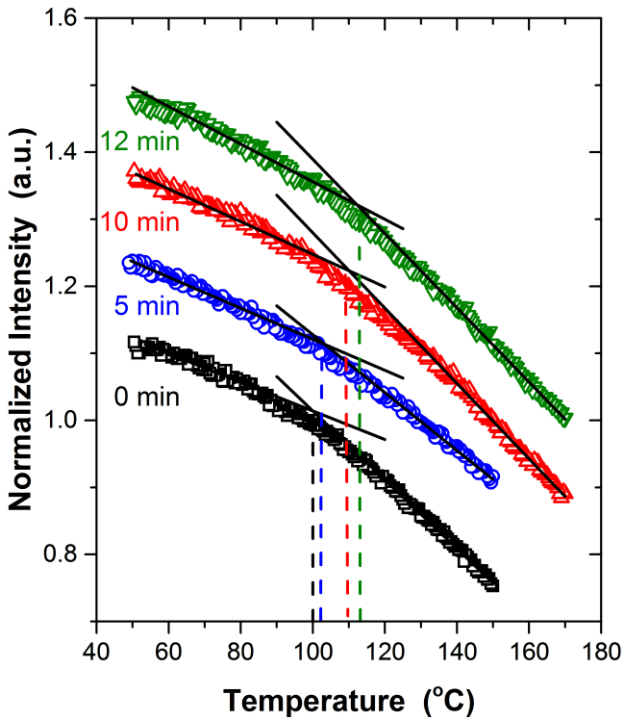

Fig. 5.2. Temperature dependence of the fluorescence intensity at 379 nm measured on cooling at 1 °C/min for four representative samples with increasing exposure time to the HF vapor that etches the silica substrate: 0 min (typical flat silica substrate) gives a local T_g = 100 ± 2 °C next

to the silica substrate, 5 min exposure gives a local T_g = 102 ± 2 ^oC, 10 min exposure gives a local T_g = 110 ± 2 ^oC, and 12 min exposure gives a local T_g = 112 ± 2 ^oC.

As the exposure time of the silica substrates to HF vapor increases, progressively more etching takes place making the silica substrates rougher. Figure 5.3 plots the local T_g measured next to the silica substrates as a function of the RMS roughness R_{rms}. We see that as the substrate roughness increases from an R_{rms} = 0.5 nm characteristic of a typical flat silica substrate to an R_{rms} = 10.9 nm for the 12 min of HF exposure, the experimentally measured local T_g next to the silica substrate increases by 10 ± 2 K with increasing substrate roughness. Thus, we have experimentally observed the same qualitative trend observed in numerous computer simulations[6,7,12-18] that increasing substrate roughness leads to slower dynamics and a local increase in T_g.

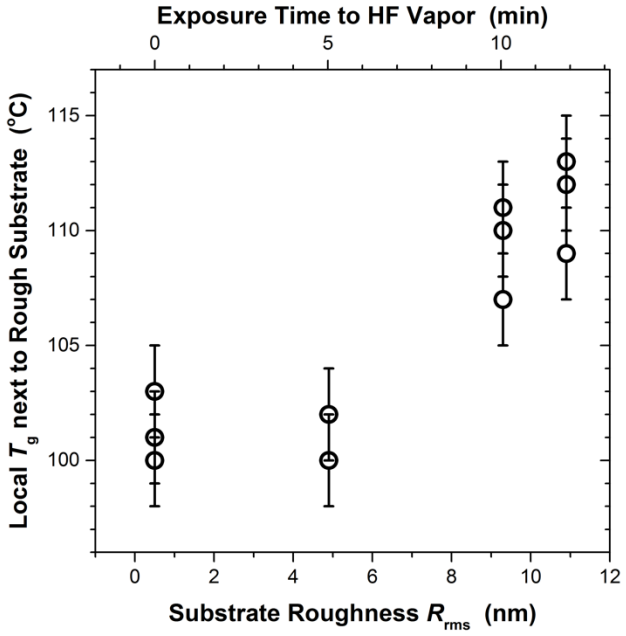

Fig. 5.3. Experimentally measured local T_g of 12-nm thick pyrene-labeled PS layers next to silica substrates with different roughnesses showing a 10 ± 2 K increase in local T_g with increasing substrate roughness. Top *x*-axis plots the exposure time to HF vapor used to create the roughened substrate, while the bottom *x*-axis plots the measured RMS roughness R_{rms} of the substrate surface.

As a point of discussion, Baglay and Roth recently observed large and long-ranged $T_g(z)$ perturbations near polymer-polymer interfaces.[27,28] They suggested three possibilities for why polymer-polymer interfaces may exhibit differences in comparison to a polymer-free surface interface: increased interfacial width, chain connectivity across the interface, and increased interfacial roughness.[28] We consider here how the substrate roughness needed to create a T_g change with the HF vapor treated silica compares to the interfacial roughness of a polymer-polymer interface. Bilayer films of PS (~150 nm, M_w = 48.1 kg/mol, M_w/M_n = 1.01) and poly(methyl methacrylate) (PMMA) (~200 nm, M_w = 387 kg/mol, M_w/M_n = 1.14) were made and annealed at 170 °C for 2 hours under vacuum, allowing the PS/PMMA to establish an equilibrium interface. The roughness of the PS/PMMA interface was then exposed by removing the top PS layer by immersing the bilayer sample into a 87/13 vol% cyclohexane/toluene mixture for 12 h, following the procedure by Zhang et al..[38] The undissolved PMMA layer was then dried and measured by AFM where the surface roughness was found to be R_{rms} = 1.2 nm (for a 10 μm × 10 μm scan area), not much rougher than a typical experimentally flat silica substrate. Given these results, we conclude that interfacial roughness at polymer-polymer interfaces is unlikely to have any impact on the $T_g(z)$ perturbation observed by Baglay and Roth,[27,28] although we note

that their study used higher molecular weights. As discussed in Huang and Roth,[29] the $T_g(z)$ behavior observed for polymer-polymer interfaces is likely primarily due to chain connectivity across the interface. We note that much larger PS/PMMA interfacial roughnesses ($R_{rms} \approx 15$ nm) can be obtained with the use of large amounts of compatibilizers and much lower molecular weights as demonstrated by Zhang et al..[38]

5.4.2 Characterizing substrate roughness

The computer simulation studies that observed slower local dynamics next to rough interfaces[6,7,12-18] typically did not formally quantify their substrate roughness. In many cases the difference between "smooth" and "rough" was primarily a qualitative designation where "smooth" often refers to a computationally smooth interface with no lateral (x,y) features, while "rough" refers to interfaces that contain some lateral structure to the interface in an attempt to render more accurately an experimentally realistic surface. As such the experimentally smooth scale essentially starts at what was computationally designated as rough. In computer simulations, the slowing of local dynamics near a rough interface has typically been associated with the removal of lateral sliding that can occur next to a (x,y)-featureless wall,[15,16] which was considered experimentally unrealistic. Thus, unfortunately we are left with little insight from computational studies regarding why increasing substrate roughness would experimentally lead to local increases in T_g.

To gain a better understanding of what might be the underlying cause for the experimentally observed local increase in T_g with increasing substrate roughness shown in Figure 5.3, we experimentally characterize the roughness of the substrates used in this study.

Unfortunately, meaningfully characterizing surface roughness is a non-trivial problem. There are numerous roughness parameters that have been defined.[39,40] The most common is the RMS roughness

$$R_{\mathrm{rms}} = \sum_{i=1}^{N} \sqrt{\frac{{z_i}^2}{N}} \qquad (3)$$

where z_i is the vertical distance between the i^{th} measure of the vertical coordinate z and the mean plane defined by $\sum z_i = 0$. Another common measure is the mean roughness

$$R_{\mathrm{a}} = \frac{1}{N} \sum_{i=1}^{N} |z_i| \qquad (4)$$

A surface profile that contains no large deviations from the mean plane will have similar values of R_{rms} and R_{a}. However, neither R_{rms} nor R_{a} informs us about the preference of bumps or holes on the surface. To extract more information about the up or down preference, we need to quantify the height distribution. This is typically done through the skewness R_{sk} and kurtosis R_{ku} to separately describe the symmetry and sharpness of the height distribution:

$$R_{sk} = \frac{1}{N\, {R_{\mathrm{rms}}}^3} \sum_{i=1}^{N} z_i^3 \qquad (5)$$

$$R_{ku} = \frac{1}{N\, {R_{\mathrm{rms}}}^4} \sum_{i=1}^{N} z_i^4 \qquad (6)$$

Skewness is a non-dimensional quantity that is typically evaluated in terms of having positive or negative values. A skewness of zero suggests an even distribution of data around the mean plane, while a strongly nonzero value indicates an asymmetric, one-tailed distribution with either frequent peaks ($R_{\mathrm{sk}} > 0$) or valleys ($R_{\mathrm{sk}} < 0$). Kurtosis as the fourth central moment of the height distribution indicates the sharpness of the distribution where a Gaussian normal distribution would correspond to a kurtosis value of $R_{\mathrm{ku}} = 3$. Thus, a sharp distribution of $R_{\mathrm{ku}} < 3$ would indicate few high peaks or valleys and a broad distribution $R_{\mathrm{ku}} > 3$ would indicate many.

Table I gives the measured value of R_{rms}, R_a, R_{sk}, and R_{ku} for the four different roughness substrates in this study, along with average local T_g value next to the substrates measured using fluorescence. Values are based on AFM measurements of at least three different randomly chosen spots on the substrate surface with scan sizes ranging from 3 μm × 3 μm to 10 μm × 10 μm. The R_{rms} and R_a values both indicate that the substrate roughness increases with increasing HF exposure time, while the skewness R_{sk} parameter is close to zero and the kurtosis parameter is around 3 indicating a basically symmetric normal distribution for the height profiles. There is no distinctive change observed in the numerical values between the 5 min and 10 min HF exposure times where the large change in local T_g occurs. On average the R_{rms} and R_a roughness values at 5 min are half as rough as those at 10 min. We also looked for possible correlations between the measured local T_g values and other roughness parameters, but found none that stood out. Figure 5.4 plots the height distribution function for these four rough substrates.

TABLE 5.1. Measured values of the root-mean-square (RMS) roughness R_{rms}, the mean roughness R_a, and values for the skewness R_{sk} and kurtosis R_{ku} of the height distribution, for the four different rough substrates investigate in this study along with the average local T_g measured next to the substrate.

HF Exposure	0 min	5 min	10 min	12 min
Local T_g (^{o}C)	101 ± 1.5	101 ± 1	109 ± 2	111 ± 2
R_{rms} (nm)	0.5 ± 0.1	4.9 ± 1.3	9.3 ± 2.4	10.9 ± 4.2
mean R_a (nm)	0.3 ± 0.1	3.5 ± 1.0	6.9 ± 1.8	7.9 ± 3.2
skewness R_{sk}	– 0.01 ± 0.2	– 0.4 ± 0.2	0.5 ± 0.1	– 0.02 ± 0.1
kurtosis R_{ku}	3.0 ± 0.2	3.8 ± 1.0	3.9 ± 0.1	2.7 ± 0.1

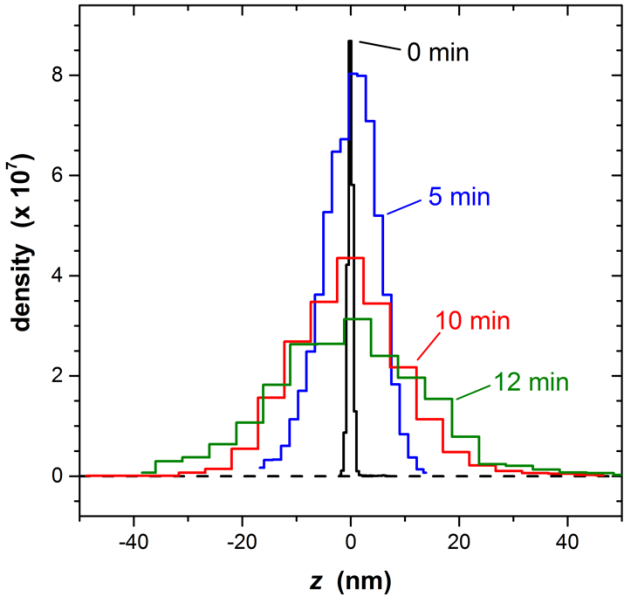

Fig. 5.4. Height distribution function for the four rough substrates created with different exposure times to the HF vapor.

Perhaps more visually informative is the actual rendering of the 3D surface profiles of the substrates as measured by AFM. Figure 5.5 graphs representative 3D topographies of the measured height profiles for the four different substrates investigated. Visually it is clear that the substrate surfaces become rougher with increasing HF exposure time, consistent with the

quantified R_{rms} and R_a values given in Table I. The topographies of the 10 and 12 min HF exposure times are noticeably rougher than that for only 5 min of exposure, and all are significantly rougher than a flat unexposed silica substrate. Typical of AFM micrographs, the images visually distort the relative scale of the vertical *z*-direction (in nanometers) relative to the horizontal *x*,*y*-dimensions (in micrometers). Keeping this in mind, we see that the roughness scale at 10 min of HF exposure needed to create an experimental change in local T_g is enormous, and especially surprising that the roughness scale at 5 min of exposure did not cause a measureable change in local T_g outside of experimental error.

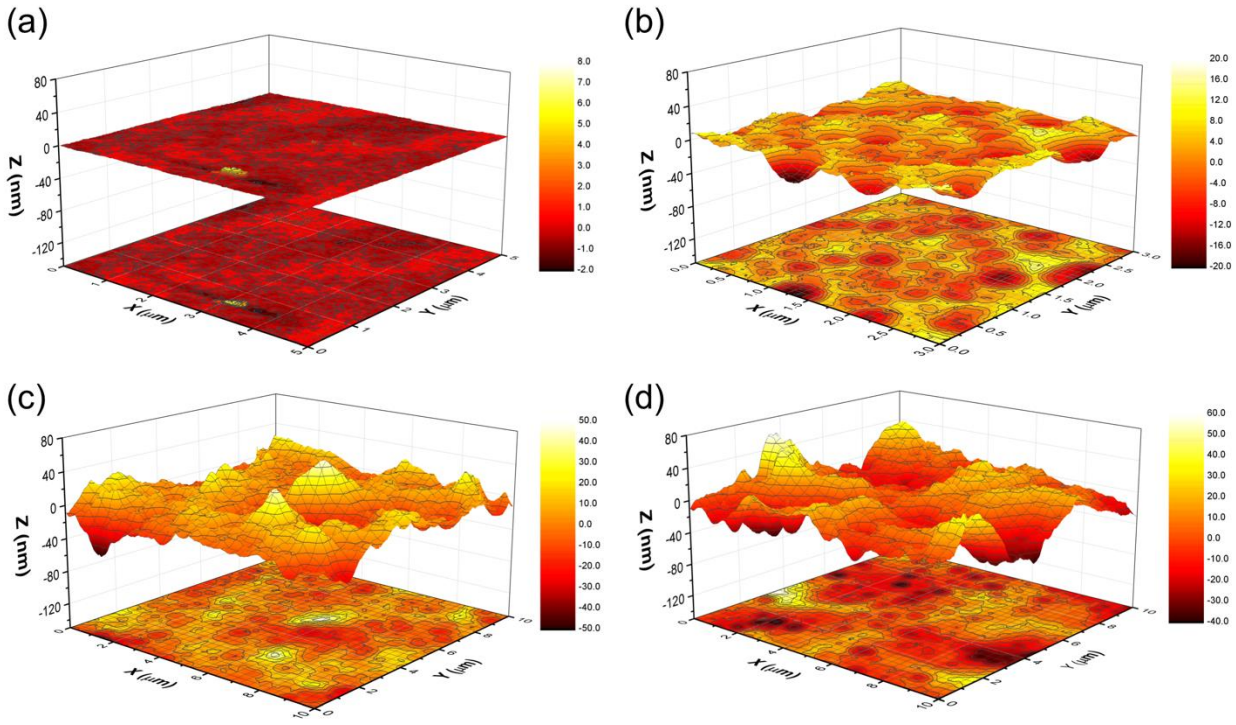

Fig. 5.5. Representative 3D AFM topographies with their projected landscapes of the rough silica substrates investigated in this study, where the *z*-scale has been made the same in all four images for direct comparison. (b) 5 min (3 μm × 3 μm), (c) 10 min (10 μm × 10 μm), and (d) 12

min (10 μm × 10 μm) of HF vapor exposure, while (a) represents an unexposed flat silica substrate (5 μm × 5 μm).

Figure 5.6 plots the 2D isotropic power spectral density (PSD) curves calculated from the AFM profiles shown in Fig. 5.5. As the Fourier transform of the surface profiles, the PSD curve characterizes any repeating lateral features of the roughness profile. The continuous shape of the PSD curves demonstrates that there is no dominating characteristic length scales associated with the surface roughness. The three substrates exposed to HF vapor are all rougher than the unexposed flat silica substrate. As the HF exposure time increases, the roughness increases by forming progressively larger feature sizes, where the 10 and 12 min HF exposure times are characterized as having micron-sized roughness. All three HF exposure times appear to have the same roughness at small wavelengths down to 20 nm, the smallest roughness feature our 8-nm AFM tip can resolve. Thus, we are left to conclude the substrate roughness features that lead to an experimental change in local T_g (i.e., between the 5 and 10 min of HF exposure) are size scales that would seem unreasonably large to be associated with the glass transition.

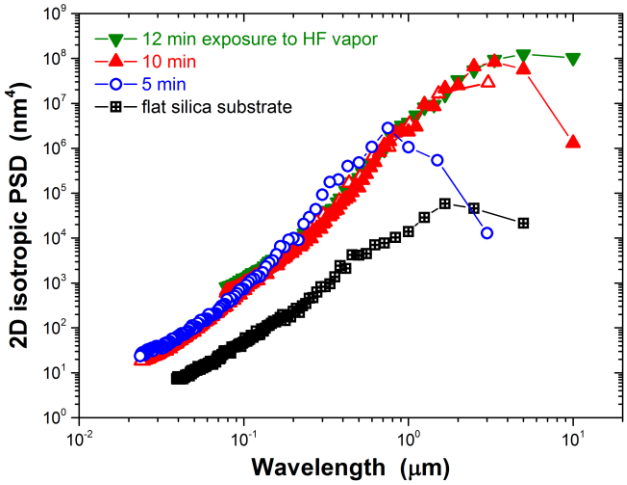

Fig. 5.6. Power spectral density (PSD) curves as a function of wavelength corresponding to the four different rough substrates shown in Fig. 5.5. (a) Flat silica substrate (from 5 μm × 5 μm scan, black squares), (b) 5 min HF exposure (from 3 μm × 3 μm, open blue circles), (c) 10 min (from 3 μm × 3 μm, open red up triangles, from 10 μm × 10 μm, closed red up triangles), and (d) 12 min (from 10 μm × 10 μm, closed green down triangles).

5.4.3 Other possible influences of increasing substrate roughness: Increased chain adsorption?

Is it possible that the roughened substrate could be having some different kind of influence that manifests itself as an increase in local T_g? Theoretical efforts by Douglas suggest that polymer adsorption could occur more readily at a rough substrate interface compared to a typical flat interface.[41] Polymer adsorption to interfaces occurs by the sticking of monomer units to the substrate because of small favorable interactions, whose enthalpic contribution multiplies as more monomers make contact with the substrate.[42-46] However, there in an entropy cost associated with chain segments remaining in contact with the interface because the chain must

distort itself from its natural Gaussian conformation to make these contacts. At a rough interface, the entropy penalty for chain segments making contact with the interface can be less, suggesting chain adsorption may occur more readily.[41] Unfortunately, we cannot experimentally test whether the amount of chain adsorption is larger on our roughened substrates. It is also not clear if the presence of such adsorbed chains would result in a local T_g increase. There are recent indications in the literature that this could be the case.[47-51]

To investigate this possibility further, we carried out experiments on flat substrates to determine if the local T_g near the substrate increases when an adsorbed layer is present. Samples were constructed with adsorbed PS layers (M_w = 400 kg/mol) of known thickness h_{ads} by the typical method of annealing a bulk film for multiple hours at 150 ^oC under vacuum, and then rinsing off any unattached chains with toluene.[52,53] The resulting thickness h_{ads} of the adsorbed layer was then measured. Multilayer samples for fluorescence measurements were assembled by floating on a 12 nm thick pyrene-labeled PS layer and annealing this structure at 170 ^oC for 2 h to intermix the adsorbed chains with the pyrene-labeled probe layer. A bulk PS overlay was then added to eliminate the competing effects of the free surface, and fluorescence measurements were carried out as described above to measure the local T_g next to these substrates with adsorbed chains. A series of samples were studied with increasing annealing time at 150 ^oC to grow progressively larger adsorbed layers. Figure 5.7 plots the measured adsorbed layer thickness h_{ads} for these samples along with the measured local T_g value next to the adsorbed layer substrate as a function of the annealing time at 150 ^oC used to create the adsorbed layer. No change in local T_g near the substrate is observed for approximately the first 10 hours of annealing at 150 ^oC even though some modest growth in h_{ads} is observed. After 25 hours of annealing, a

local T_g increase of ~15 K is observed next to the substrate, where the increase in T_g is found to be monotonic with annealing time of the adsorbed layer. However, the thickness of the adsorbed layer h_{ads} was not found to grow monotonically with annealing time. The data in Fig. 5.7 are somewhat complicated by the experimental limitations that the ellipsometry measurements of the h_{ads} thickness need to be done on silicon wafers, while the fluorescence measurements of T_g need to be done on silica substrates. Although both silicon and silica substrates have the same surface chemistry and both underwent the same sample preparation treatment together, they are nonetheless technically measurements on different samples. Additional measurements by our group have not found the adsorbed layer thickness h_{ads} to be a particularly robust parameter with considerable variability observed between samples that have undergone the same sample preparation procedure. This suggests to us that h_{ads} may not be the best parameter to capture the impact of the adsorbed layer on local T_g.

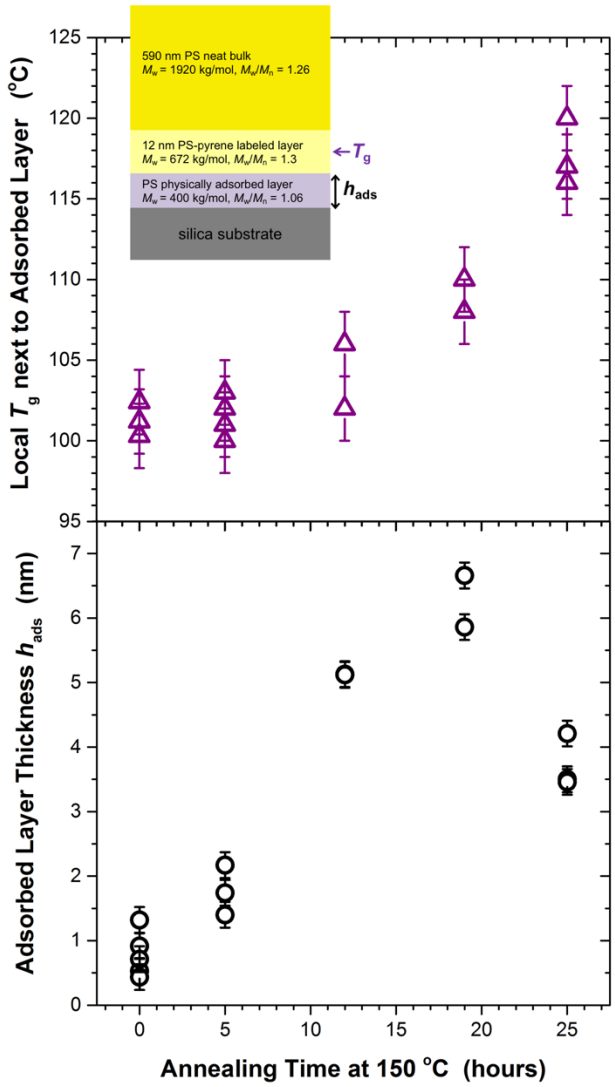

Fig. 5.7. Local glass transition temperature T_g next to substrates with PS adsorbed layers using fluorescence and the adsorbed layer thickness h_{ads} measured using ellipsometry, as a function of the annealing time at 150 °C under vacuum used to grow the adsorbed layers on flat substrates.

It is not clear by what mechanism adsorbed chains could be locally increasing T_g. The structure of the adsorbed layer in solutions and melts has been described in terms of trains, loops, and tails.[42-45,54-56] Some studies suggest that the early stage of adsorption may be dominated with

short loops and trains, while at longer growth times, tails and larger more loosely bonded loops dominate the structure of the adsorbed layer.[45,54,55,57] The monotonic increase in T_g with increasing annealing time of the adsorbed layer, in contrast to the non-monotonic change in the measured adsorbed layer thickness h_{ads}, may be associated with such internal changes to the structure of the adsorbed layer where a predominance of tails at long annealing times may be necessary to cause a T_g increase. The higher prevalence of tails in the late stages of the adsorption process may be compared to our recent work investigating the local glass transition temperature $T_g(z)$ near end-tethered substrate interfaces.[29] In this study, we observed a large, maximum increase in local $T_g(z = 0)$ next to the end-tethered PS substrates of 49 ± 2 K for an optimal grafting density $\sigma = 0.011$ chains/nm^2 within the mushroom-to-brush transition region. Although it is not clear why such a handful (~10 vol%) end-tethered chains near a substrate interface could have such a large increase in local T_g as the glass transition is not typically associated with chain connectivity effects,[29] it is possible that adsorbed layers with a predominance of tails could behave in a similar fashion. Thus, it is possible that the local T_g increase observed next to the roughened substrates with such large roughness features results from a greater preponderance of adsorbed chains that contain tails, which may then behave in an analogous manner to end-tethered chains. However, we caution that these results are far from conclusive, and much additional research is required to better understand the observed behavior.

5.5 Conclusions

We have experimentally measured the local glass transition temperature T_g next to rough silica substrates using a local fluorescence method. Roughened silica substrates were fabricated

using a HF vapor treatment that leaves the surface chemistry unchanged. Our results show an increase of 10 ± 2 K in the local T_g near the substrate with increasing roughness for R_{rms} values of 0.5 to 10.9 nm. This is qualitatively consistent with numerous computer simulations that have compared local dynamics near smooth and rough interfaces, finding slower dynamics and increases in T_g next to rough interfaces.[6,7,12-18] However, the size scale of the roughness features we require to experimentally observe an increase in local T_g are significantly larger (micrometer sized) compared with length scales typically associated with the glass transition. We investigated one possible explanation for the experimentally observed increase in local T_g near such rough interfaces, whereby polymer chains may adsorb more readily to rougher substrates as the entropic penalty for monomer units to make contact with the substrate becomes reduced.[41] In this fashion adsorbed layers with perhaps a predominance of tails could behave in a similar fashion to end-tethered chains, which we have recently shown can cause a large increase in local T_g near the substrate with only a handful of chains within the "mushroom-to-brush" crossover region.[29]

5.6 References

[1] M.D. Ediger and J.A. Forrest, Macromolecules **47**, 471 (2014).

[2] J.L. Keddie, R.A.L. Jones, and R.A. Cory, Europhys Lett **27**, 59 (1994).

[3] J.L. Keddie, R.A.L. Jones, and R.A. Cory, Faraday Discuss **98**, 219 (1994).

[4] M. Alcoutlabi and G.B. McKenna, J Phys: Condens Matter **17**, R461 (2005).

[5] C.B. Roth and J.R. Dutcher, J Electroanal Chem **584**, 13 (2005).

[6] J. Baschnagel and F. Varnik, J Phys: Condens Matter **17**, R851 (2005).

[7] P.Z. Hanakata, J.F. Douglas, and F.W. Starr, Nat Commun **5**, 4163 (2014).

[8] C.J. Ellison and J.M. Torkelson, Nature Materials **2**, 695 (2003).

[9] C.M. Evans, H. Deng, W.F. Jager, and J.M. Torkelson, Macromolecules **46**, 6091 (2013).

[10] C.B. Roth, J.E. Pye, and R.R. Baglay, in *Polymer Glasses*, edited by C.B. Roth (CRC Press, Taylor & Francis Group, 2016), pp. 181–204.

[11] S. Napolitano, E. Glynos, and N.B. Tito, Rep Prog Phys **80**, 036602 (2017).

[12] P. Scheidler, W. Kob, and K. Binder, Europhys Lett **59**, 701 (2002).

[13] P. Scheidler, W. Kob, and K. Binder, J Phys Chem B **108**, 6673 (2004).

[14] G.D. Smith, D. Bedrov, and O. Borodin, Phys Rev Lett **90**, 226103 (2003).

[15] K. Binder, J. Baschnagel, and W. Paul, Prog Polym Sci **28**, 115 (2003).

[16] P.Z. Hanakata, J.F. Douglas, and F.W. Starr, J Chem Phys **137**, 244901 (2012).

[17] P.Z. Hanakata, B.A. Pazmiño Betancourt, J.F. Douglas, and F.W. Starr, J Chem Phys **142**, 234907 (2015).

[18] T. Davris and A.V. Lyulin, J Chem Phys **143**, 074906 (2015).

[19] C. Cao, X. Huang, C.B. Roth, and E.R. Weeks, J Chem Phys **147**, 224505 (2017).

[20] C.M. Evans, S. Narayanan, Z. Jiang, and J.M. Torkelson, Phys Rev Lett **109**, 038302 (2012).

[21] D. Christie, C. Zhang, J. Fu, B. Koel, and R.D. Priestley, J Polym Sci, Part B: Polym Phys **54**, 1776 (2016).

[22] O.K.C. Tsui, T.P. Russell, and C.J. Hawker, Macromolecules **34**, 5535 (2001).

[23] D.S. Fryer, R.D. Peters, E.J. Kim, J.E. Tomaszewski, J.J. de Pablo, P.F. Nealey, C.C. White, and W.L. Wu, Macromolecules **34**, 5627 (2001).

[24] C.R. Helms and B.E. Deal, Journal of Vacuum Science Technology A: Vacuum, Surfaces, and Films **10**, 806 (1992).

[25] L.T. Zhuravlev, Colloids and Surfaces A: Physicochemical and Engineering Aspects **173**, 1 (2000).

[26] P.M. Rauscher, J.E. Pye, R.R. Baglay, and C.B. Roth, Macromolecules **46**, 9806 (2013).

[27] R.R. Baglay and C.B. Roth, J Chem Phys **143**, 111101 (2015).

[28] R.R. Baglay and C.B. Roth, J Chem Phys **146**, 203307 (2017).

[29] X. Huang and C.B. Roth, ACS Macro Lett. **7**, 269 (2018).

[30] G.A.C.M. Spierings, J Mater Sci **28**, 6261 (1993).

[31] S. Shih, K.H. Jung, D.L. Kwong, M. Kovar, and J.M. White, Appl Phys Lett **62**, 1904 (1998).

[32] J.L. Hor, H. Wang, Z. Fakhraai, and D. Lee, Soft Matter **14**, 23 (2018).

[33] M. Zhang, P. Dobriyal, J.T. Chen, T.P. Russell, J. Olmo, and A. Merry, Nano Lett **6**, 1075 (2006).

[34] X. Huang and C.B. Roth, J Chem Phys **144**, 234903 (2016).

[35] C.J. Clarke, Polymer **37**, 4747 (1996).

[36] R.A.L. Jones and R.W. Richards, *Polymers at Surfaces and Interfaces* (Cambridge University Press, 1999).

[37] S. Kim, S.A. Hewlett, C.B. Roth, and J.M. Torkelson, Eur Phys J E **30**, 83 (2009).

[38] J. Zhang, T.P. Lodge, and C.W. Macosko, Macromolecules **38**, 6586 (2005).

[39] E.S. Gadelmawla, M.M. Koura, T.M.A. Maksoud, I.M. Elewa, and H.H. Soliman, Journal of Materials Processing Technology **123**, 133 (2002).

[40] J.M. Bennett and L. Mattsson, *Introduction to Surface Roughness and Scattering* (Optical Society of America, Washington, DC (1989), pp. 38–56.

[41] J.F. Douglas, Macromolecules **22**, 3707 (1989).

[42] B. O'Shaughnessy and D. Vavylonis, J Phys: Condens Mater **17**, R63 (2005).

[43] J.M.H.M. Scheutjens and G.J. Fleer, J Phys Chem **83**, 1619 (1979).

[44] O. Guiselin, Europhys Lett **17**, 225 (1992).

[45] M. Sen, N. Jiang, J. Cheung, M.K. Endoh, T. Koga, D. Kawaguchi, and K. Tanaka, ACS Macro Lett. **5**, 504 (2016).

[46] D.N. Simavilla, W. Huang, P. Vandestrick, J.P. Ryckaert, M. Sferrazza, and S. Napolitano, ACS Macro Lett. **6**, 975 (2017).

[47] S. Napolitano and M. Wübbenhorst, Nat Commun **2**, 260 (2011).

[48] T. Koga, N. Jiang, P. Gin, M.K. Endoh, S. Narayanan, L.B. Lurio, and S.K. Sinha, Phys Rev Lett **107**, 225901 (2011).

[49] S. Napolitano, S. Capponi, and B. Vanroy, Eur Phys J E **36**, 61 (2013).

[50] M.J. Burroughs, S. Napolitano, D. Cangialosi, and R.D. Priestley, Macromolecules **49**, 4647 (2016).

[51] N.G. Perez-de-Eulate, M. Sferrazza, D. Cangialosi, and S. Napolitano, ACS Macro Lett. **6**, 354 (2017).

[52] Y. Fujii, Z. Yang, J. Leach, H. Atarashi, K. Tanaka, and O.K.C. Tsui, Macromolecules **42**, 7418 (2009).

[53] C. Housmans, M. Sferrazza, and S. Napolitano, Macromolecules **47**, 3390 (2014).

[54] P. Gin, N. Jiang, C. Liang, T. Taniguchi, B. Akgun, S.K. Satija, M.K. Endoh, and T. Koga, Phys Rev Lett **±9**, 265501 (2012).

[55] N. Jiang, J. Shang, X. Di, M.K. Endoh, and T. Koga, Macromolecules **47**, 2682 (2014).

[56] A. De Virgiliis, A. Milchev, V.G. Rostiashvili, and T.A. Vilgis, Eur Phys J E **35**, 97 (2012).

[57] H.M. Schneider, P. Frantz, and S. Granick, Langmuir **12**, 994 (1996).

Chapter 6

Summary and Conclusions

In this dissertation, I measured the global and local material properties of polymer films under different boundary conditions using ellipsometry and a modified fluorescence technique originally developed by Torkelson's group.[1] Ellipsometry was used to study how the glass transition temperature T_g and specific volume v_{sp} changed as I decreased the total film thickness h of PS on flat silicon wafers. Spectrofluorometry locally measured $T_g(z)$ inside PS matrices near both end-tethered and rough silica substrates without the free surface effect. To achieve such local T_g measurements, a 12 ± 1 nm thick labeled PS layer with a fluorescence T_g sensitive pyrene dye was inserted at a distance z from different interfaces, thereby mapping the local $T_g(z)$ profiles.

The fundamentals of $T_g(h)$ variations in thin polymer films has puzzled the field for over 20 years. How do other material properties correlate with this whole film $T_g(h)$ change? People also observed different interfacial conditions, such as polymer-air, polymer-substrate, polymer-liquid and dissimilar polymer-polymer interfaces, that can significantly alter local dynamics of polymer films and eventually affect the whole film glass transition behavior. Are there any intrinsic material length scales that are coupled to the observed perturbative effects due to interfaces? How similar and different are those perturbations regarding their strength in altering local dynamics?

Prior to my work published as an editor's choice in 2016 *Journal of Chemical Physics*,[2] there existed experimental studies trying to correlate $T_g(h)$ variations with other material

properties including physical aging,[3–7] viscosity,[8–10] modulus,[11–14], and permeability.[15] However, changes in mass density ρ (or specific volume v_{sp}) in thin polymer films have been little studied with a controversy in the trends of $\rho(h)$. In the late 1990s, studies on both supported and freestanding PS films using neutron reflectivity[16] and Brillouin light scattering[17] showed no change in the density of PS films to within ± 1 % down to film thickness of 6.5 nm. Some recent studies claim to see a density increase of 25-30 % for film thicknesses below ~25 nm.[18,19] In 2011, theoretically, a thermodynamic model proposed by White and Lipson predicted the temperature-dependent specific volume for the liquid state in thin freestanding PS films.[20] In this equation-of-state model, film expansion with decreasing thickness arises from a reduction in the attractive energy between polymer segments due to the missing interactions at the free surface. Based on the small predicted increase in the liquid v_{sp} of ~ 0.5 %, their calculated T_g values are in remarkable agreement with the experimental low MW PS freestanding films from literature.[21] More recently, they have also expanded this model to incorporate substrate interactions and treat supported polymer films.[22] Unfortunately, the lack of precision and controversy in the previous density measurements in polymer thin films were not able to provide evidence for White and Lipson's theory. Before my contributions in Chapter 3, the field did not have such a detailed ellipsometry study of supported PS thin films while exploring the validity of Lorentz-Lorenz formula in converting $n(h)$ into $v_{sp}(h)$.

One of my significant contributions to the literature is showing the lack of correlation between the specific volume v_{sp} and $T_g(h)$ depression in supported PS films. In Chapter 3, I found that both the liquid and glassy v_{sp} are non-monotonic as a function of film thickness h. They start to deviate from bulk at ~120 nm, and at 65 nm they have a maximum increase of (0.4

± 0.2) %, and then specific volume drops back to the bulk value at ~40 nm. This magnitude in percentage increase in v_{sp} is consistent with the theoretical prediction by White and Lipson and all within the experimental error of previous studies ± 1 %.[16,17] For films thinner than 30 nm, we believe the dramatic decrease in the specific volume is not real and likely due to the breakdown of the Lorentz-Lorenz formula. The non-monotonic behavior of v_{sp} in both liquid and glassy states suggest that there is no correlation between the monotonic $T_g(h)$ decrease and the density change in supported PS films. Most recently, inspired by this work, Yixuan Han and Alan Rohrbach are looking into the specific volume changes v_{sp} of supported poly(methyl methacrylate) (PMMA) and poly(2-vinyl pyridine) (P2VP) films as a function of film thickness h using exactly the same experimental procedures, in order to see whether or not different polymer-substrate interactions affect the density variations in polymer films.

After my work in Chapter 3, two computer simulations works were published looking into density variations in freestanding polymer films with decreasing film thickness that both cited my paper.[2] Both Stevenson et al.[23] and Lock et al.[24] observed density (specific volume) changes as they decreased the film thickness in their molecular dynamics simulations. Specifically, Stevenson et al. used a standard bead-spring model to simulate freestanding polymer films with their results supporting the idea that the shift in T_g of thin polymer films is controlled by molecular packing or density.[23] This is in contradiction with what I observed experimentally.[2] Lock et al. did atomistic level simulations studying molecular packing of polysulfone (PSF) to look into different kinds of physical properties of thin PSF freestanding films.[24] They found that T_g shifts with film thickness did not happen at the same film thicknesses, from 100 nm to 10 nm, as the specific volume changes, in qualitative agreement with my

experimental observations. Neither of the simulation works observes a nonmonotonic behavior in the specific volume as a function of film thickness.

The unknown influence of the free surface effect in Chapter 3 causes difficulty in interpreting our thin film data. As a result, for the second half of my dissertation, I focused on studying the local glass transition temperature T_g near different substrate conditions without the free surface effect using fluorescence spectroscopy. Previously in our lab, Baglay and Roth successfully measured the local $T_g(z)$ profiles across dissimilar polymer-polymer interfaces avoiding the free surface.[25–27] To achieve the long length scale of T_g as a function of distance z from a polymer-polymer interface, they have to anneal the interface to equilibrium. Therefore, Baglay and Roth proposed three potential explanations for the hundreds of nanometers long $T_g(z)$ profiles that arise during the annealing procedure, especially compared to a polymer-air interface.[26] First, there is a broadening of the interfacial region. The interfacial width of a polymer-air interface is only ~0.5 nm, which is about ten times smaller than that at a polymer-polymer interface.[26] Second, there is chain interpenetration happening at the polymer-polymer interfaces. Chapter 4 in this dissertation aimed to independently study how chain tethering at the interface perturbs a PS matrix with different grafting densities.[28] Third, there is more interfacial roughening at polymer-polymer interfaces due to the smaller interfacial tension compared to a polymer-air interface. Chapter 5 of my dissertation focused on isolating the effects from a rough substrate and investigated how various surface roughnesses alter the local T_g dynamics.

Prior to my work of Chapter 4 published in 2017 *ACS Macro Letters*,[28] studies of the average glass transition temperature $T_g(h)$ of thin PS films with substrate grafted chains dated back to Keddie and Jones in 1995.[29] Over the last two decades, people have reported both

increases,[30-32] and decreases[33] in the whole film $T_g(h)$ value relative to films of equivalent thickness on grafted substrates. However, such measurements are complicated by the presence of a strong and potentially dominating, free surface effect. The only existing study measuring the local T_g at a tethered substrate without the free surface effect is from Lan and Torkelson.[34] They observed a large T_g increase of ~35 K of chains end-tethered to a substrate with a grafting density of ~0.3 chains/nm^2.

In Chapter 4, I measured the local $T_g(z = 0)$ at the tethered substrate with grafting densities from 0.004-0.042 chains/nm^2 and observed an optimum grafting density of $\sigma = 0.011$ chains/nm^2 that results in a maximum T_g increase of 49 ± 2 K, which corresponds to the "mushroom-to-brush" crossover regime. The length scale of the optimum grafting density over which this $T_g(z)$ perturbation persists from the interface is ~100-125 nm, and is comparable to our group's recent work of PS next to a higher-T_g polymer such as polysulfone.[26] I made two significant contributions to the literature in this Chapter 4. One is finding that the volume fraction of tethered chains near the substrate region that leads to this maximum T_g increase is only ~10 %. This tells us it does not take many grafted chains to have a big impact on T_g. The other is suggesting that chain tethering may play a dominating role in deciding the long ranged $T_g(z)$ profiles near polymer-polymer interfaces, compared to the interfacial roughness effect studied in Chapter 5.

In Chapter 5, I am interested in studying how surface roughness changes the local T_g dynamics. Prior to my work, there is no published experimental study of measuring polymer dynamics next to a rough substrate because of many experimental difficulties. The only related experimental work is from an American Physical Society (APS) presentation by Panagopoulou

and Napolitano, who looked into how surface roughness influenced the segmental mobility of thin polymer films using dielectric spectroscopy.[35] However, their results contradict with the slowing down motion observed in many simulation works.[36-39]

The rough substrates with similar surface chemistry were made by exposing flat silica substrates to hydrofluoric (HF) vapor for different lengths of time. I observed a monotonic T_g increase of up to 111 ± 2 ^{0}C as the root-mean square roughness R_q increases from 0.5 nm to 10.9 nm. One possible explanation for the T_g increase we investigated was the theoretical suggestion that adsorption can occur more readily at a rough substrate due to a smaller entropy penalty.[40] To test this idea, we grew different adsorbed layers on flat silica substrates and locally measured T_g at various adsorbed layers avoiding the free surface effect. Our results indicate that T_g also increases monotonically with adsorption at longer times suggesting that adsorption on a rough substrate may be the reason why T_g increases. The 10 ± 2 K increase in T_g next to a rough interface is almost five times smaller than the T_g increase next to a tethered substrate with a grafting density of σ = 0.011 chains/nm^2.[28] This suggests that interfacial roughness may not play as important a role as chain tethering in deciding the $T_g(z)$ profiles next to dissimilar polymer-polymer interfaces.

These results of my Ph.D. work have left a number of open questions regarding the mechanism behind the slow down motion next to both end-tethered and rough substrates. Why and how does T_g increase at the grafted substrate? We suspect that this chain connectivity effect may be related to when chain dynamics can follow Gaussian dynamics.[28] Do the tethered chains alter local mobility in a similar way as free chain ends? I can imagine simulation work looking at the tethered chains' conformation in a polymer matrix would be very interesting and possibly

helping explain local T_g increases at a tethered interface. Is the adsorption the only and real explanation for the T_g increase observed at the rough substrate? Or is it perhaps a pure geometric effect? Douglas also suggested more interactions can happen between polymer chains and a rough wall compared to a flat wall.[40] Does the rough substrate somehow change the interfacial interactions? Finally, is it appropriate to suspect that the microstructure of adsorbed layers at longer annealing times contribute to T_g increases next the rough substrate? How similar are tails of adsorbed layers to end-tethered chains? At a first glance, they do not look that different.

References

[1] C.J. Ellison and J.M. Torkelson, Nat. Mater. **2**, 695 (2003).

[2] X. Huang and C.B. Roth, J. Chem. Phys. **144**, 234903 (2016).

[3] S. Kawana and R.A.L. Jones, Eur. Phys. J. E **10**, 223 (2003).

[4] R.D. Priestley, C.J. Ellison, L.J. Broadbelt, and J.M. Torkelson, Science **309**, 456 (2005).

[5] R.D. Priestley, L.J. Broadbelt, and J.M. Torkelson, Macromolecules **38**, 654 (2005).

[6] J.E. Pye, K.A. Rohald, E.A. Baker, and C.B. Roth, Macromolecules **43**, 8296 (2010).

[7] B. Frieberg, E. Glynos, and P.F. Green, Phys. Rev. Lett. **108**, 268304 (2012).

[8] Z. Yang, Y. Fujii, F.K. Lee, C.H. Lam, and O.K.C. Tsui, Science **328**, 1676 (2010).

[9] C.B. Roth and J.R. Dutcher, Phys. Rev. E **72**, 021803 (2005).

[10] C.B. Roth and J.R. Dutcher, J. Polym. Sci., Part B: Polym. Phys. **44**, 3011 (2006).

[11] C.M. Stafford, B.D. Vogt, C. Harrison, D. Julthongpiput, and R. Huang, Macromolecules **39**, 5095 (2006).

[12] J.M. Torres, C.M. Stafford, and B.D. Vogt, ACS Nano **3**, 2677 (2009).

[13] T.B. Karim and G.B. McKenna, Polym. **54**, 5928 (2013).

[14] T.B. Karim and G.B. McKenna, Macromolecules **45**, 9697 (2012).

[15] B.W. Rowe, B.D. Freeman, and D.R. Paul, Polym. **50**, 5565 (2009).

[16] W.E. Wallace, N.C. Beck Tan, W.L. Wu, and S. Satija, J. Chem. Phys. **108**, 3798 (1998).

[17] J.A. Forrest, K. Dalnoki-Veress, and J.R. Dutcher, Phys. Rev. E **58**, 6109 (1998).

[18] G. Vignaud, M.S. Chebil, J.K. Bal, N. Delorme, T. Beuvier, Y. Grohens, and A. Gibaud, Langmuir **30**, 11599 (2014).

[19] S. Ata, K. Kuboyama, K. Ito, Y. Kobayashi, and T. Ougizawa, Polym. **53**, 1028 (2012).

[20] R.P. White and J.E.G. Lipson, Phys. Rev. E **84**, 041801 (2011).

[21] J. Mattsson, J.A. Forrest, and L. Börjesson, Phys. Rev. E **62**, 5187 (2000).

[22] R.P. White, C.C. Price, and J.E.G. Lipson, Macromolecules **48**, 4132 (2015).

[23]C.S. Stevenson, J.G. Curro, and J.D. McCoy, J. Chem. Phys. **146**, 203322 (2017)

[24] S.S.M. Lock, K.K. Lau, A.M. Shariff, Y.F. Yeong, and M.A. Bustam, RSC Adv. **7**, 44376 (2017).

[25] R.R. Baglay and C.B. Roth, J. Chem. Phys. **143**, 111101 (2015).

[26] R.R. Baglay and C.B. Roth, J. Chem. Phys. **146**, 203307 (2017).

[27] R.R. Baglay and C.B. Roth, ACS Macro Lett. **6**, 887 (2017).

[28] X. Huang and C.B. Roth, ACS Macro Lett. **7**, 269 (2018).

[29] J.L. Keddie and R.A.L. Jones, Isreal J. Chem. **35**, 21 (1995)

[30] R.S. Tate, D.S. Fryer, S. Paqualini, M.F. Montague, J.J. De Pablo, and P.F. Nealey, J. Chem. Phys. **115**, 9982 (2001).

[31] A. Clough, D. Peng, Z. Yang, and O.K.C. Tsui, Macromolecules **44**, 1649 (2011).

[32] B. Zuo, S. Zhang, C. Niu, H. Zhou, S. Sun, and X. Wang, Soft Matter **13**, 2426 (2017).

[33] H. Lee, H. Ahn, S. Naidu, B.S. Seong, D.Y. Ryu, D.M. Trombly, and V. Ganesan, Macromolecules **43**, 9892 (2010).

[34] T. Lan and J.M. Torkelson, Polym. **64**, 183 (2015).

[35] A. Panagopoulou and S. Napolitano, *Impact of Substrate Roughness on the Segmental Mobility of Thin Polymer Films*, presented at APS March Meeting, New Orleans, LA, USA (2017).

[36] P. Scheidler, W. Kob, and K. Binder, J. Phys. Chem. B **108**, 6673 (2004).

[37] P.Z. Hanakata, J.F. Douglas, and F.W. Starr, Nat. Commun. **5**, 4163 (2014).

[38] P.Z. Hanakata, B.A. Pazmiño Betancourt, J.F. Douglas, and F.W. Starr, J. Chem. Phys. **142**, 234907 (2015).

[39] T. Davris and A.V. Lyulin, J. Chem. Phys. **143**, 074906 (2015).

[40] J.F. Douglas, Macromolecules **22**, 3707 (1989).